The Molecular mechanisms of aminergic release at type II synaptic terminals of *Drosophila melanogaster* and the effects of spermidine on mitochondrial redox status.

Inaugural-Dissertation

to obtain the academic degree Doctor rerum naturalium (Dr. rer. nat.)

Submitted to the Department of Biology, Chemistry, Pharmacy of Freie Universität Berlin

by

Jason Chun Kit See

from Berlin, Germany

2024

The experimental part of this thesis was conducted from May 2019 till May 2022 under the supervision of Prof. Dr. Stephan Sigrist and Prof. Dr. Hans-Joachim Pflüger at the Institute of Biology/Genetics of the Freie Universität Berlin and at the CharitéCrossOver at the Charité Campus Mitte.

1st Reviewer: Prof. Dr. Stephan Sigrist

2nd Reviewer: Prof. Dr. Mathias Wernet

Date of defence: 12.04.2024

1

Acknowledgements

together and the support they gave me throughout the years. I also like to thank my cat Shii, who kept distracting me in writing my thesis by sitting on my lap or walking in front of my monitor or by waking me up every day because she was hungry. I love you, regardless.

I would like to finish by thanking my close friends for always supporting me and keeping me company. Thank you, Anny and Bobby, for being there for me and putting up with me. Your emotional and moral support helped me a lot in writing my thesis.

Statement of Authorship

I hereby affirm that I wrote this thesis independently, and that I used no other sources than tools than quoted. All parts that were taken literally or correspondingly from publications are indicated as such. Intellectual property of other authors has been marked accordingly. I also declare that I have not applied for an examination procedure at any other institution and that I have not submitted the dissertation in this or any other form to any other faculty as a dissertation.

_____

Jason Chun Kit See

Contents

6

1.Introduction

1.1 The Chemical Synapse

The human brain is a highly complex organ that has been researched for a long time. It is seen as the central unit of our nervous system that is responsible for information processing with more than an estimated 100 billion neurons [19]. These neurons are highly specialized cells that have unique functions in the organism. An organism requires the ability to respond to environmental influences and adapt accordingly which is accomplished through the evolutionary result of neurons. These cells fulfil highly specific tasks in the organism, allowing it to process environmental changes. This includes e.g. visual, olfactory, mechanical stimuli which are perceived by sensory receptors and are transmitted to neurons in the central nervous system (CNS) by creating an electrical currents where they are then processed cells [20]. Neurons can be divided into a soma (the cell body), an axon and multiple dendrites. They are able to transmit information through electrical or chemical signals to other neuronal, or non-neuronal cells, such as muscles, through asymmetrical intercellular junctions [21], which are also known as synapses. The fundamental difference between an electrical and a chemical synapse lies in their transmission speed and the form of information transmission. An electrical synapse has faster transmission due to the connection of pre- and postsynapse via integral membrane proteins called "gap junctions" allowing for direct cytoplasmatic exchange of ions and smaller metabolites [22], while slower chemical synapses relay information through the release of neurotransmitters into the synaptic cleft which then bind to postsynaptic ionotropic (through ligand-gating ion channels) or metabotropic (through G-protein mediated second messenger signalling) receptors [1][23]. These emitted neurotransmitters are initially located in the presynapse within synaptic vesicles (SV).
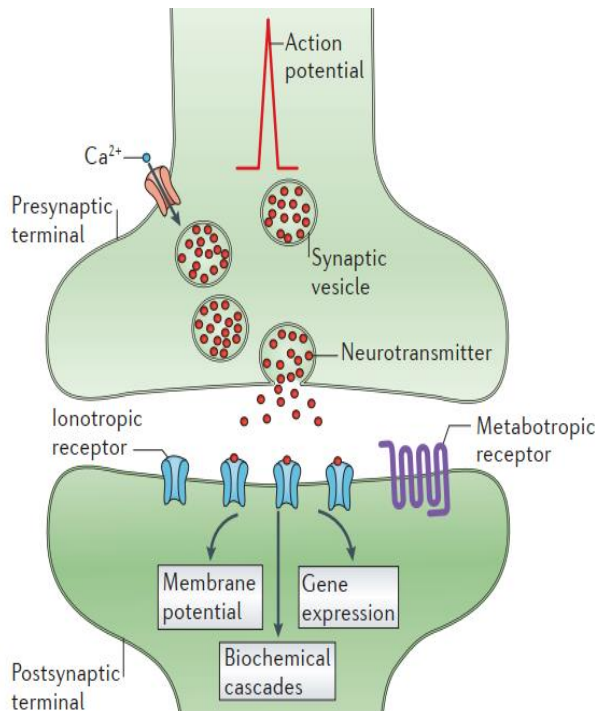
Figure 1: Simplified illustration of a chemical synapse and the transmission of an action potential.

An action potential travels to a presynaptic terminal triggering the activation of voltage-gated calcium channels (orange). Synaptic vesicles filled with neurotransmitters (red dots) are guided to the presynaptic membrane to fuse and release their content into the synaptic cleft because of the Ca^{2+} influx. These neurotransmitters are recognized by ionotropic receptors (blue) or metabotropic receptors (purple) in the postsynaptic density. The activation of these receptors leads to different postsynaptic events such as a change of membrane potential, triggering of a biochemical cascade or a change in gene expression. Illustration taken and modified from Pereda, 2014 [9].

Chemical synapses consist of a presynapse, a synaptic cleft and a postsynapse and play a crucial part in signal transmission. Upon the arrival of an action potential the voltage gated Ca^{2+} channels (VGCC) are activated. This results into an influx of Ca^{2+} which triggers synaptic vesicles within the presynapse to release their neurotransmitter via exocytosis at highly specialized areas of the presynaptic plasma membrane, also known as active zones (AZs). The active zone is a presynaptic plasma membrane region with electron-dense material at which SV docking and release takes place through an influx of Ca^{2+} ions [24]. The electron-dense material is also known as T-bar and contains a diversity of different active zone proteins such as Rab3-interacting molecules (RIM), RIM-binding protein (RBP), ELKS/Bruchpilot (BRP) proteins, Munc13/Unc13s and Liprin-α [25-28] . Through exocytosis of SVs with the presynaptic plasma membrane, neurotransmitters are released into the synaptic cleft which then are recognized by corresponding postsynaptic receptor proteins. SVs have a diameter of roughly 40 nm and contain around 1500 - 2000 neurotransmitter molecules [10]. These neurotransmitters can be either excitatory (e.g., acetylcholine, glutamate) or inhibitory (GABA, glycine) and lead to either a de- or hyperpolarization of the following cell. This is achieved by an ionotropic or metabotropic uptake of the

presynaptically released neurotransmitter. In case of an excitatory postsynapse, an electron-dense structure also known as post synaptic density (PSD) can be found and is precisely aligned with the AZ of the presynapse [25]. The PSD contains a variety of tyrosine kinases, G protein-coupled receptors, ion channels and cell adhesion molecules [23].

1.2 The presynaptic compartment

1.2.1 Synaptic vesicles

Synaptic vesicles are uniform organelles that are central for neurotransmitter release in synapses with a diameter of around 40 nm (Figure 2). The release of neurotransmitters from the presynapse is triggered by an incoming action potential that depolarizes the presynaptic plasma membrane. The Ca^{2+} influx triggers the exocytosis of SVs by binding to synaptotagmin, which results into the release of neurotransmitters into the synaptic cleft [29]. This process is repeated multiple times per milliseconds. To restore the synaptic vesicle pool in the presynapse, the released neurotransmitters are recycled into SVs via endocytosis.

Figure 2: „Molecular model of an Average SV".

A 3D constructed model of the outside view of a SV by using an array of modern molecular techniques by Takamori et al. Image taken and slightly modified from Takamori et al, 2006 [10].

1.2.2 The Synaptic Vesicle Cycle and the release machinery

The synaptic vesicle cycle is an interplay of exo- and endocytosis of SVs, required for a quick and repeated neurotransmitter release at the AZ. The major processes involved are SV docking and priming, recycling and reclustering, exocytosis and endocytosis [15] (Figure 3).

The SV cycle begins with the recruitment of SVs to the AZ site and continues by tethering and docking them at the AZ close to where VGCCs are located. Following the docking, the SVs are molecularly primed, which is a process that involves several priming reactions that leaves the SVs in a metastable state and prepares them for fast Ca^{2+}-triggered fusion with the plasma membrane [30]. The SVs that have been primed

and are ready for membrane fusion constitutes the readily releasable pool (RRP). Once SVs have been released, the release site needs to undergo clearing process, to remove the remaining SV membrane proteins to allow further fusion events to happen (Figure 3).

Aside from the RRP, there are two additional synaptic vesical pools: The recycling pool and the reserve pool. The recycling pool is defined as the pool of vesicles that maintain the release upon moderate stimulation and is thought to consist of around 5%-20% of all vesicles, whereas the reserve pool is defined as the depot of SVs that are only released through intense stimulation and is estimated to be constituted by the majority of SVs in the presynaptic terminal (around 80-90%) [31]. The arrival of an action potential causes the influx of Ca^{2+}-ions which are recognized by the Ca2+ sensor on the SV and leads to the fusion of the vesicles in the RRP. The vesicles in the RRP are already docked and primed and can therefore be used for immediate fusion with the presynaptic membrane.

The core proteins in the exocytotic release machinery include SNARE proteins (soluble N-ethylmaleimide-sensitive factor attachment protein receptors), which can further be divided into vesicular (v-SNARE) and target (t-SNARE) SNARE proteins. In neurons, the v-SNARE protein is synaptobrevin (also known as VAMP, vesicle-associated-membrane protein) [32, 33] and the t-SNARE proteins, which are located in the plasma membrane, are SNAP-25 (synaptosomal-associated-protein 25) [34] and Syntaxin-1 [35]. The v-SNARE protein synaptobrevin forms a complex with the t-SNARE proteins syntaxin-1 and SNAP-25 [36] at the synapse to mediate fusion of the SV. Syntaxin-1 is present in a closed conformation and cannot engage with the SNARE-complex formation in that state. Therefore, it is necessary to change the conformation of synaptobrevin from a closed into an activated open conformation to proceed with the SNARE-complex formation. This is done with the help of the priming factor (M)Unc13 (mammalian homologue of *D.melanogaster's* and *C.elegans*' Uncoordinated-13 protein) [37]. This results in a trans-complex between 3 SNARE proteins which coiled-coil regions form a helix that's twisting around each other and brings SV membrane and plasma membrane closely together without fusing them yet. This process is also known as SV priming, which makes the SV fusion competent. To fuse the SV with the membrane, the influx of Ca^{2+} ions via VGCC upon an action potential arrival, is required. The SV membrane protein Synaptotagmin-1, which is

known as a Ca^{2+} sensor, is able to sense the local changes of Ca^{2+} concentration and initiates the fusion of SV with the synaptic plasma membrane with the help of the co-factor complexin [26, 38]. Furthermore (M)Unc18 is thought to play a crucial role in the
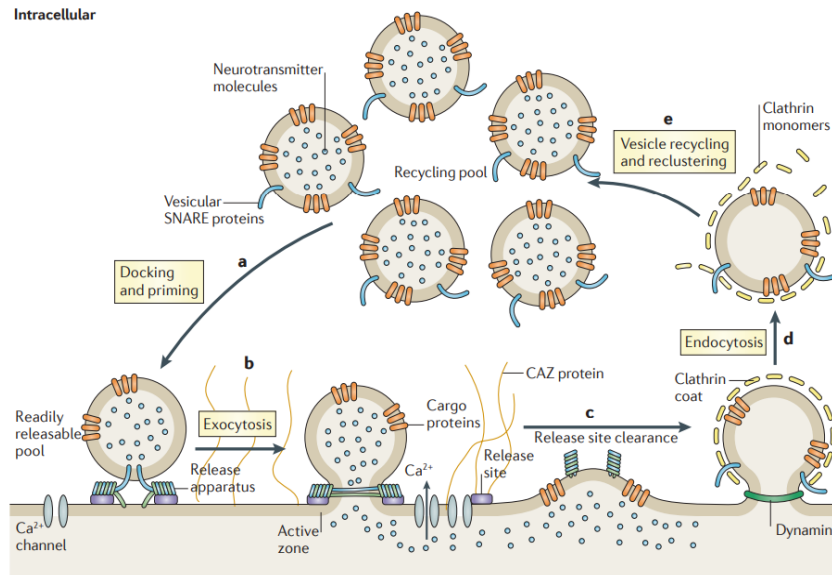
Figure 3: Overview of the synaptic vesicle cycle.

The readily releasable pool constitutes of the docked and primed SVs. Upon Ca^{2+} influx the exocytosis of those SVs is triggered and neurotransmitter release into the synaptic cleft takes place. The exocytosis of SVs occurs at the AZ of the presynaptic membrane which, after release, must be cleared for subsequent SV release. The clathrin-mediated endocytosis of new synaptic vesicle membranes then happens at the peri-active zone that surrounds the AZ area and are then excised by dynamin. After the clathrin uncoating and the neurotransmitter uptake took place, the SVs return into recycling pool where they are reclustered once again. Image from Haucke et al., 2011 [15].

fusion process. It's bound to Syntaxin-1 prior the conformation changes and remains bound throughout the whole SNARE complex assembly until the neurotransmitter release [37, 39]. Once SV fuse at the presynaptic membrane, the release site must be cleared of the remaining SV membrane proteins and the SNARE complex must be disassembled to recycle the SNARE proteins within. This is achieved by the hydrolysis of ATP through the evolutionary conserved ATPase NSF (N-ethylmaleimide-sensitive factor) [40]. With the help of SNAPs (soluble NSF attachment proteins) as a co-factor NSF is able to bind onto the SNARE complex and finally disassemble the complex

[41]. Lastly, the now broken down complex can be recycled via clathrin- and dynamin-mediated exocytosis [29].
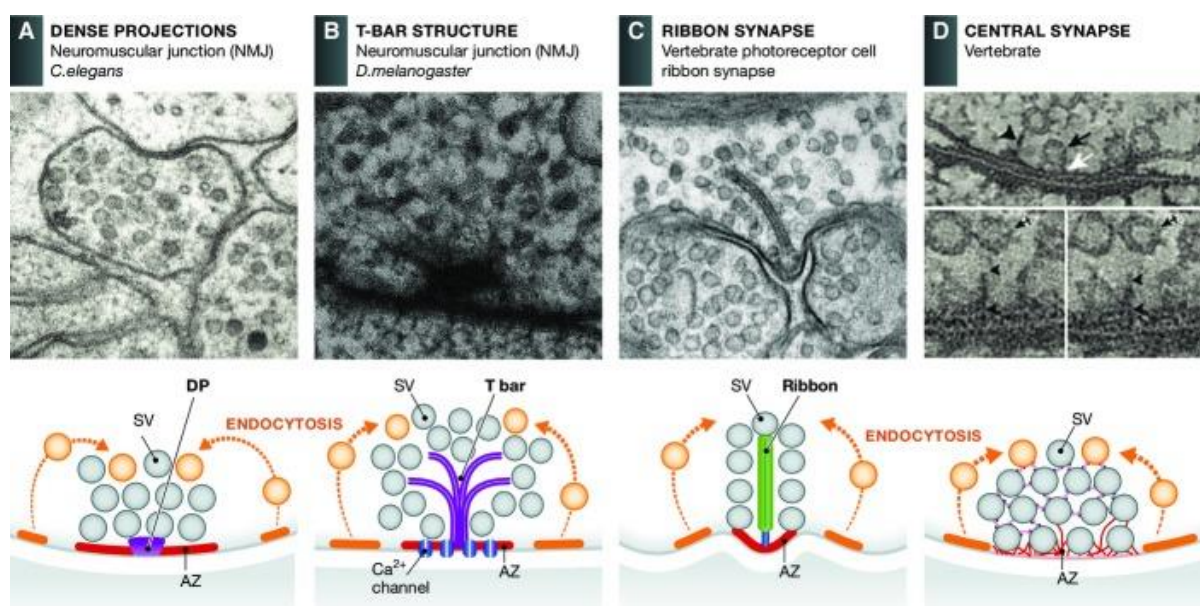
Figure 4: Electron micrographs and schematic drawings of active zones in different species.

Electron microscopic images show the difference in AZ morphology between different species and synapses within the same species. **(A)** AZ of C.elegans at the NMJ. They are generally characterized as broad surface of plasma membranes in between the dense projection and flanking cellular tight junctions. **(B)** An AZ at the NMJ in Drosophila. The electron dense projection in Drosophila is also known as T-bar and has typically a platform consisting of a meshwork of filaments overlaying a pedestal. **(C)** AZ of a vertebrate photoreceptor cell ribbon synapse. These synapses have large AZs with a specialized organelle called the synaptic ribbon. This organelle tethers large numbers of SVs and facilitate fast-sustained synaptic transmission. **(D)** AZ of a central synapse in vertebrate. They are less complex than sensory synapses exhibiting fine filamentous projections which connect docked SVs. Images and text taken and modified from Ackermann et al. 2015 [2].

1.3 The active zone as synaptic vesicle release site

The active zones at presynaptic terminals are highly specialized regions at the plasma membrane where neurotransmitter release happens. It is a central structure for every nerve terminal and is a major contributor for signal transmission, which downstream also defines the action potential shape and frequency, as well as the information that is delivered to the post-synapse. This membrane region contains a variety of channels and transmembrane proteins which forms an electron-dense structure when observed under an electron microscope (Figure 4). The cytomatrix of the active zone (CAZ) is a

meshwork of proteins that also depicts as an electron-dense structure in electron microscopic pictures. This dense projection varies in its appearance between organisms and even synapses [2, 25] (Figure 4), and is an indicator of the presence of an extended molecular scaffold [28]. As my work focusses on the molecular mechanisms in *D.melanogaster* as my model organism, I will focus on the neuromuscular junction (NMJ) of *D.melanogaster*.

1.3.1 Ca2+-Channels

VGCCs are a family of ion channels that are evolutionary highly conserved and are structurally related to K^+- and Na^+-channels [42]. They are vital for the neurotransmitter release in synapses. Upon action potential (AP) arrival, the calcium channels open and allow the flood of calcium ions into the cell, resulting in an increase of intracellular Ca^{2+} concentration. The result of this influx triggers the onset of the exocytotic machinery at the synaptic terminal and initiates the start of the exocytosis of primed SVs [43]. Additionally, they are also involved in other processes, such as cell growth, differentiation, muscle contraction, hormone release and more [44]. VGCCs are composed of 5 subunits ($\alpha 1, \alpha 2, \beta, \gamma, \delta$) that form a complex. Initial electrophysiological characterizations categorized Ca^{2+}-channels into two different types: Low-voltage activated (LVA) or high-voltage-activated (HVA) [45]. The activation voltage threshold of LVA is at around >-70 mV while HVA types have a threshold at >-40 mV. LVA Ca^{2+} channels have a small channel conductance and are fast inactivating (also termed as T-type, for "transient" or "tiny"), unlike HVA Ca^{2+} channels that exhibit a large single channel conductance and slower inactivation. The latter channels can also be further divided into following subcategories: L-type ("L" stands for "long-lasting"), N-types, P/Q-types and R-types [42]. Studies have shown that only Ca_{V2} subfamily channels are enriched at synaptic terminals and are the major Ca^{2+} channel family that is involved in neurotransmitter release [46]. The subunit $\alpha 1$ is the subunit that controls the voltage-dependent activation by their voltage-sensing domains [44]. It was shown, that in *D.melanogaster* the gene *cacophony* (cac) [47] encodes a synaptic calcium $\alpha 1$ subunit and interacts with the N-terminus of BRP in vitro [48]. The clustering of Ca^{2+} channels at the presynaptic membrane is mainly mediated by BRP and Rab3-Interacting Molecule binding proteins (RIM-BP) [48, 49].

1.3.2 ELKS/BRP

The protein BRP in *D.melanogaster* is encoded by the gene "*brp*" and possesses an N-terminal domain with significant sequence homology to the vertebrate ELKS/CAST/ERC, and a C-terminal rich in coiled-coil structures and is around 200 kDa big. Studies have shown, that *brp* mutant flies exhibit defects in locomotion in general, but also have unstable flight behaviour resulting in constant crashes, hence labelled as "Bruchpilot" (Bruchpilot is german and translates into English as "crash pilot") [50]. In *Drosophila,* BRP is the core protein defining the electron dense projection in the presynaptic CAZ, as *brp^{Null}* mutants show an absent of the usual T-bar structure in electron microscopic images [49]. Furthermore, *brp^{Null}* mutants show reduced amplitudes of evoked excitatory postsynaptic currents of around 25% (eEPSC), reduced RRP size and a declustering of Ca^{2+} channels at NMJs [48, 49, 51]. In previous studies, it has been revealed, that by staining BRP with the monoclonal antibody NC82 and with the help of stimulated emission depletion (STED) fluorescence microscopy, BRP organizes in a donut-shape at the AZ around a central Ca^{2+} channel opposing a glutamate receptor field of the postsynapse [49, 52]. In addition, it has been shown that BRP's N-terminal is mediating the clustering of VGCC and interacts with the α subunit of Ca^{2+} channels [48, 50, 53].

In *Drosophila,* there are two main isoforms of BRP that is expressed: BRP-170 (size of 170 kDa) and BRP-190 (size of 190 kDa). Both isoforms contribute to the T-bar cytomatrix assembly very similarly and alternate in a circular array. Mutants of either isoform did not result in an abolishment of the cytomatrix or Ca^{2+} channel clustering, but instead lead to a reduction in size and baseline transmission [51]. Unlike in mammalians, where Piccolo and Bassoon, two large coiled-coil proteins are required in the assembly of the AZ, *Drosophila* only has one Piccolo homologue known as "Fife", but no known Bassoon homologue [54, 55]. It is assumed that BRP mediates the functions of mammalian proteins ELKS and Bassoon in *Drosophila* and plays a crucial role in SV recruitment [27, 56].

1.3.3 Rim-Binding Protein

RIM-BP (or RBP) are multidomain proteins composed with a string of identifiable modules, that are involved in the organization of the AZ and the localization of BRP [27, 57, 58]. It has been suggested that they contribute to linking the AZ protein network with the Ca^{2+} channels by interacting with RIM and Unc13A, but also in Ca^{2+}

channel recruitment [57, 59, 60]. All RBPs contain one N-terminal and two C-terminal SH3 domains, two to three central Fibronectin-3 domains [58, 61]. The C-terminal SH3 domains have been shown to bind to PxxP motifs of the intracellular tail of the α1 subunit of Ca^{2+} channels [62, 63], RIM [57] and *Drosophila* Unc13A [59]. The loss of RBP in an RBP mutant results into an almost complete abolishment of evoked neurotransmitter release in *Drosophila* [58] and a decrease in Ca^{2+} channel release site coupling in mammals [64]. The reduction of Ca^{2+} channel recruitment in RIM mutant synapses can be rescued with only a RIM fragment that contains only its PDZ-domain and its RBP interaction domain [57]. This suggests that RBP has other interactions within the presynaptic AZ, besides from binding to RIM and Ca^{2+} channels, to function [27, 57].

1.3.4 Liprin-α and Syd-1

Liprin-α family proteins are evolutionary conserved multi-domain proteins required in the assembly, organization, and function of the AZ, but also vesicular trafficking regulation [28, 65-67]. They were first identified as interaction partners for LAR (Leukocyte common antigen-related) protein-tyrosine phosphatases at focal adhesions [68]. Liprins can be structurally segmented in an N-terminal rich in coiled-coil structures, containing evolutionary conserved "Liprin-α Homology regions 1 (LH1) and 2 (LH2)" [69]. The N-terminal half is capable of forming homodimers [70] which then can interact with other AZ proteins, e.g. RIM [69] and ELKS/ERC/CAST [71]. The C-terminal halves contain three conserved SAM ("Sterile-Alpha-Motif") domains which can bind to LAR-type receptor protein tyrosine phosphatase [72]. Loss of function (LoF) mutations of Liprin-α result in fewer, but bigger AZs [48, 65, 73]. In *Drosophila* it was shown that Liprin-α together with Syd-1 ("synapse-defective-1"), another large scaffolding protein, act as an early arriving scaffold component involved in AZ seeding and the stabilization of late arriving BRP/RBP scaffold [48, 74, 75].

Syd-1 is a binding partner of Liprin-α and forms a transsynaptic complex with Neurexin-1 in the presynapse and Neuroligin-1 in the postsynapse [74, 75]. It's a large scaffolding protein crucial for alignment of pre- and postsynapse as well as AZ maturation. It was shown that Syd-1, together with Liprin-α, arrives early at the AZ, hours before the incorporation of other AZ proteins such as ELKS/BRP at *Drosophila* NMJs [48, 74-76] and Syd-1 stalls Liprin-α at newly formed AZ sites. A missense mutation in the LH1 domain of Liprin-α resulted in a gain of function (GoF) effect where

Syd-1 was not necessary anymore for the assembly process [76]. The same effect can be achieved by overexpressing Liprin-α, indicating that Syd-1's function during the process is recruiting Liprin-α [76, 77].

1.3.5 Unc13

Unc13 is an evolutionary conserved multidomain protein which was first described in *C.elegans*, whose mutation resulted in "uncoordinated" movements [78]. It is a large protein (>200 kDa) that plays an important role at the CAZ and especially in the SV priming process [27]. The deletion of this protein leads to an almost complete abolishment of spontaneous and evoked neurotransmitter release in vertebrates and invertebrates [79-81]. In mammals, there are 5 Munc-13 genes [27, 82-84]: Munc13-1, Munc13-2 and Munc13-3 which are expressed mainly in brain, while the other two isoforms Munc13-4 and BAP3 (BAI1-associated protein 3) are primarily expressed outside of the brain [27, 83, 85].

In *C.elegans* there are also two Unc13 isoforms: Unc13S (S = Short) and Unc13L (L = Long) that are essential in controlling different kinetics of synaptic transmission. The Unc13L isoform mediates fast synchronous release, whereas Unc13S is required for the slow-release component. The localization of both isoforms corresponds to their functionality within the presynaptic terminal: Unc13L clusters close to the AZ, while Unc13S appears rather diffuse [80, 86]. In *Drosophila* neuronal cells, two main isoforms are expressed: Unc13A and Unc13B, which are transcribed from a single Unc13 gene locus by using alternative promoters [87]. Additionally, both isoforms, in *C.elegans* and *D.melanogaster*, only differ in their N-terminal protein structure [59, 82]. In super-resolution light microscopy images, it has been shown, that Unc13A localizes closely to the AZ, while the B isoform is located around 50 nm towards the periphery in *Drosophila* larval NMJ. Previous knockout experiments of early or late scaffold complex suggested a stabilization of Unc13B via Liprin-α and Syd-1, whereas RBP and BRP anchors Unc13A to the AZ. It also has been suggested that their different location at the AZ and therefore their proximity to the Ca^{2+}-channel, just like in *C.elegans*, reflect their function in SV release. An Unc13A mutant resulted into an almost abolishment of neurotransmitter release, while a mutation in Unc13B resulted in only a minor synaptic transmission defect at the *Drosophila* larval NMJ [59].

1.4 The postsynaptic compartment

The postsynapse is at the receiving end in the action potential transmission process and is closely and precisely aligned opposite of the presynapse. The released neurotransmitters of the presynapse bind to postsynaptic receptors leading into an ionotropic or metabotropic reaction transforming the chemical reaction back into an electrical signal. Ionotropic receptors allow specific ions to directly osmose from the synaptic cleft into the postsynaptic cell leading to a membrane potential change. Unlike ionotropic receptors, metabotropic receptors (also known as G-protein coupled receptors) don't enable a direct influx of ions into the postsynaptic compartment but trigger an intracellular second-messenger response upon neurotransmitter binding [24, 27]. The result of the ion influx depends on the ion that enters the postsynapse itself. The flow of cations into the postsynapse leads to a depolarization resulting into an excitatory signal transmission, while an influx of anions leads to a hyperpolarization and an inhibitory signal. The effect on the postsynapse can typically be attributed to specific neurotransmitters. For example, inhibitory synapses use γ-aminobutyric acid (GABA) or glycine to activate distinct but homologous classes of chloride-permeable ion channels [88], while excitatory synapses differ specifically depending on species. In mammalian CNS, glutamate is the predominant excitatory neurotransmitter [89], while acetylcholine (ACh) is the case in vertebrate NMJ.

As I focus on *Drosophila,* as my model organism, in my thesis, I will write about it in more detail in the following paragraphs, as I will elucidate the model organism itself.

1.5 Drosophila melanogaster as a genetic model organism in Neurobiology

Drosophila melanogaster is a fruit fly that has been used as a model organism for more than one hundred centuries. It's an organism well suited for research due to its short life cycle and generation time (Figure 5), low cost and excellent genetic tools that have been developed in due of time. With the increase in molecular tools, the fly
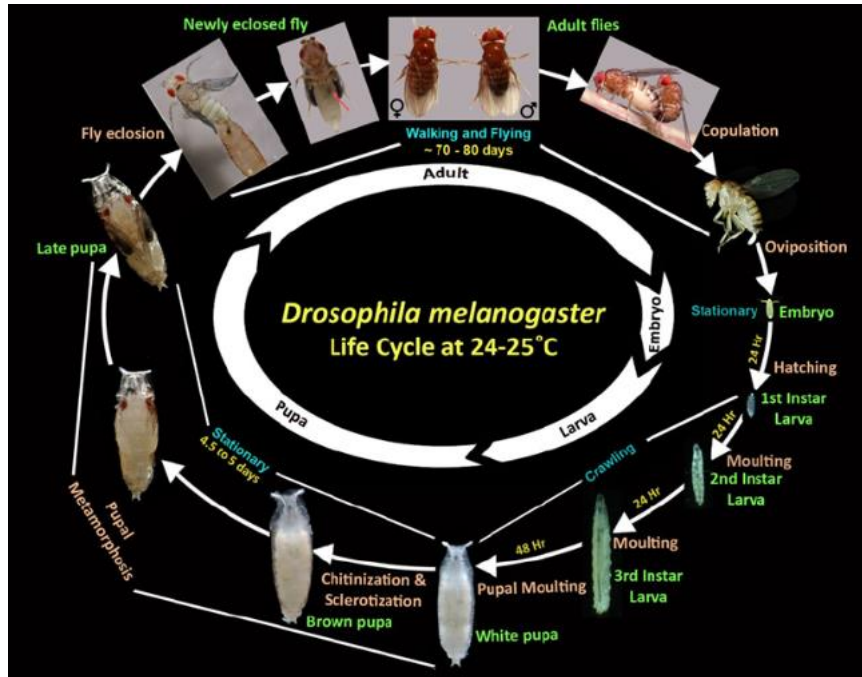
Figure 5: Life cycle of *Drosophila melanogaster*.

After mating, female flies lay up to 100 eggs per day. After embryogenesis, that takes up to 24 hours, the embryos hatch into 1st instar larva, which then feed and grow for two consecutive larval stages. Once they reach the 3rd instar larva stage, they start to crawl out of the food and pupate (in fly vials on the sides of the vial). Once the pupal moulting happened, the larva, which now is a pupa, undergoes metamorphosis, where great reorganization of inner organs take place. After around 4 to 5 days, the pupa starts to hatch, and an adult fly emerges. The length of the stages heavily depends on temperature. The given numbers here are the life cycle at around 24-25°C. Image modified from the book "Rearing and handling of Drosophila – A primer for laboratory experiments" by Chaudhary et al. [6].

Drosophila has become an even more popular genetic organism to use in basic research [90]. Historically, Thomas Hunt Morgan (1866-1945) was the one that used the fly to prove chromosomal theory of inheritance, showing that the *white* gene is located on the X-chromosome, for which he received a Nobel prize [91]. This was followed by his protégés that defined many genetic principles, including the effect of X-rays on mutation rates [92]. All the work that has been done on *Drosophila*, along with its low generation time, high reproduction rate as well as low simple and cost-effective rearing conditions, makes it a very popular genetic model organism to study neuroscientific and neurodevelopmental questions on [93, 94]. Genetically, *Drosophila* offers a variety of methods as well. Due to P-element based genetics, a huge genetical tool kit to modify the genome, or especially single genes or proteins, are possible. Particularly the establishment of the GAL4-UAS system allows for local and temporal

specific expression of desired genes [95]. Genome analysis have shown that 75% of human disease genes have homologues in *Drosophila*, albeit with lesser redundancy [96]. One of the better characterized synaptic models is the NMJ at *Drosophila* L3 larva, which consists of glutamatergic synapses, unlike in vertebrates, where they primarily use acetylcholine as neurotransmitter. The excitatory larval NMJ synapses show similarities to synapses in vertebrate CNS. In *Drosophila*, larval NMJ synapses use glutamate receptors (GluR) that are homologous to AMPA-type GluR in mammalian brain [97].

1.5.1 The larval NMJ in Drosophila melanogaster and larval locomotion

The neuromuscular junction (NMJ) within the larval body wall muscles in *Drosophila* have become a very popular genetic model system to study a plethora of questions in neuroscience and were first used back in the 1970s [98, 99].
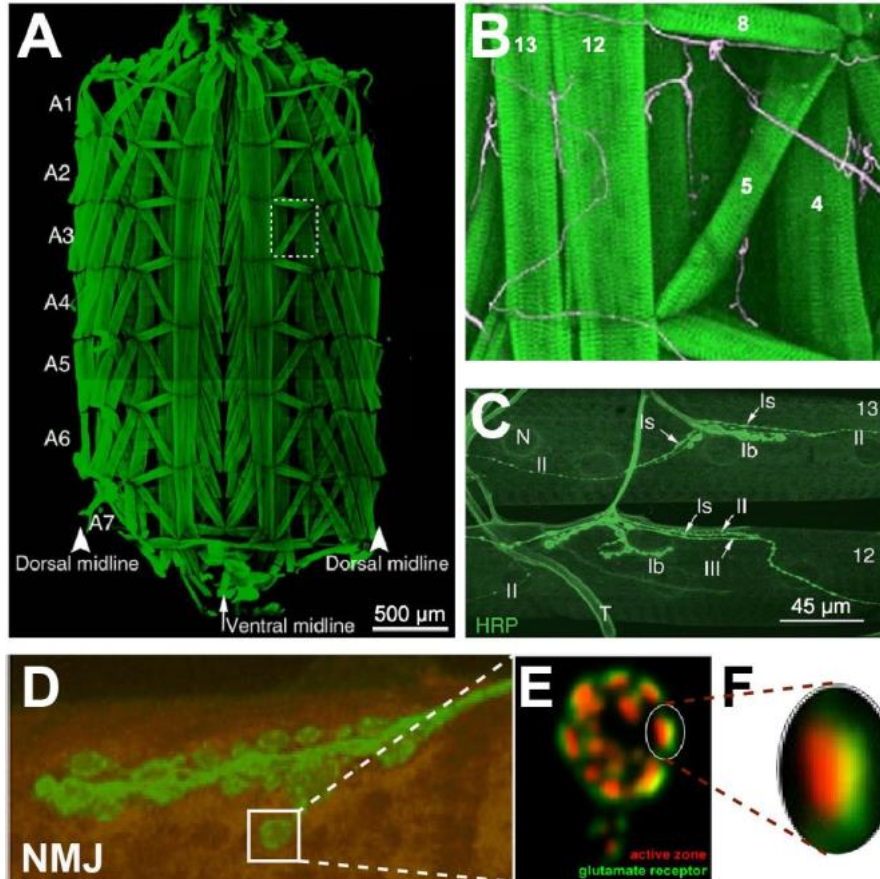
Figure 6: The Neuromuscular Junction at *Drosophila melanogaster.*

(A) shows a 3rd instar larva body wall muscles preparation. The preparation used FITC-conjugated phalloidin staining for F-actin. The larva has 7 abdominal segments (A1 to A7), which have a repeating muscle pattern, aside from A1. **(B)** A magnification of a hemisegment at the muscles 13, 12, 8, 5 and 4 (magnification of the region in the dashed area in (A). Muscles are shown in green with phalloidin and neuronal membrane in white with the antibody HRP (Horseradish peroxidase). **(C)** Different types of boutons at the NMJ at muscle 12 and 13 stained with anti-HRP. There are type Ib (big), type-Is (small), type-II and type-III boutons. Usually, type-I boutons innervate a single muscle and release glutamate as neurotransmitter, while type-II and type-III are modulatory. Type-II motoneurons innervate multiple muscles and use octopamine as neurotransmitter and type-III are peptidergic. **(D)** Larval muscle (orange) innervated by a motoneuron (green). The square area is a bouton magnified in **(E,F)** A magnification of a bouton. The presynaptic active zone (red) is colocalized to the glutamate receptor field (green). Images and descriptions taken and modified from [13], [18], Matthias Sieber, PhD thesis, Matthias Böhme, PhD thesis.

It is now used to study a broad variety of neuroscientific questions such as synapse physiology, development and plasticity [100]. The advantage of using the NMJ of *Drosophila* is the availability of modern genetic tools that e.g. allow spatiotemporally controlled gene expression [101] and various other experimental techniques such as electrophysiology, immunohistochemistry, electron microscopy, STED and live imaging. Additionally, *Drosophila* NMJ synapses show structural plasticity and are glutamatergic [102]. Furthermore, *Drosophila's* larval body wall muscles are easily accessible via simple dissection methods and the preparation can be categorized in different abdominal segments with a bilateral organized muscle pattern (Figure 6). The muscles in *Drosophila* larvae are attached at to the inner body wall surface with a very stereotypical muscle pattern ranging from A2 (Abdominal segment) to A7 (only A1 slightly differs) with only 32 motor neurons in each abdominal hemisegment [103]. The neurons innervating the NMJs originate from the ventral nerve cord (VNC). There are three classes of neurons at the *Drosophila* NMJ: type-Ib (big) and type-Is (small), type-II and type-III. Type-Ib and type-Is are the main excitatory neurons, usually innervating a single muscle fibre [100].

The larval body wall muscles are innervated by glutamatergic, peptidergic and octopaminergic motor neurons, which synaptic endings are organized into synaptic boutons and forming the presynaptic compartment of the NMJ. The postsynaptic membrane contains the GluR field that is exactly aligned opposite of the presynaptic AZ, creating the location of synaptic transmission. With the growth of the larva, the muscles increase in size as well, which requires the system to be able to compensate for the changes on synaptic levels. The bone morphogenic protein (BMP) pathway has been shown to be a vital player in pre- and postsynaptic communication [104]. It initiates a retrograde signal by which muscles influence presynaptic growth. Additionally, WNTs regulate the pre- and postsynaptic apparatus in a retrograde and autocrine way. A mutation of *wingless* (also known as WNT1) lead to the development of so-called "ghost boutons", which are boutons filled with SVs, but devoid of AZs, postsynaptic specializations and mitochondria, which are all critical components for synaptic terminals, indicating a central role in of *wingless* in synapse differentiation [105, 106].

Locomotion for *Drosophila* larvae is of utmost importance, as during their life cycle as larvae their main objective is to forage and take up nutrients to grow and reach their

requirement to be able to metamorphose and grow into their adult form. Natural crawling behaviour entails different larval actions such as forward and backward
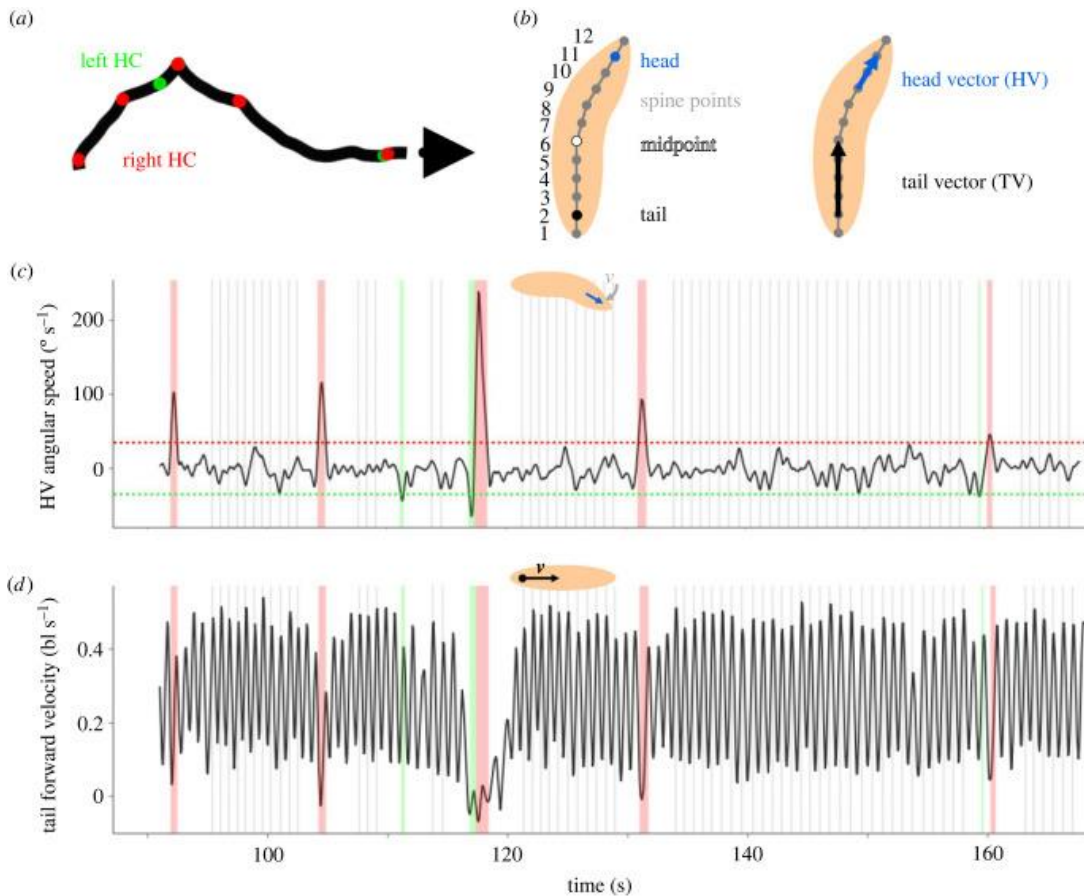
Figure 7 Basic overview of the analysis data from using IMBA.

(a) A sample of the tracking of a larva. Green dots represent left HC while red dots right HCs and the big arrow indicates the end of the track. **(b)** On the left, the 12 spine points along the spine of the larvae with equal distance between each point are determined, while spine point 1 equals the tail and spine point 12 the head of the larva. Spine point 11 (2nd from the front) is taken as an indicative of the head and the spine point 2 (2nd from the rear) is an indicative of the tail. On the right graphic is the depiction of the larva and the HV (Spine points 9 to 11) and the tail vector (Spine points 2 to 6). **(c)** The angular speed of the head vector of the track seen in (a), negative values depict left movement and positive values right movement. The red, strippled line symbolizes the +/- 35°/s threshold of the HV angular speed. Green shaded events show left HCs and red shaded ones depict right HCs. **(d)** The forward velocity of the tail in body lengths per second (bl/s) of the larval track (a). Each oscillation represents one cycle of peristaltic forward movement and during a run the velocity oscillates regularly. During a run, each tail forward velocity peak is therefore defined as one step (grey lines). 1.5s before and after a HC, the regular forward movement is stopped, and no steps are observed in the meantime. Image and caption taken and modified from M. Thane's paper [4].

locomotion, turning, head casts, pauses, bending, rolling, hunching, and burrowing

[107-109]. Larval locomotion is achieved through abdominal somatic body wall muscle contractions that can go either from posterior to anterior, resulting in a forward movement, or the other way around from anterior to posterior, enabling backward locomotion [110-113]. Continuous, relatively straight, forward peristaltic movement can be described as run phases, while reorientation events happen after lateral head casts (HC), which are followed by a significant decrease in speed and a change of direction [4, 114]. A HC is defined in the paper of Michael Tane in 2023 [4] as a movement of the angular speed of the head vector (HV; vector between 9th and 11th spine point, Figure 7) that exceeds the value of +/- 35°/s. More locomotive microbehaviour that can be observed and analysed will be discussed later in this thesis.

1.5.2 The properties of type II boutons and the role of octopamine and tyramine

Type-II terminal neurons use the biogenic amine octopamine and tyramine, while type-III neurons are peptidergic and contain insulin as co-transmitter [115]. Neuromodulation for different behaviours is mediated by epinephrine and norepinephrine in vertebrates, while the invertebrate counterparts are octopamine (OA) and tyramine (TA). OA and TA are decarboxylation products of the amino acid tyrosine, while is TA the biological precursor of OA (Figure 8) [116]. They have been shown to regulate a diversity of physiological, cellular, and behavioural processes in conjunction with peptides [116-119]. OA is involved in modulation of a wide variety of behaviour e.g. the stimulation of a single dorsal unpaired median (DUM) neuron in locust resulted in the modulation of neuromuscular potentials, indicating a direct adaption of motor functions in response to environmental changes [120]. OA also controls fight or flight response in *Drosophila* on different levels by neurons releasing it onto different peripheral organs and can trigger the release of adipokinetic hormones [116]. During flight take-off phase and rest, OA activates the potent glycolytic activator fructose 2,6-biphosphate leading to glycolytic activities in the flight muscle, while during flight, OA levels in flight muscles decrease, resulting in reduced glycolysis and a switch towards fat as main energy source fuelling flight muscles. Interestingly, while OA in flight muscles decreases, the levels in the hemolymph actually increases during that period [116]. As to what effects it has and where it comes from remains elusive. Additionally, in *Drosophila,* OA may modulate different behaviours such as aggression, sleep, egg-laying behaviour, ethanol tolerance, as well as learning and memory [115, 121-127]. The release of OA in type II terminals onto insect skeletal muscles produces

a small increase in twitch tension (up to 10%) and an increase in skeletal muscle relaxation rate [128-130]. Surprisingly, TA regulates motor behaviours in an antagonistic behaviour to OA [131]. Larval *Drosophila* crawling and adult flight initiation and maintenance are enhanced by OA but reduced by TA signalling [132, 133]. Compared to OA, TA has not been described as well as OA, but previous work show, that TA is also acting on CPG circuits, muscle contraction properties, metabolism and likely on sensory systems [130, 134-136].
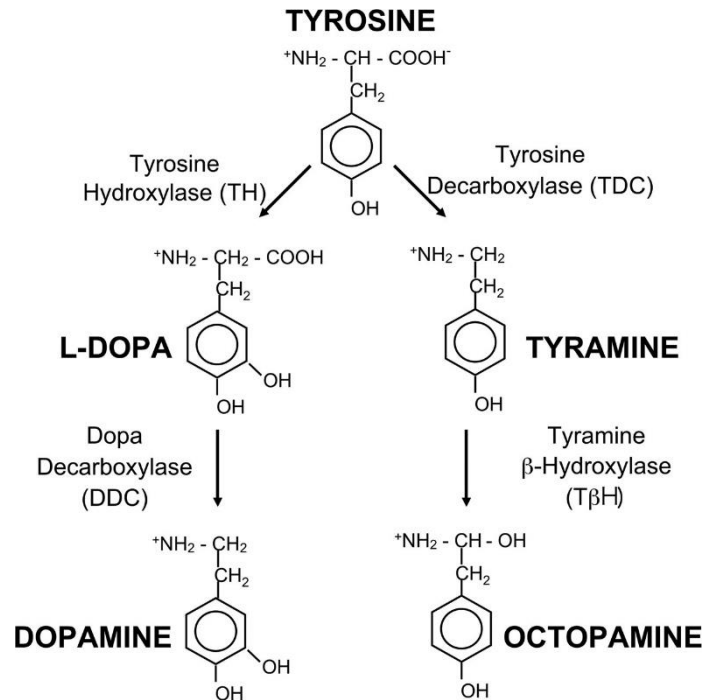
TYROSINE

Figure 8: Biosynthesis pathway of dopamine, octopamine and tyramine in Drosophila melanogaster.

On the left side is the biosynthesis pathway of tyrosine into dopamine and on the right from tyrosine to octopamine. Tyrosine is decarboxylated by tyrosine decarboxylase (TDC), forming tyramine. Tyramine is then hydroxylated using tyramine β-hydroxylase (TβH). Image taken from Cole et al, 2005 [8].

My work focusses on the neuromodulatory type-II synapses, which in contrast to the heavily researched type-I boutons, are smaller in size. Type-I endings have relatively large boutons with a diameter of around 3 µm to 4 µm, while type-II endings consist of characteristically long, trailing filaments with small boutons (around 1 to 2 µm) [137]. Initially, TA was thought to be just an intermediate product of OA synthesis from tyrosine. The discovery of a TA receptor in *Drosophila melanogaster*'s genome suggested the role of a signalling molecule for this biogenic amine [138, 139]. A hypomorphic TA receptor mutant, *honoka* [136] and *Tdc2^{RO54}* (a mutation of the rate-

limiting tyrosine decarboxylase enzyme in the OA biosynthesis; resulting in the lack of OA and TA) [8], supported these suggestions. OA exhibits excitatory effects on muscle contraction, while TA reduces muscle contraction due to inhibitory effects on evoked excitatory junction potentials (EJP) on body wall muscles. A complete lack of inhibition of evoked EJPs was observed in *honoka* mutants [136], further supporting the idea of OA and TA having contrary effects at body wall muscles. Additional studies showed that TβH (Tyramine β-Hydroxylase mutants; mutants are not able to convert TA into OA) mutant larvae showed an increase in TA and decrease of OA, while also exhibiting reduced larval forward locomotion due to more frequent directional changes of greater than 20° than in wildtype larvae and also increased pause episodes [132, 140]. These locomotion phenotypes could partially be rescued by octopamine feeding. Supplying these mutant larvae with yohimbine, an agent inhibiting TA receptors, also showed a partial rescue. Feeding the mutant larvae OA and yohimbine showed an even greater rescue effect, while feeding TβH mutant larvae with additional TA lead to an even severe impaired forward locomotion phenotype [132]. These results support the assumption of OA and TA having oppositional effects on larval locomotion. A very recent study from Natalie Schützer et al in 2019, shows supporting evidence of the enhancing effects that OA has on larval locomotion when in a nutrient-deprived state, whereas TA reduces locomotion when they are satiated [1, 141]. Starvation of 2 hours resulted in a significant increase in total crawling distance and mean crawling speed, while feeding the larva with TA significantly decreased crawling distance and speed [141]. They also showed indication that TDC2 positive neurons are also in contact with motor neuron (MN) dendrites and that TA decreases MN excitability. Noteworthy is also, that TβH mutant adults do not show any phenotypes in locomotion, while mutant flies lacking both, OA, and TA, showcase a defective locomotion phenotype [8, 142-145]. OA is mainly synthesized in unpaired median (UM) neurons in insects. The bilaterally symmetrical axons of those neurons have their cell bodies located either ventrally (VUM) or dorsally (DUM) in the suboesophageal ganglion (SOG) and the VNC [146-149]. DUM/VUM neurons can further be divided into subpopulations which are differently recruited in different motor behaviour, e.g. jumping, walking, flying, or crawling [131, 150-155]. These octopaminergic/tyraminergic (OA/TA) neurons also have metabolic functions, as they are involved in glycolysis regulation (only at increasing glycolysis) [156]. During flight these neurons are switched off [152, 156], while shortly before flight, OA release may prepare the flight muscles for the high

25

energy consumption and therefore high glycolytic rates during take-off [131]. OA is also an important modulator in the CNS for e.g. activating the central pattern generator (CPG) for flight [157-159] and further non-flight muscle motor neurons that are
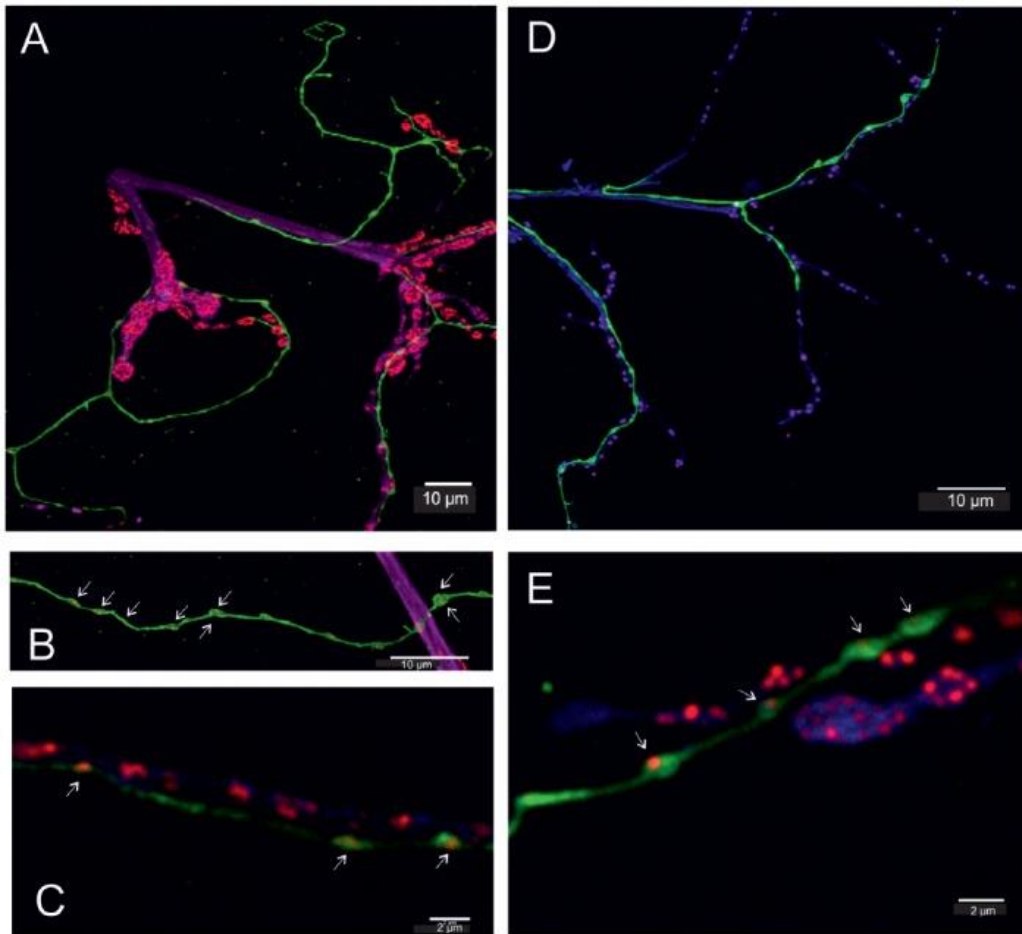
Figure 9: Images of transgenic Drosophila melanogaster (TDC2-Gal4 > UAS-CD8-GFP, green) larva (A-C) and adult (D,E).

An additional anti-horseradish peroxidase (HRP) labelling (magenta) was used to visualize motor axons of body wall muscles, Nc82 to stain for BRP^{C-term} (red) and GFP for octopaminergic/tyraminergic axons (green). **(A)** The GFP-labelled octopaminergic/tyraminergic neurons show one or two BRP-labels in each bouton (varicosities in B) and C), white arrows). **(B)** Magnification of an OA/TA fibre with BRP-labels in each bouton. **(C)** BRP labels are also observed in motor axons. **(D, E)** Adult DLM flight muscles images, with anti-HRP in magenta visualizing axon motors, showing the relationship between green-labelled VUM-neurons and red-labelled active zones. Structural differences of adult and larval NMJ are particularly well observed in E). Scale bars: (A,B,D): 10 μm, (C,E): 2 μm. Image and caption taken and modified from Stocker et al., 2018 [17].

involved in flying to the flight rhythm [134]. Flies with an OA deficiency exhibit severe flight performance defects with less flight duration compared to control flies [133]. OA

and TA positive neurons in *Drosophila* in the VNC extend to the periphery in larva [149], where they innervate the majority of muscles with exception of muscle 6, 7 and 28 [160]. The axonal extension of those DUM/VUM neurons show characteristic structures along the muscles they innervate. These octopaminergic neurons form "beaded fibre" structures, which are varicosities along the axon containing type-II terminals (first described in locust by Platonikova [161] and later studied in more detail by Hoyle [162] and reviewed by Bräunig and Pflüger [163]. The dendritic processes of all DUM/VUM-neurons are labelled by TA and OA antibodies [164] and also BRP (BRP^{NC82}) [17].
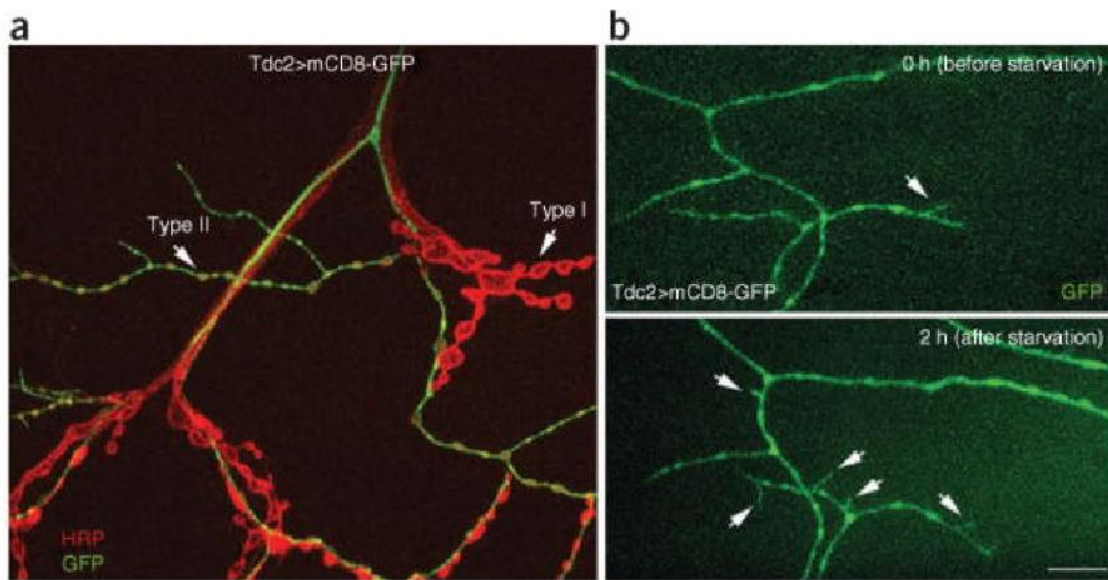
Figure 10: Images of the NMJs at muscle 12 and 13 of a third-instar larva expressing mCD8-GFP in OA/TA neurons.

(a) The Type I and type II endings are indicated with white arrows and their corresponding labels and were stained for anti-GFP (green) and anti-HRP (red). **()** Live imaging of OA/TA neurons through cuticle of intact larva before and after 2 hours of starvation. White arrows point at synaptopods. Imaged taken and modified from Koon et al, 2011 [1].

The octopaminergic system was found to be linked to hunger and stress as well [164, 165]. *Drosophila* wild type larvae's neurons with type II terminals showed the formation of additional synaptopods, which are described as filipodia-like extensions, after food-deprivation, that could extend and retract in a matter of few minutes [1]. Synaptopods that are present or formed prior starvation are also labelled as "natural synaptopods", while upon starvation the number of synaptopods was significantly increased [1]. Similar, results were found in Stocker et al from 2018, where after 2 hours of starvation,

a decrease in synaptopods was observed and only after 6 hours a significant increase in synaptopods was observed (Figure 10) [17].

Interestingly, when eliminating OA neurons by expressing head involution defective protein (hid; a cell-death protein) a drastic decrease in locomotion speed and starvation behaviour was the result. Similar results can be observed when testing OA mutants (tbh^{nM18} and tdc2^{R054}), indicating that the increased locomotor speed due to starvation leads to structural changes in type II endings [1]. Furthermore, eliminating OA in *tbh*-null mutants decreased the number of natural synaptopods significantly and bathing wild-type preparations for 15 minutes in OA lead to a dose-dependent increase in synaptopods, while tyramine did not exhibit any effects [1]. These findings showcase a certain degree of plasticity that octopaminergic/tyraminergic neurons possess.

1.5.3 Octopamine and Tyramine in invertebrates and the difference of type I and type II terminals
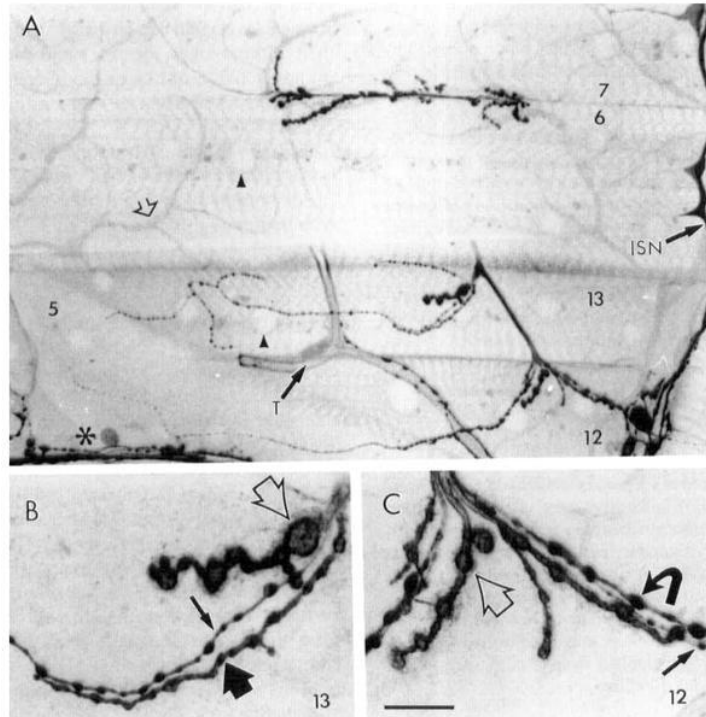
Figure 11: Confocal images of muscles 6,7, 12 and 13 in A3.

(A) Overview of innervation of all 4 muscles stained with anti-HRP. Arrowheads indicate numerous nuclei, open arrows tracheoles and the asterisk the innervation to muscle 5 and 8. T: large Trachea. **(B)** Zoom of branch point at muscle 13 showing different bouton types. Open arrow: Type Ib, thin arrow: Type II, wide arrow: Type Is. **(C)** Zoom of branch point at muscle 12. Curved arrow: Type III. Anterior is on the right. Scale bar: 40 µm in A), 10 µm in B) and C). Image and caption taken and slightly modified from Budnik et al. 2015 [14].

Octopamine is a biogenic amine first discovered in the salivary glands of *Octopus vulgaris* [166] and is a structural analogue of vertebrate norepinephrine in invertebrates. It has a variety of effects as described before and is synthesized from L-tyrosine in a two-step de novo pathway. Tyramine is the result of the decarboxylation of tyrosine by tyrosine decarboxylase. After the decarboxylation, a hydroxylation reaction takes place with the help of the rate-limiting enzyme tyramine β-hydroxylase, which product is then Octopamine (Figure 8) [167]. The most prominent and best characterized octopaminergic/tyraminergic neurons are the DUM/VUM neurons, which extend from the CNS to the periphery in *Drosophila* and innervate the majority of the muscles [149]. These neuronal endings are type II terminals, that differ from the common and better characterized type I terminal morphology. They are smaller (1-2

µm) than type I terminals (3 - 5 µm) and use different neurotransmitters. Type I terminal neurons use glutamate [168], while type II use Octopamine [115]. Ultrastructurally, both terminals also show differences: Type I terminals show in electron microscopic images an electron-dense structure, also known as T-bar at the AZ and a plethora of clear and round vesicles with a diameter of around 40-50 nm [10], while type II neuronal terminals show an absence of an electron-dense structure and contain only clear elliptical (around 33 nm) and dense core vesicles (DCV) of around 100 - 150 nm in diameter, filled with OA (Figure 12) [17, 169]. Figure 12C also shows the exocytosis of such DCV via OA immuno-gold labels, supporting the hypothesis that OA is acting as a neurotransmitter in type II terminals. Aside from these ultrastructural differences, some AZ proteins have been found in both type of terminals, such as BRP [17], synaptotagmin and synapsin [170], indicating a common release machinery in both neuron types. The presence of synaptotagmin and synapsin in type II terminals may also suggest the existence of different SV pools such as the reserve and release pool in those neurons. Additionally, it has been reported, that around 70% of the OA neurons in the adult nervous system of *Drosophila melanogaster* express dVGLUT, indicating the capability of dual transmission [171].

OA/TA neurons also exhibit very dynamic features. Upon environmental change, they can be adaptively altered. After a starvation time of around 2 hours synaptopods formation takes place and type II terminal boutons undergo morphological changes (Figure 10) according to Koon et al [1], while Stocker et al. [17] showed an initial decrease in synaptopod numbers in the first 2 hours, but a significant increase after 6 hours of starvation. It was mentioned that this difference could have been due to the different ages of the used animals. During synaptopod formation, Fascillin II (FasII) has been shown to be present in all synaptopods at all stages [1]. FasII is a 95 kDa cell membrane glycoprotein that is expressed in a subset of neuronal tracts and other nervous system pathways, as well as in axons and growth cones of other axonal tracts [172-175]. It acts as an adhesion-competent membrane protein and helps mediating neuronal migration as well as axonal guiding [172, 173, 176, 177]. Other proteins involved in synaptopod formation were synaptotagmin 1, TβH, BRP and Futsch. Synaptotagmin 1 was present only 40% of the times, albeit it being always present during the onset of varicosity formation. TβH, indicating the onset of octopamine synthesis, was never observed before the start of the new varicosity formation, but

was observed to be present in every matured synaptopod. BRP was present in 27% of the synaptopods, after TβH expression. Futsch, a MAP1B-related (microtubule-associated protein) protein, which is necessary for axonal growth and dendritic morphology [178], was observed in synaptopods, only after the formation of a secondary varicosity [1]. These results indicate the presence of AZ proteins of type I terminal AZ proteins in type II terminals. Furthermore, they also have shown the importance of OA in this process by eliminating OA in *tbh*-null mutants, which resulted in a significant decrease in natural synaptopods numbers. They also showed a significant increase in synaptopods by bathing wild-type preparations in octopamine. The increase in synaptopod numbers showed a dependence on OA concentration, while tyramine bath application did not show any effects. The induction of synaptopod also required normal Ca^{2+} levels (1.5 mM) [1]. When impairing activity in octopaminergic neurons, type II innervation at body wall muscles did not happen [1]. Through further experimentations, it was shown that the cAMP pathway and synaptopod formation were downstream of OA, as *dnc*^{M14} (dunce) and *rut*^{2080} (rutabaga) mutant showed a decrease in natural synaptopod numbers, which could not be rescued by the octopamine application. Additionally, expressing a dCREB dominant-negative transgene (CREBdn/dCREB2-b) also lead to a decrease in natural synaptopod numbers, suggesting that the formation of type II synapses requires CREB-mediated transcription activated by cAMP cascades [1]. Furthermore, TDC2 positive neurons have suggested to be in contact with larval crawling motoneurons, as TDC2 neurons show overlapping regions and presynaptic BRP labelling with those motoneurons [141].
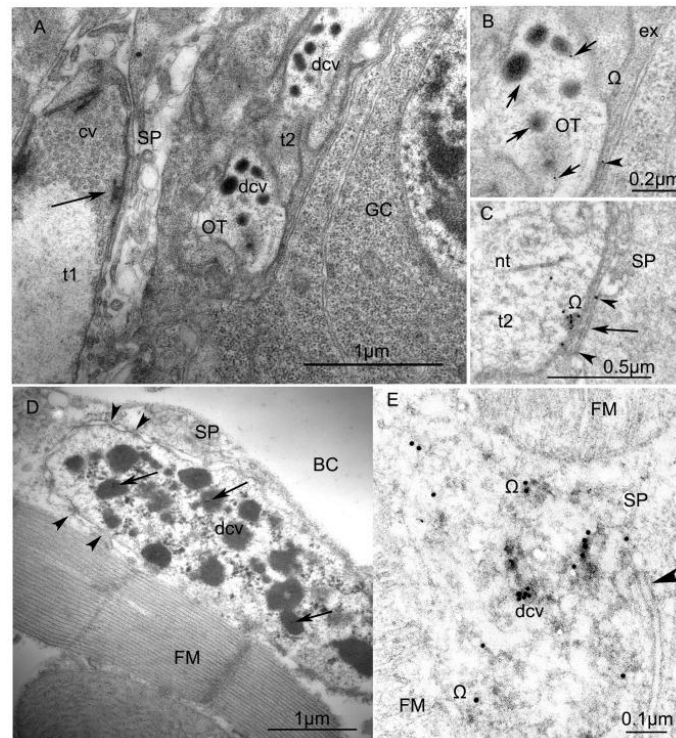
Figure 12: Ultrastructure of VUM neuron terminals in *Drosophila melanogaster* larva.

(A, B) and adult flies **(C, D)**. **(A)** Two terminals (type I and type II) at the larval body-wall muscle. The type I terminal (t1) contains an electron-dense structure (the black arrow) and clear vesicles (cv), indicating the AZ, and meets the sarcoplasmatic processes (SP). The other is an octopaminergic type II (t2) terminal (OT), which contains only dense core vesicles (DCV) with anti-octopamine Immuno-Gold labels. It's surrounded by a glial cell (GC). Scale = 1 µm. **(B)** Magnification of part of the type II terminal in (A). Black arrows point at immunogold labels. Abbreviations: ex = extracellular matrix, Ω = omega-profile on membrane release-site. **(C)** DCV in the middle of exocytosis indicated by the accumulation of immune-gold labels in the DCV and synaptic cleft (arrowheads). **(D)** An octopaminergic type II axon terminal at the dorsal longitudinal flight muscle (DLFM) of an adult Drosophila fly, labelled with 12 nm Immuno-gold particles (arrows). The axon terminals contain many dcv. Other abbreviation: BC = body cavity. Scale = 1 µm. **(E)** Higher magnification of anti-OT-immunogold labelling in DCV and release site (arrowhead). Scale = 1 µm. Image and text taken and modified from Stocker et al, 2018 [17].

1.5.4 How do Octopamine and Tyramine act on the synapse and what is known of octopamine receptors?

Octopamine is a biogenic amine and is responsible for a variety of biological functions as mentioned earlier. The amine was first discovered in the salivary glands of *Octopus vulgaris* by Erspamer and Boretti in 1951 [166] and 20 years after its discovery, Nathanson and Greengard in 1973 [179], found evidence of a biological relevance of

OA. It can act as a neurohormone, but also as a neuromodulator and has roles in learning and memory processes in *Drosophila melanogaster* and *Apis mellifera* [180, 181]. Insect OA receptors are G-protein coupled receptors that affect intracellular cyclic AMP concentrations or generate intracellular calcium signals [116, 182]. The initial classification of OA receptors were suggested by Evans in 1981 [183] via a pharmacological characterization in locust. Receptors were distinguished into Octopamine$_1$ class receptors, mediating the reduction in myogenic rhythm speed via an increase in intracellular calcium level [184] and Octopamine$_2$ class receptors, responsible for mediating the OA modulation of neuromuscular transmission mediated by slow motor neurons. This class receptor can be further divided into two subcategories: Octopamine$_{2A}$ and Octopamine$_{2B}$. The first subcategory is presynaptically mediating an increase in NT release, while the latter is located postsynaptically and involved in the increase of relaxation rate of tension of the muscle. Subsequently, it was discovered that both subcategories mediate their actions by increasing the levels of cyclic AMP [185, 186]. Later on, Evans and Maqueira in 2005 [187] suggested, that a solely pharmacological approach in characterization of receptor types might not be sufficient and requires further molecular and genetical investigation [187]. The first potential octopamine receptor cloned from *Drosophila* (Oct-TyrR; CG7485) initially experienced a more potent receptor stimulation through tyramine than octopamine, suggesting it to be a tyraminergic receptor rather than an octopaminergic one [118, 139, 188]. Further investigations revealed the "agonist-specific coupling" or "agonist trafficking" nature of this receptor [189], showing the induction of different conformation changes upon docking of different agonists onto the receptor, which can result in a differential coupling to a different second messenger system [190, 191]. This receptor was revealed to be a dual OA/TA receptor, capable of binding to both amine depending on neuromodulatory or neuronal input it receives [192]. The receptor preferably bound with tyramine to inhibit adenylyl cyclase, while OA coupling resulted in an induction of calcium signal.

The first OA receptor cloned in *Drosophila* that preferred OA over TA was the OA receptor OAMB from the mushroom bodies (CG3856) [193]. The mushroom bodies (MB) are considered to be essential for a plethora of learning and memory tasks in insects [194]. It was additionally shown, that OA stimulates adenylyl cyclase activity in fly head homogenates [195] which suggested OAMB to be associated with important

33

neural functions such as synaptic modulation and other behavioural plasticity [193, 196]. Contrary to these assumptions, Balfanz et al [197] suggested the function of OAMB receptor to be mediated via elevation of intracellular calcium, rather than increase in cAMP levels. This would classify OAMB as an Octopamine$_1$ rather than an Octopamine$_2$ receptor and would question its major role in octopaminergic modulation in insect learning and memory. However, it was demonstrated that OAMB not only expresses in *Drosophila* brain, but also in other tissues such as abdominal and thoracic ganglia, as well as in oviducts and other parts of the reproductive system and was also expressed as two different transcripts: OAMB-K3 and OAMB-AS by alternative splicing of the last exon [196]. These isoforms were shown to be present in all tissues that express the gene.

Later on, Evans and Maqueira [187] proposed a new classification of octopaminergic receptors in insects in 2005. They suggested a distinction between β-adrenergic-like octopamine receptor (OctβR) and an α-adrenergic-like octopamine receptor (OctαRs). The first mentioned group, that includes several OA receptors such as DmOctβ1R (CG6919), DmOctβ2R (CG6989) and DmOctβ3R (CG7078), show structural and signalling similarities, but also the highest phylogenetic homologies to β-adrenergic receptors in vertebrates [187]. These receptors are closely related to the β-adrenergic receptors in vertebrates and subsequently show similar responsiveness to adrenaline and noradrenaline and their capability to selectively activate adenylyl cyclase. The second group of OA receptors, OctαRs, show closer similarities to the α-adrenergic receptors in vertebrates, and are pharmacologically similar as well. Similarly, they act upon increasing the intracellular calcium levels [193]. Additionally, a third group, octopamine/tyramine group of receptors was suggested, that includes the dual OA/TA receptor OAR Drome (Oct-TyrR; CG7485) [138]. This group is structurally and pharmacologically more similar to α-adrenergic receptors, even though it still remains elusive, whether this group of receptors can be categorized as OA receptors, since they could also just be a type of tyramine receptor due to their preference in binding to TA [118, 188].

To summarize, OA receptors are distinguishable via their mode of actions: OctαRs, which were initially categorized as Octopamine$_2$ receptors, act through activation of adenylyl cyclase and one of the representative receptors is OAMB (*Drosophila* mushroom body receptor). They are structurally and pharmacologically like α-

adrenergic receptors in vertebrates. OctβRs were initially known as Octopamine$_1$ receptors and act upon increasing of cyclic AMP levels and show homologies to vertebrate β-adrenergic receptors. DmOctβ1R (CG6919), DmOctβ2R (CG6989) and DmOctβ3R (CG7078) are known OctβRs. The third group, the octopamine/tyramine group of receptors such as Oct-TyrR (CG7485), is structurally and pharmacologically more like α-adrenergic receptors, but preferably binds to tyramine over octopamine, suggesting it to be more of a tyraminergic receptor, rather than an octopaminergic one.

Tyramine, identical to Octopamine, is also a monoamine and synthesized from the same amino acid: Tyrosine. It's a precursor product in the biosynthesis pathway of OA and is the result of decarboxylation of tyrosine via TDC [198]. There also may be a salvage pathway that does not require TDC to produce TA. Theoretically, Tyrosine can be hydroxylated into 3,4-dihydroxyphenylalanine through tyrosine hydroxylase (TH) pathway and further transformed to dopamine via 3,4 dihydroxyphenylalanine-decarboxylase. Dopamine can then be used to produce TA via the dopamine dehydroxylase pathway. The biological importance of this round-about TA synthesis pathway remains unclear. TA can be released as a standard neurotransmitter into a synaptic cleft, as a local modulator over a tissue or as a neurohormone [199] and all major neuropils of brains and ganglia are densely supplied by OA/TA fibres [146, 200]. The whole interaction of all actors (TA, OA, TA-receptors, OA-receptors, OA/TA-receptors) has yet to be completely understood. Three different tyramine receptors (TyrR) are known in *Drosophila melanogaster*: TyrR, TyrRII and TyrRIII. While the first receptor was found early on in 1990 by Saudou et al. [139], the latter two were found later in 2005 by Cazzamali et al. [201] and their signalling properties partly characterized by Bayliss et al in 2013 [202]. The receptor cloned by Cazzamali et al. in 2005 [201] is defined as a fully tyramine specific receptor, since it doesn't exhibit any cross-reactivity to tryptamine, OA, DOPA, dopamine, β-phenylethylamine, noradrenaline, histamine, adrenaline or serotonin up to 100 μM in Chinese hamster ovary (CHO) [201]. Unlike octopamine receptors, tyramine receptors have not been extensively studied yet. One of the first works were from Sadou et al. in 1990, where they found out, that tyramine results into dose-dependent reduction of forskolin-stimulated cAMP levels. This cAMP reduction caused by tyramine can be antagonized by yohimbine, a pharmacological agent which is an α$_2$-adrenergic receptor antagonist and has a high affinity to tyramine receptors [139]. Although TA has not been

characterized as well as OA, previous works of Arakawa et al. [138] and Robb et al. [189] showed that the dual OA/TA receptor is capable of inhibiting adenylyl cyclase activity, but also in elevating intracellular calcium levels by utilizing different G-protein coupled pathways. It's been speculated, that TA and OA are coupled to different second messenger system utilizing the same receptor and the classification of tyramine and octopamine receptor has been questioned due to property of these receptors being able to bind to either monoamine, albeit with different potency and preference [203].

The research in both monoamines and their molecular effects in organisms has seen progress, but many questions remain. My thesis questions the molecular mechanisms of the aminergic release at type II synaptic terminals and what happens to them during metamorphosis. Previous works show that TA and OA act via DUM/VUM neurons and affect larval locomotion in response to hunger and stress, but also has effects on the adult animal. Therefore, I will now start to elaborate the process of metabolism and will focus on the development of the NMJ and what happens to the neurons during metamorphosis.

1.6 Development of *Drosophila melanogaster* larva into an adult

1.6.1 Development and plasticity of *Drosophila melanogaster* NMJ

In my thesis I focus on the larval NMJ, the progression of them during metamorphosis and the indirect flight muscles (IFM) in adult flies. The development starts with embryogenesis after the egg has been laid. At 25° C the embryogenesis takes around 20 to 22 hours for the first-instar larva to emerge and during the first 10 hours of embryogenesis segregation of neuroblasts from the neuroectoderm takes place and differentiate and divide neurons and glial cells [204]. 10 hours after egg laying (AEL) the axons of postmitotic motor neurons extend along cell-specific paths and during the 3 next hours they leave the CNS and extend towards targets along the body wall through the still developing muscle fields [205]. They innervate ventral muscles first, as they are the first they come in contact with and continue with dorsal muscles, therefore synaptogenesis of NMJs develop in a "wave"-like manner from ventral to dorsal muscles [206]. During the wave-like extension of axons, finding the correct innervation target is secured through specific molecular cues (such as TOLL, fasciclin III and others [207, 208]) which are integrated by intracellular signalling processes within the growth cone, that then responds positive or negative, depending on the

desired or inappropriate target [206]. There are three pathways the motor axons take when leaving the CNS to find their muscle targets: The segmental (SN) and intersegmental (ISN) nerve roots and the transverse nerve. SN and ISN further split into five separate nerve pathways in the periphery: SNa (innervating lateral muscles), SNc (innervating ventral muscles), ISN (innervating dorsal muscles), ISNb (innervating ventrolateral muscles) and ISNd (innervating other ventral muscles). The pathways the motor axons take to their muscle fibre targets are genetically predetermined [100].

In *Drosophila melanogaster* embryo and larvae muscles are formed through the fusion of myoblasts [209]. While the initial growth cone comes in contact with the muscles, they already finished fusing, but are typically connected to neighbouring muscles via cytoplasmatic bridges and also have thin patchy basal laminae [210]. During that period, voltage-gated calcium currents and then different types of potassium currents appear and signal a quick development of the muscles' electrical membrane properties [211]. Cell surface adhesion markers such as FasIII III are located in the postsynapse for the innervation process and are also present in neural muscles indicating that muscles are responsible for defining the site of innervation [212]. The absence of FasIII does not hinder NMJ formation, nor does it restrict functional NMJs [213, 214], but affected animals only showed a slight impairment in target recognition. This also supports the idea that multiple redundant recognition cues are responsible for direction of the first steps of synaptogenesis. Meanwhile, ahead of muscle innervation, glutamate receptors are distributed, but fail to localize without neural induction [212]. Upon arrival of the growth cone at the intended target, the cone enlarges and forms boutons [210]. The number of presynaptic structures appears to not be influenced by postsynaptic compartments [215] and NMJs can form morphologically, and most likely also functionally, normal even with the absence of myoblast fusion. AZ localization still requires postsynaptic interplay and close apposition of pre- and postsynaptic membranes [215, 216]. During embryogenesis an immature, but already functional NMJ can be formed within an hour of growth cone contact with the muscle, but continues to mature throughout hatching and larval stages [205]. Around 20h AEL at 25°C, the first instar larva emerges from the embryo and starts its life cycle as described in Figure 5. During larval development, the presynaptic bouton is engulfed by an infolded membranous structure known as the "subsynaptic reticulum" that

contains neurotransmitter receptors, scaffolding proteins, and postsynaptic signalling complexes [97, 169, 206, 217]. The major changes in the presynapse during larval development is the result of elaboration of nerve terminal branches and the increase in boutons and subsequently active release sites and AZs [218].

Aside from the NMJs as target region for research in my thesis, IFM are also a target of interest for my thesis, as OA and TA are also known to play a part in the CPG in flight in *Drosophila melanogaster*. The IFMs are a major organ in the thorax of an adult fly and contribute to the functionality of powering wing strokes during flight behaviour [219, 220]. These muscles consist of dorsal longitudinal flight muscles (DLM) and dorsoventral flight muscles (DVM). During pupation, muscle histolysis and major reorganisation of organs take place, meaning that almost all the existing larval muscles and their innervation disappear and must reorganize themselves while the larva transforms into its adult form. The histolysis of muscles that takes place during the pupal stages occur in waves. The first wave eliminates the majority of head and thoracic segment muscles, while sparing most abdominal muscles and dilatory muscles of the pharynx or the larval oblique muscles (LOM; consisting of 3 pairs of dorsal thoracic muscles) which later on are remodelled to form DLMs in the adult [221-223]. Three of those LOMs are not part of the histolysis process and remain unscathed during pupation. 6 hours after puparium formation (APF), only 3 LOMs (muscles 9, 10 and 19') are still present and appear to be intact and remain birefringent while myoblast start to migrate towards the templates [224]. 8h APF those LOMs show vacuoles and a significantly reduced birefringence when observed under polarized light. At 10h APF, LOMs exhibit high vacuolation and distorted shape appearance and 2 hours after, they elongate while the vacuoles are less visible [224]. The LOMs lose their sarcomeric organization, but their plasma membrane does not undergo phagocytosis and therefore remain intact. As they proceed with elongation, ultimately, they end up splitting into 6 template IFMs around 14h APF. Interestingly, the most dorsal LOM retains its vacuolation, where the other two lose them before splitting and also splits 16h APF instead of 14h APF [224]. At 20 hours APF, the splitting of the LOMs has completed and the result are 6 template DLMs in each hemisegment. Contrary to the DLMs which develop from existing LOMs, DVMs develop de novo from the fusion of myoblasts at the same time as DLM development. For DLMs, myoblasts migrate towards the three LOMs that consist of *Dumbfounded* (*Duf*) – expressing cells and

form the developing fibre, while for DVMs *Duf*-expressing myoblast fuse with nearby myoblasts and form a primary fibre that continues to incorporate myoblasts. Myoblast fusion continues throughout the first quarter of metamorphosis. After the fusion events end, the developing fibre transitions into myofibrillogenesis which result into the development of nascent myotubes into myofibers. Those myofibers consist of myofibrils which in turn consist of sarcomeres that are formed by actin and myosin filaments [225].

1.6.2 Innervation of the DLM during pupal stages

6 hours APF, most larval muscles have been histolyzed, aside from muscles 9, 10 and 19' [224] which in result obviously means a regression of innervation at the NMJ. At this time point, type I and type II boutons can still be observed at the still present muscles [226]. Around 8 hours APF, muscle 10 and 19' are devoid of type I innervations, while type II remain. After 2 further hours, type I boutons are nowhere to be seen, while type II endings are still visible until 12h APF. Between 10 and 12 hours APF the innervation shows rapid changes, possibly due to the begin of adult innervation and at 12h APF, when the muscles transformed into pretemplates, neurite outgrowth happens and branches of ISN are visible over each pretemplate. During this phase and even after, some faulty contacts and retraction of those can take place. In contrary to the DLM, the branches to the pretemplates located at the most ventral side and the developing DVM III are not as visible and the ones that can be observed have fine processes, even along the nerve trunk [226]. At 16 hours APF, each branch that gravitates toward the splitting muscle templates derived from muscle 10 and 19' consists of two components, that most likely are the axons and two different neurons that are extending to innervate the developing DLM template. The two components separate by 18 hours APF and each of them innervate one DLM template by 20 hours APF. The ISN branches to the dorsal most pretemplates do not show different components and subsequently the two most dorsal DLM fibres are innervated by a single contralateral neuron, motor neuron 5 [226, 227]. The innervation pattern at 20 hours APF is very similar to the adult innervation [228]. The muscles elongate until around 36 hours APF and after around 100 hours the adult fly emerges.

1.6.3 Innervation of the DVM during pupal stages

The DVM bundles are subdivided into DVM I with 3, DVM II with 2 and DVM III with 2 fibres. DVM I and DVM II develop in a lateral position, while DVM III is the shortest

bundle of the three and is located below the developing DLMs [223, 226, 229]. Between DVM I and DVM II is the jump muscle (tergal depressor of the trochanter, TDT). Unlike the innervation at DLMs, DVMs form de novo during metamorphosis and therefore there is no known prior innervation present for future DVMs, since the histolysis wave dissolves the preexisting larval muscles at the DVM development sites. Although there are no visible signs for DVM development at 10 hours APF, some signs can be observed such as short branching of the ISN and the SN in the region, but also myoblast segregation into clusters [226]. At 12 hours APF, short branches of the ISN and SN at the DVM development site associate with the myoblast clusters and an outgrowth at the posterior of the ISN is extending towards the new developing DVM III. After 14 hours of puparium formation the segregation between DVM I and DVM II is almost finished and at 18 hours APF two nerves exit the ventral ganglion one extending anteriorly towards the dorsal region innervating the TDT, DVM I and the other one with three distinct branches innervating DVM II and a direct muscle [226]. The innervation pattern at the current time point is most likely close to the adult innervation and barely changes in the next 6 hours, when the DLM innervation pattern is also at an adult-like state.

1.6.4 Innervation of abdominal muscles during metamorphosis

In the first 24 hours APF, most larval muscles are subjected to histolysis and therefore a major reconstruction of innervation is also necessary. During the time when muscles are histolyzed and nerves are retracted, a single major nerve trunk maintains the innervation of persisting muscles and remains in contact with the epidermis at four positions in each hemisegment (Figure 13) [16]. As metamorphosis progresses, adult innervation begins at three out of four of the nerve/epidermis contact points, where nerve growth is initiated and fine filopodial extensions are extending. The growth cones of the contact points of nerve/epidermis originate from larval cells, that are replaced by proliferating histoblasts, thus enabling the growth cone to continue its migration over to the adult epidermis. At around 26 hours APF, the growth cones follow an advancing front of histoblasts, and the dorsal growth cones emerge out on the epidermis while making short lateral projections on their way. At 36 hours APF the dorsal growth cone has migrated from its lateral position to the dorsal midline and at 48 hours APF only lateral projections remain that innervate adult muscles. While the dorsal growth cone follows ventrally migrating histoblast cells and extends a multitude

of short lateral projections along the way, the lateral innervation develops differently. The growth cone for lateral innervation extends fine, branching processes towards parallel muscles in its targeted regions in each segment and the axons will innervate
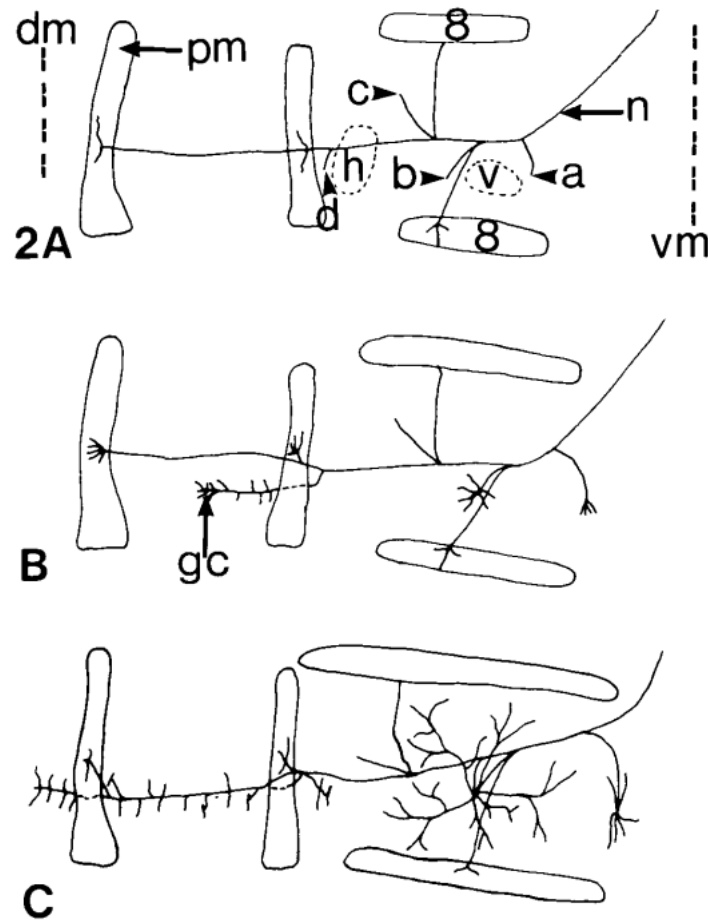
Figure 13: A diagrammatic representation of a hemisegment of the pupal abdomen and the position and migration of nerves.

(A) shows the innervation 10h APF, **(B)** 30h APF and **(C)** 90h APF. Abbreviations: vm = ventral midline; dm = dorsal midline; n = nerve; pm = persistent larval muscle; gc = growth cones from nerves; 8 = muscle no. 8 (pleural internal transverse); h = dorsal histoblast nest; v = ventral histoblast nest; a-d = Attachment points of nerves to the epidermis. Anterior is up. Image and description taken and slightly modified from Paper of D.A. Currie and M. Bate, 1991 [16].

the final adult ventral muscle that is located medioventrally [16].

1.6.5 Adult innervation of IFMs and abdominal muscles

The *Drosophila* thorax harbours 6 DLMs of which every is innervated by a total of five motoneurons. Every DLM aside from the two most dorsal located DLM are innervated

by 1 motoneuron each, the 2 exceptions are innervated by one motoneuron (MN5) [230]. DVM innervations are thought to stem from persistent larval neurons as they are still observed after histolysis of the larval muscles at DVM development sites, aside from DVM III where there are no such nerve endings visible. Therefore it is suggested that DVM III is innervated by motoneurons without prior larval target [226].

The abdominal muscles in adult flies are located at the abdominal segments 1 to 7 (A1-7), while the muscle pattern in terminal abdominal segment is more complicated due to the existence of genitalia and analia at those segments, A1 also shows a slightly different pattern [229]. In the other segments, A2 – A7, are groups of dorsal, lateral, and ventral muscles and a small muscle in each hemisegment that associates with the lateral spiracle. Every hemisegment consists of 17-22 dorsal parallel longitudinal fibres, 20 lateral dorsoventrally parallel fibres and 5-8 ventral fibres located ventrally to the midline [231]. During metamorphosis, a subset of body wall muscles withstands histolysis and survives until adulthood. The muscles that are located dorsally at the abdomen are labelled dorsal internal oblique muscles (DIOM). The amount of DIOMs per segment differs, the first and second have 3 pairs of DIOMs (DIOM 1,2 and 3), the third and fourth contains 2 pairs (DIOM 1 and 3) and the fifth has 1 pair (DIOM1) [232]. DIOMs were located basally beneath dorsal external oblique muscles (DEOMs), which were subjected to programmed cell death ahead of head eversion. These histolysis resistant larval DIOMs experience muscle atrophy around 0 to 50 h after head eversion followed by a hypertrophy between 50 h and 100 h after head eversion, transforming into temporary adult muscles and are subjected to degeneration within the first 24 hours of eclosion [233].

The abdominal muscles in the adult are innervated by at least five motoneurons which include two VUM neurons [234]. Each hemisegment in the abdominal part of the adult fly is innervated by a single major nerve trunk which forms extended short motor branches towards each DLM and form NMJs on each of them with one rostrad and one caudad primary branch and occasionally by secondary branches [235, 236].

Depending on age the branches show different length, and the distribution of boutons is also different. While younger flies (3 days after eclosion) show shorter branches, "mid adult" flies (around 15 days after eclosion) show significantly longer and slightly more branches and larger bouton sizes. At 30 days posteclosion, adult fly innervation

starts to decline, branch length shortens, and a slight tendency of branch thickness reduction were observed, while the number in branches remained around the same, albeit with increased bouton sizes. In old flies (60 days after eclosion), half the population survive and the still alive flies showed an increase in muscle size with signs
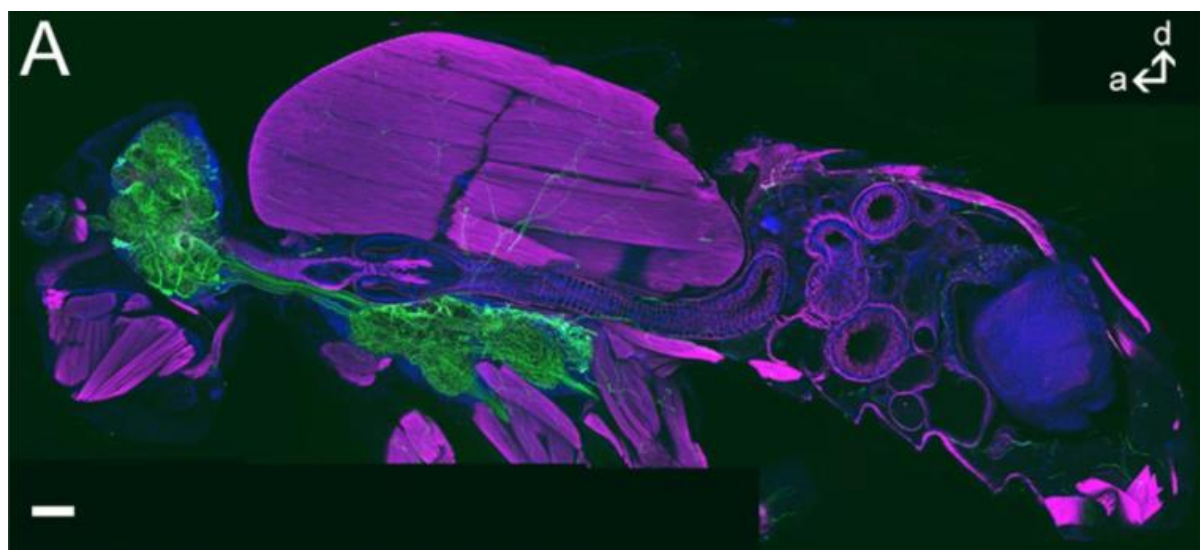
Figure 14: TDC2-Gal4 arborization in a whole fly section.

(A) shows the TDC2-Gal4 arborization in a whole fly section, visualizing the innervation of TDC2-positive neurons at the IFM. Green: TDC2 > 10xmyr::GFP; Magenta: Phalloidin, Fas2, BRP; Blue: DAPI. Scale bar: 50 µm. Image and caption taken and modified from D. Pauls et al. 2018 [3].

of degeneration such as defective mitochondria, autophagosomes and unnatural sarcomeric structures, albeit no significant alteration in its muscle numbers and other gross anatomical features and nuclei properties [236].

1.7 Aging

In the second part of my thesis, I was interested in the effects of aging in flies and its effects on mitochondrial transport and brain oxidation status in association with dietary spermidine supplementation as a continuation of my master's thesis.

1.7.1 Aging and the connection to oxidative stress and mitochondria and aerobic respiration

The process of aging is a mainly ununderstood process that has been researched extensively and is accompanied by changes in brain that adds to progressive cognitive decline. Previous studies have shown many hallmarks of aging such as "(1) mitochondrial dysfunction; (2) intracellular accumulation of oxidatively damages proteins, nucleic acids and lipids; (3) dysregulation of metabolism; (4) impairment of cellular waste disposal mechanisms such as autophagylysosomes and proteasome functionalities; (5) impairment of adaptive stress response signalling; (6) compromised DNA repair; (7) aberrant neuronal network activity; (8) dysregulation of neuronal Ca^{2+} handling; (9) stem cell exhaustion and (10) inflammation" [237, 238]. As these effects of aging have been observed, the process itself remains poorly understood and multiple theories have been proposed as an explanatory attempt [239-242]. One theory proposed by D. Harman in 1956 [243] is the "free radical theory of aging and radiation chemistry" and suggests the involvement of reactive oxygen species (ROS) in aging. This theory describes the possibility of an accumulation of oxidative stress through production of ROS during aerobic respiration which could be linked to aging and death [243]. Approximately 90% of ROS are produced in mitochondria during aerobic respiration that are capable of damaging cellular macromolecules such as DNA, lipids, and proteins [244, 245]. Aerobic respiration is a metabolic process that breaks down nutrients to produce energy for the cell and consists of three major reactions: Glycolysis, citric acid cycle and oxidative phosphorylation. The first step is the glycolysis which converts the nutrient molecules such as glucose into pyruvate which then is oxidized into acetyl-CoA by pyruvate dehydrogenase complex located in the cytoplasm and then enters the citric acid cycle inside the mitochondrial matrix. Acetyl-CoA serves as a point of entry for the citric acid cycle (also known as tricarboxylic acid cycle or Krebs cycle). Acetyl-CoA and oxalacetate are converted with the help of citrate synthase into citrate which in turn is further converted into isocitrate by aconitase and isocitrate is then oxidized into α-ketoglutarate which leads to a

reduction of NAD^+ into NADH. α-ketoglutarate, which derived from the hydrolysis of extracellular glutamine to glutamate through glutaminase I and II pathways, enters the citric acid cycle and is subjected to oxidative decarboxylation with NAD^+ and CoA-SH and forms succinyl-CoA, NADH, CO_2 and H^+. Succinyl-CoA is hydrolysed forming succinate, CoA-SH, and guanosine triphosphate (GTP, a form of energy) and succinate is then oxidized into fumarate by complex II/succinate dehydrogenase while converting FAD into $FADH_2$. Oxalacetate, NADH and H^+ are then products by the oxidation of L-malate which is the result of the hydration of fumarate by fumarase and marks the completion of the citric acid cycle [246-248]. The main products generated by the citric acid cycle are the electrons provided by NADH and $FADH_2$ that are used for the mitochondrial electron transport chain (ETC). The ETC consists of five protein complexes that are integrated into the mitochondrial inner membrane. NADH and $FADH_2$ donate a pair of electrons to Complex I and Complex II respectively. Through the transfer of electrons from Complex I to the Q cycle, a net of 4 protons is acquired and pumped across the inner membrane into the intermembrane space of the mitochondria. Complex I or Complex II then donate 2 electrons to ubiquinone (Q) which in result is then reduced to ubiquinol (QH_2). Electron movement is generated by oxidization of ubiquinol by Complex III, resulting into the movement of a single electron at a time through cytochrome c. An electron transferred to cytochrome c translates into the pumping of 2 protons in form of H^+ into the intramembrane space, resulting into 4 H^+ being pumped into the intramembrane space for every electron pair moving through the cycle. Electrons are then transported to Complex IV by cytochrome c where oxygen acts as a terminal electron acceptor and is reduced to water. Reducing oxygen (O_2) into water (H_2O) would lead to the pumping of 4 protons into the intramembrane space, but due to 2 protons being consumed during the process, a total of 2 H^+ protons are pumped at Complex IV. This interplay of electron transportation results into the movement of protons from the mitochondrial matrix into the intermembrane space which subsequently creates a protonmotive force, resulting into the re-entry of H^+ back into the matrix through Complex V which is coupled to the adenosine triphosphate (ATP) production from adenosine diphosphate (ADP) [247, 248]. It is still unclear where exactly ROS is generated in these processes, but it was hypothesized, that any disturbance in the oxidative phosphorylation process might lead to increased ROS production [249]. Furthermore, recent studies have shown that ROS could also act as important secondary messengers mediating intracellular pathways [250-252], but this

is heavily dependent on the amount of ROS generation. Production of a large amount of ROS leads to lipid peroxidation, DNA damage, protein oxidation, irreversible impairment of mitochondria, insufficient ATP generation and then ultimately also cell death [248, 253].

1.7.2 Mitochondria, ROS, oxidative stress, and glutathione

Mitochondria are double-membrane-bound organelles compromised of two separate functionally distinct outer membrane and inner membranes that encapsulates the intermembrane space and the matrix compartments and contain a circular genome also known as mitochondrial DNA (mtDNA) and are essential for energy production and calcium homeostasis in most eukaryotic cells [249, 254, 255]. The origin of mitochondria is thought to originate one to two billion years ago and arose from the incorporation of an alpha-proteobacterium by a eukaryotic progenitor, leading to a mutualistic relationship [254, 256, 257]. The mitochondria, also widely known as the "powerhouse of the cell" [258], is best known as an important organelle producing ATP via oxidative phosphorylation for the cell, but its functions are not limited to only energy production. Multiple studies have demonstrated that mitochondrial ROS also affect homeostatic signalling pathways and act as secondary messenger [250, 251, 259, 260]. In larger amounts, ROS can have detrimental effects, making maintaining mitochondrial integrity an essential task for the cell. It has been shown that mitochondrial quality declines with age and results into an altered morphology, damaged mtDNA, and an increase in oxidants, despite a decrease in ATP production and that mitochondria and ROS accumulate in aging brains [261, 262]. ROS are O_2-derived free radicals e.g. superoxide anions (O_2^-), hydroxyl (HO), peroxyl (RO_2) and alkoxyl (RO) radicals, but also O_2 non-radical species such as hydrogen peroxide (H_2O_2) have been demonstrated to cause oxidative damage and can induce apoptosis [263, 264]. Around 1-2% of mitochondrial O_2 that's being consumed are diverted for ROS formation, mainly at Complex I and Complex III of the respiratory chain [265, 266]. The O_2^- derived from mitochondria is dismutated to H_2O_2 by manganese superoxide dismutase, and can generate the highly reactive HO via Fenton and/or Haber-Weiss reactions, when metal ions are present which can lead to significant damage to proteins, lipids and DNA [264]. To maintain physiological low levels of ROS, cellular redox systems are of importance. Cells have their own way to deal with adequate amount of ROS within the cells by utilizing so called "reduction-oxidation"

(redox) systems. Redox systems consist of redox couples that maintain intracellular redox environment and are not in equilibrium to each other, but appear to be kinetically controlled [267]. The redox couples are capable of exchanging electrons by either donating or accepting reduction equivalents and can represent as good cofactors in redox enzymatic reactions [268]. Initially, an imbalance of these redox couples were defined as oxidative stress [269], which has been updated by the author as more accurately: "An imbalance between oxidants and antioxidants in favour of oxidants, potentially leading to damage, is termed "oxidative stress"" [270]. To counteract oxidative stress, cells are using these redox couples to maintain a healthy intracellular redox environment. The relative amount of oxidized and reduced form of these redox couples are indicator of the cellular redox status, which can be shifted towards oxidized or reduced condition [268]. The most common three redox systems in cells are thioredoxin (TRX_{red}/TRX_{ox}), nicotinamide adenine dinucleotide phosphate ($NADPH/NADP^+$) and glutathione (GSH/GSSG) [268]. The GSH/GSSG concentration is about 500- to 1000-fold higher than TRX and NADPH and therefore appears to be more important than the other redox couples [271].

Glutathione is a well-recognized tripeptide and has been shown to play an important role in apoptotic signalling and previous studies have linked mitochondrial GSH loss to enhanced cytotoxicity [272]. Glutathione is present in different forms such as the reduced form (GSH) and two oxidized forms: glutathione disulphide (GSSG), but also as glutathione mixed disulfide with protein thiols (GS-R) [273]. Glutathione's functions are not only limited to being an intracellular redox buffer but can also act as a modulator for thiol-dependent enzyme activities or as a cofactor for antioxidant enzymes such as GSH-peroxidase [274-276]. In response to oxidative stress, it was shown that the GSH/GSSG ratio increases in favour of glutathione disulphide or by decreasing the amount of reduced glutathione [268]. Previous works have also shown the importance of GSH in programmed cell death and its massive extrusion through specific membrane translocator, which was coupled with the release of cytochrome c, upon an apoptotic stimulus [277-279]. Glutathione is synthesized in the cytosol and entails two ATP-dependent steps which are catalysed by glutamate-cysteine ligase (GSH1) and glutathione synthase (GSH2). Upon oxidative stress through toxic oxygen radicals such as superoxide anion ($O2^-$) and hydrogen peroxide (H_2O_2), the enzyme superoxide dismutase (SOD) converts $O2^-$ into H_2O_2 which is then reduced by GSH

with the selenium-dependent enzyme GSH peroxidase in the cytosol and mitochondria [12]. During this process, GSH is oxidized to GSSG which can then be reduced again with NADPH, thus resulting in a redox cycle (ability to oxidize and reduce back to both forms is a defining trait of a redox couple). Within the cell, it is also possible to deal with H_2O_2 by reducing it with catalase in peroxisomes, which is not present in mitochondria. This further emphasizes the importance of GSH/GSSG in mitochondria as a defence mechanism against oxidative stress (Figure 15). Furthermore, the cell is capable of actively exporting out GSSG under immense oxidative stress situations, forming mixed disulfides, which leads to the depletion of cellular GSH [12]. GSH also has been linked to modulation of certain cell responses as well as growth promotion and DNA synthesis modulation [280-285]. Additionally, GSH has also been connected to modulation of apoptosis, involving chromatin condensation and fragmentation, internucleosomal DNA cleavage and the other extreme cell death pathway necrosis [12, 286, 287]. These cell death pathways involve mitochondria and is modulated by GSH by regulation of redox state of proteins' thiol residues such as NFκB, stress kinases and caspases [286]. By modulating mitochondrial ROS content, GSH can influence cell death pathways and mitochondrial GSH depletion can lead to increased ROS levels leading to degradation of mitochondrial quality resulting into mitochondrial dysfunction as well as ATP depletion [286].
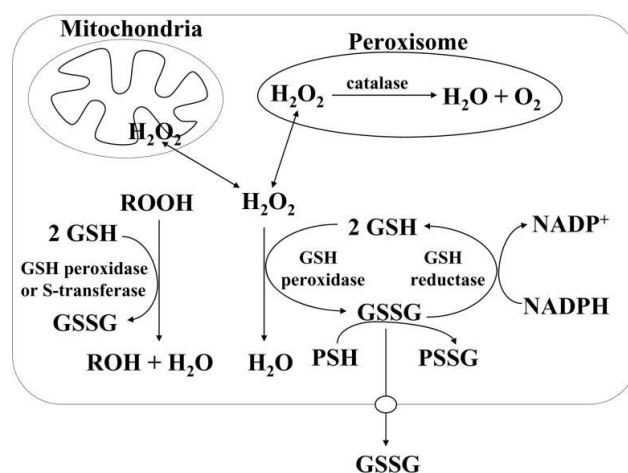
Figure 15: Antioxidant effects of GSH.

H_2O_2 production is the result of aerobic metabolism which can be broken down in the cytosol or mitochondria by GSH peroxidase, resulting into the oxidation of GSH into GSSG, or inside peroxisomes via catalase. The produced GSSG can be reduced back using GSSG reductase at the expense of NADPH, resulting in a redox cycle. To maintain the redox equilibrium of the redox couple, GSSG can be actively exported out of the cell or form mixed disulfides (PSSG) by reacting with protein sulfhydryl (PSH). Image taken and slightly modified from Lu, S.C., 2009 [12].

Knowing the importance of GSH in detoxification as well as maintaining intracellular redox equilibrium, we used the mito-roGFP2-Grx1 construct to measure the fluorescence ratio of mitochondrial GSH and GSSG in *Drosophila melanogaster* adult fly brains to measure oxidative stress.

1.7.3 Autophagy, spermidine and hypusination

The progressive decline in cognitive capabilities during aging is accompanied by the loss of mitochondrial quality with age [262]. For the cell to maintain its own integrity, autophagy is necessary. Autophagy is a cellular "self-cleaning mechanism" which can be classified in three different types, which depends on the pathway used to transport biomolecules for degradation to lysosomes: Macroautophagy, microautophagy and chaperone-mediated autophagy [288]. Mitophagy is a form of macroautophagy, which will be the I will be addressing here, and is necessary to maintain mitochondrial quality. It targets damaged and non-functional mitochondria and marks them for degradation [288]. Macroautophagy itself is an evolutionary conserved, genetically programmed process that's responsible for degradation of cellular proteins and damaged or excessive organelles [288]. Through macroautophagy, the target for degradation is encapsulated by a double-membrane structure, also known as autophagosomes, which are then moved along microtubules. The autophagosomal outer membrane fuses with the lysosome resulting into an autophagolysosome where degradation of the target and the inner membrane by hydrolases takes place [289-291]. Once degradation is done, the content is released back into the cytoplasm through permeases and then used for anabolic or catabolic reactions [291-295]. Most autophagy-related gene (Atg) proteins form multi-molecule complexes for regulation of autophagosome formation which include the ULK1 kinase complex, the Beclin 1-VPS34 class III phosphoinositide 3-kinase (PI3K), the Atg9-Atg2-Atg18 complex, the Atg5-Atg12-Atg16 complex as well as the Atg8/LC3 conjugation system [296-298]. In yeast, the autophagosome induction and formation are mediated by an interplay of multiple proteins such as the Atg1-Atg13-Atg17 complex, phosphatidylinositol 3-kinase complex and the Atg5-Atg12-Atg16 multimere complex [299]. Additionally, the control of autophagy has been linked to involve the nutritional conditions of the cells, it is inhibited by insulin and promoted by glucagon and the inhibition of the mammalian target of rapamycin (mTOR), which is a protein kinase in the PI3K-related kinase (PIKK) family, involved in multiple critical cellular processes [300-302]. An inhibition of

mTOR due to nutrient-deprivation, leads to initiation of autophagy by the activation of insulin-like growth receptor (IGF1R) which relays a signal through tyrosine kinase activities to insulin receptor substrates (IRS1 and IRS2). The result of mTOR activation through IGF1R signalling is the inhibition of autophagy, while the reverse is true under nutrient-deprived situations, mTOR is inhibited resulting into the activation of autophagy. The inhibition of TOR is mediated by AMP-activated protein kinase (AMPK) which with TOR control autophagy induction [303-305].

Another selective autophagy form is mitophagy, which specifically aims at superfluous or damaged mitochondria. Atg32 had been shown to be required for mitophagy, and its expression and mitophagy process itself were suppressed by N-acetylcysteine (NAC), which is the precursor of glutathione [306]. When mitochondria are damaged, their membrane potential decreases and parkin is recruited and translocated from the cytosol into the mitochondria, via the activity of PTEN-induced kinase 1 (PINK1), to promote autophagy [307, 308]. The ability to distinguish healthy and non-healthy mitochondria of the kinase remains to be researched, but PINK1 is thought to be expressed and then imported into all mitochondria where it is degraded by proteolysis, and only in dysfunctional mitochondria, PINK1 proteolysis is impaired, which results in an accumulation of PINK1 in damaged mitochondria, which is then followed by the recruitment of Parkin, inducing mitophagy [309, 310].

Spermidine (Spd) is a natural polyamine that has been shown to extend lifespan in different species through autophagy-related mechanisms [311-313]. Dietary Spd in murine cardiomyocytes have shown to induce mitophagy and suppresses age-induced memory impairment as well as preserve synaptic flexibilities in flies [314-317]. Polyamines such as spermidine, spermine and putrescine are polycations and able to react with negatively charged molecules such as DNA, RNA, lipids, or proteins. Furthermore, spermidine acts as an amino-butyl group donor for the synthesis of hypusine (Nε-[4-amino-2-hydroxybutyl]-lysine) to a specific lysine residue of the eukaryotic translation initiation factor 5A (eIF5A). Hypusine is an unusual amino acid that is synthesized posttranslationally in two enzymatic steps, where deoxyhypusine synthase (DHPS) catalyses the cleavage of spermidine, using its amino-butyl group for the second enzymatic step. This intermediate product is hydroxylated by deoxyhypusine hydroxylase (DOHH) and produces hypusine as final product [318, 319]. The hypusination of eIF5A has been shown to decrease with age and that dietary

spermidine supplementation can augment this until mid-aged flies and has been linked to mitochondrial functionality [320].
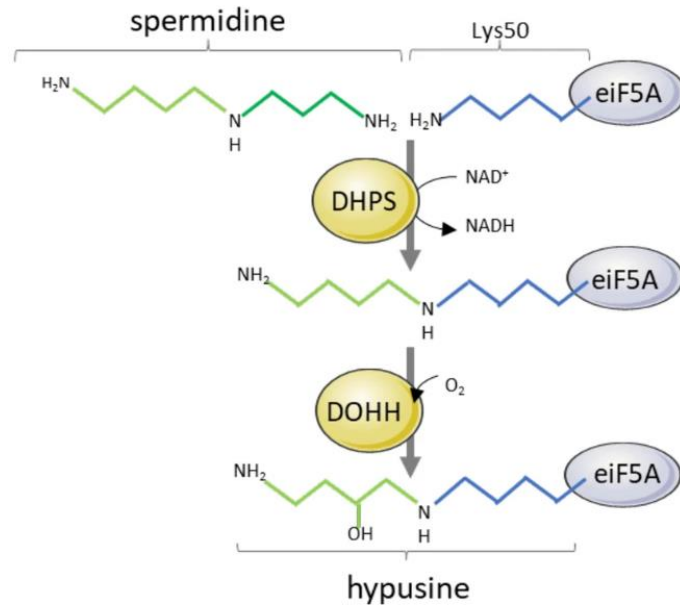
Figure 16: Spermidine acts as an amino-butyl group donor for hypusination of eIF5A.

Spermidine donates an amino-butyl group to the lysine residue at position 51 for the hypusination of eIF5A. The hypusine synthesis involves two enzymatic steps, the first is the catalysation of the cleavage of spermidine through DHPS and the second is the hydroxylation of the intermediate with DOHH, forming hypusine. Image taken and modified from Tauc et al, 2021 [7].

1.7.4 Redox-sensitive green fluorescent protein

For my thesis, we were interested in the effects of aging on redox level in adult fly brains with age and the effects spermidine and a DHPS KD mutant has on it. To measure this, we used a redox-sensitive GFP (roGFP) that allows us to measure glutathione redox potential. Through the engineering of two surface-exposed cysteines into the GFP barrel on β-strands 7 and 10, a disulfide switch is attached that can be used to exploit a structure-dependant shift through protonation status of the chromophore [321, 322]. Depending on the redox environment, the cysteine residues can form disulfide bridges which in response, slightly alters the protein barrel conformation of the GFP and lead to an alteration in protonation state of the chromophore, resulting into a difference in fluorescence [11, 323]. This engineered GFP is therefore redox-sensitive and has two fluorescence maxima (400 nm and 490 nm), depending on redox state [11]. For the experiments in this thesis, roGFP2-Grx1,

which has shown to be insensitive to pH changed within physiological range and coupled to human-glutaredoxin-1 (Grx1) that enhances the specificity for glutathione and the equilibrium kinetics of roGFP2 and the GSH/GSSG redox couple [324-326]. Depending on the oxidation state of the disulfide bond of the roGFP2, the fluorescence excitation changes. In a more oxidized state, fluorescence intensity shifts towards 400 nm, while in a reduced state, the intensity peaks at 480 nm [11].

1.7.5 Mitochondrial trafficking in axons
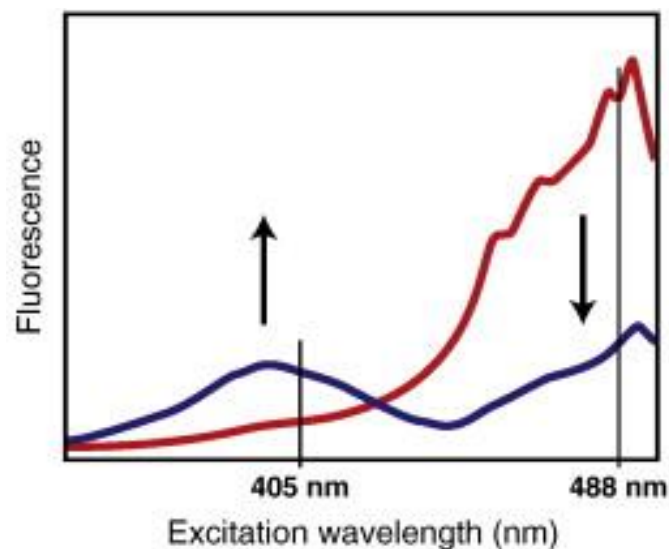
Figure 17: Excitation spectrum of roGFP2.

The red curve represents the excitation spectrum of roGFP2 in fully oxidized state, while blue shows the fully reduced state. The vertical lines show excitation wavelengths. Image taken and modified from Aller et al., 2013 [11].

Neurons are highly polarized cells that consist of distinct structural and functional domains such as the soma and a long axon and thick dendrites. These neurons require different amount of energy in each domain and therefore show nonuniform mitochondrial numbers across different domains. High-energy demanding areas such as presynaptic of postsynaptic terminals, active growth cones or axonal branches contain more mitochondria [327-330]. To satiate the need of energy, mitochondria need to be transported from soma to their final destination, even though it has been shown that mitochondrial biogenesis can occur in axons, it is thought that majority of the new mitochondria are synthesized in the soma and then transported [328, 331, 332]. Dysfunctional mitochondria are hypothesized to be transported back to the soma, where it is subjected to mitophagy, but previous works have shown that

mitochondrial movement is closely-tied to the state of the cell and organelle itself and an impairment of this transport system seems to be linked to the pathogenesis of several neurodegenerative diseases [333-335]. Transported mitochondria in axons have shown to be able to move bidirectionally, with frequent directional changes, as well as with pauses and switches to persistent docking [328, 336, 337]. The mobility of mitochondria is granted through motor adaptor proteins and mitochondrial receptor to attach to motor proteins building a motor-adaptor-receptor complex enabling mobility and transport from soma to distal axonal or dendritic regions through microtubules [338, 339]. The microtubules are formed through polymerisation of α- and β-tubulin, arranged with plus and minus ends, with axonal microtubules minus end directed towards the soma and the plus ends towards distal regions. Kinesin superfamily proteins (KIF) and cytoplasmatic dynein are responsible for long-distance transport under ATP-hydrolysis control of cargos including mitochondria [340-342]. KIF motors move towards the plus end and cytoplasmic dynein towards the minus ends of microtubule, resulting into KIF motors driving anterograde and dynein retrograde transport [339]. Previous works have shown that axonal transport experience age-related decline, and impaired mitochondrial transport has been associated in aging-associated neurodegenerative diseases [343].

1.8 Aim of the thesis

As type I terminals are in the main scope of research in the past few years and type II terminals, compared to type Is, always had had relatively low exposure in this field, my thesis questions the functionality and molecular components of those synapses and their potential role in synaptic guiding. Glutamatergic synapses are known to exhibit bigger boutons and that they're filled with BRP and other AZ proteins and a postsynaptic structure that aligns directly opposite of the AZ. For octopaminergic neurons, the release machinery is still not well researched and the absence of an electron-dense structure at the AZ poses the question how release takes place in those synapses. In my thesis, I aim to contribute few data that hopefully can shed some light on these neurons in that aspect. For this matter, I use STED and use immunohistochemical staining of BRP, GFP and RBP to visualize AZ players in type II synapses at larval NMJs and observe the organisation of the tested proteins. Another important part of my thesis is about the innervation and temporal distribution of synapses during the major reorganization of organs during metamorphosis. Most neural connections disintegrate, and the connections must form a new, on the matured adult muscles then. TDC2 positive neurons have been shown to be in contact with dendrites of larval crawling motoneurons, implying communication between both neurons. In my thesis, I aim to pinpoint the pupal stage that is essential for target-finding of adult glutamatergic and OA/TA neuron innervation and question if type I or type II terminal neurons show any dependence when finding their new innervation target. I use immunohistochemical staining in different pupal stages and image them via confocal microscopy to get an overview of muscle organization and innervation. Lastly, we collaborated with the Bertram Gerber lab and worked with the very sophisticated researcher, who has now his own group, Professor Dr. Michael Schleyer. I used their advanced larval locomotion tracking and analysis system IMBA (individual maggot behaviour tracker) to determine locomotive defects through RNAi lines of AZ proteins specifically expressed in OA/TA neurons. We tested different AZ proteins known for their importance at the AZ and knocked them down in OA/TA neurons and used IMBA to determine any locomotive defects. Furthermore, we tested BRP, RBP, Unc13A and Unc13B with this method. Using this method, we aim to find out, whether any of those AZ proteins have a role in larval locomotion and in what degree they affect it when they are downregulated. Using IMBA allowed us to analyse larval locomotion

in greater detail, that would normally not be possible via normal larval locomotion assays.

In the second part of my thesis, we were interested in the effects of aging on mitochondrial transport as well as mitochondrial redox state in combination with dietary spermidine supplementation. Here, we used genetical constructs and immunohistochemical approaches to investigate possible deficits in mitochondrial transport with age and spermidine supplementation in adult fly wings. Additionally, we checked for mitochondrial redox state with the use of mito-roGFP2-Grx1 to determine the equilibrium of GSH/GSSG that delivers information about mitochondrial oxidative stress. Furthermore, as spermidine is involved in the hypusination of eIF5A, we knocked down DHPS and investigated the effects it has on mitochondrial redox state in adult fly brains.

2. Material and Methods

2.1 Fly stocks and Husbandry

Fly strains were reared under standard laboratory conditions which were previously described [102]. Crosses and stocks were maintained at 22°C and crosses used for experiments were kept at 25°C. All flies were raised on standard food at a 60%-80% relative humidity and a 12h/12h light/dark cycle. Fly strains obtained from Vienna *Drosophila* Research Centre, Bloomington *Drosophila* Stock Centre or other labs are indicated in Table 1.

2.2 Immunohistochemistry

For immunohistochemical studied on *Drosophila* larval NMJs, 3rd instar larvae were used. Dissection and preparation of 3rd instar larvae were described previously [74]. To summarize, the larvae was pinned at its head and tail in hemolymph-like saline (HL3, see table 3) [344] with their dorsal side facing upwards and then cut open dorsally at the rostro-caudal midline. The innards were carefully removed, and the dissection fixed with 4% paraformaldehyde (PFA) in phosphate-buffered saline (PBS) for 10 minutes. For pupal dissection, the pupa was placed ventral side up, the anterior side of the puparium and internal pupa were used to open the puparium with forceps. This left the anterior side of the pupa head open and a fine scissor or the force of forceps were used to cut, or tear open the puparium along the midline parallel to the anterior-posterior axis until the posterior part of the puparium. If done correctly, the puparium can be removed with little effort, leaving the internal pupa intact, which was then cut open like a 3rd instar larva and identically fixed with 4% PFA in PBS for 10 minutes. If the internal pupa resembled an adult fly more than a larva, they were dissected as such. For adult fly preparation, the wings, legs, and abdomen were cut off, leaving only the thorax and the head. The thorax was then faced dorsal side upwards and cut in two symmetrical halves. The thorax was then spread open to reveal the IFMs for the following staining process. The IFM were then fixated with 4% PFA in PBS for 10 minutes as well. After fixation, filets were washed three times with PBS with 0.05% Triton-X 100 (PBT) for 20 minutes each on a rotator. After washing, the filets were blocked in a blocking solution consisting of 5% normal goat serum (NGS) in 0.05% PBT for an hour and afterwards incubated in a primary antibody solution at 4°C over night. On the subsequent morning, the filets were washed anew and then blocked once again as described before and then incubated with the secondary

antibody solution for 2-3 hours at room temperature and finally washed another three times for 20 minutes in PBS. Once the staining is done, the filets were mounted in Mowiol for confocal preparation or in ProLong Gold for STED experiments. Samples were stored at 4°C.

2.3 Microscopy and image analysis

2.3.1 Confocal microscopy

Pupal images were acquired at room temperature with the Leica Confocal microscopy system TCS-SP8 using a 43x optical zoom with an oil objective with NA=1.4. Images from the thorax region (T2-T3) of the pupa were taken with an image size of 246.03 µm x 246.03 µm and a corresponding pixel size of 240.50 nm x 240.50 nm x 251.77 nm and a z-step size of 0.25 µm at 8 bits. The samples were scanned bidirectional with a sequential channel scanning with a line average of 2 and at 600 Hz with varying zoom, using LAS X software (LEICA DMI 6000, Leica Microsystems, Germany). For all confocal images, analysis was performed using Fiji software (NIH, USA).

2.3.2 STED microscopy and analysis

STED microscopy and the analysis of data were done with the support of Dr. Marta Maglione (FU Berlin, Sigrist Lab, Germany). Two-color STED imaging was performed using a TCS SP8 with a tuneable white laser (470nm – 670nm) and a depletion laser at 775 nm. Type II terminals were imaged at muscles 12 and 13. Images were acquired using LAS X software (Leica Microsystems) with a 100x, 1.4x NA oil immersion objective and then deconvoluted using Huygens Professional deconvolution software (SVI, The Netherlands).

Image analyses were performed using Fiji software (NIH, USA), images were manually thresholded to remove low intensity pixels and then used for each image in the same experimental set. The average diameter and width of the type II boutons and BRP spot were manually measured using the built-in measure command in the program. The orientation of the bouton was used to determine diameter and width of the BRP spots. BRP dots that were no further apart than < 0.02 mm were still considered as one entity and regarded as a single BRP spot. If BRP dots were further away apart than 0.02 mm within a bouton, they were considered as new spot and measured and counted separately. To measure diameter and width, a vector was placed through the bouton or BRP spot and the measure function in the Fiji software was used.

2.4 Larval locomotion assay using IMBA
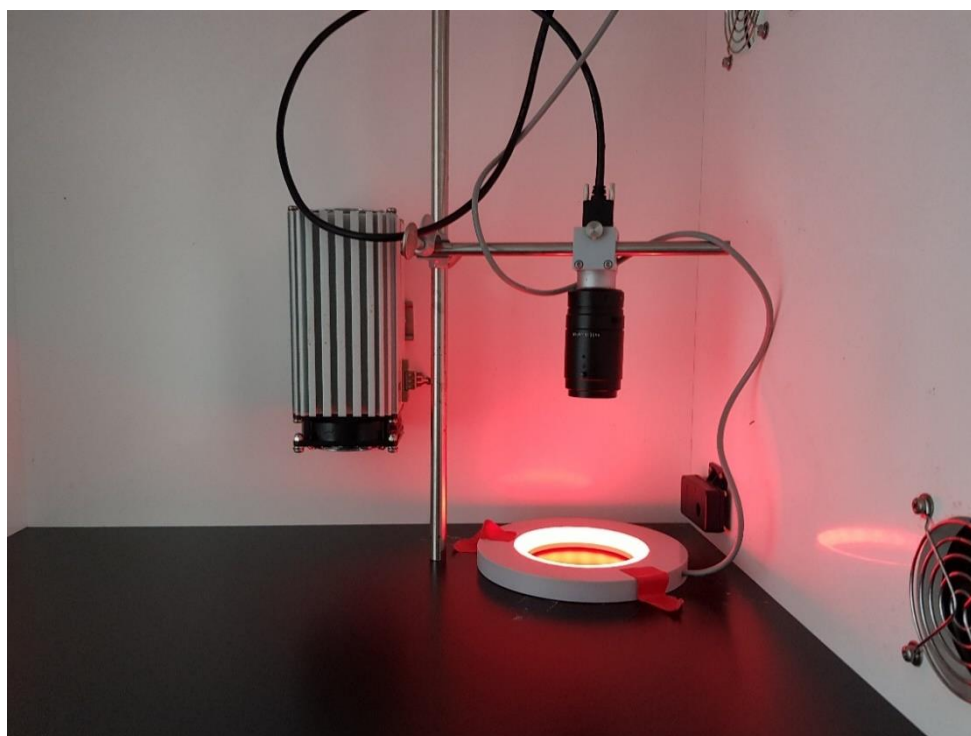
Figure 18: Setup of the larval crawling assay used for IMBA analysis.

The setup consists of a camera above the experimental area (below the camera) with an LED ring around it. The petri dish with 1% agarose and 5 to 10 larvae were put inside the LED ring and videos were captures with the camera for 3 minutes.

Third instar feeding-stage larvae (*D.melanogaster*), aged around 4-5 days AEL, were used throughout the experiment. A spoonful of food medium was taken and rinsed with tap water to select larvae for the experiment. The selected larvae were put on petri dishes with 9 cm inner diameter (Sarstedt, Nümbrecht, Germany) filled with 1% agarose (electrophoresis grade; Roth, Karlsruhe, Germany). Around 5 to 10 larvae were used per video. They were put in the middle of the petri dish, slightly separated, and were then recorded for 3 minutes from above with a camera and an LED light serving as light source. Larvae that appeared for less than 2 minutes were disregarded and not taken into video analysis. The larvae were tracked with IMBA that consists of IMBAtracker and IMBAvisualizer, that allows for tracking and analysis of individual larvae within groups.

The data extraction of the videos was generously done by Prof. Dr. Michael Schleyer and the analysis and statistics were performed using the software GraphPad Prism 6 (GraphPad Software, Inc., San Diego, CA, USA). The 3-minute-long videos were

analysed and only larvae that appeared in the videos for at least 2 minutes were eligible for statistics. IMBA was kindly provided by the Bertram Gerber Lab in the Leibniz Institute of Neurobiology in Magdeburg [4].

2.5 Fly wing assay

To investigate mitochondrial trafficking through axonal transport we used a modified protocol of Alessio Vagnoni and Simon L. Bullock [345]. A microscopic slide (76 mm x 26 mm) was modified by glueing adhesive tape on 3 different positions that were far enough apart to fit a fly in between. 3 stripes of adhesive tape were glued on top of each other to avoid the fly from being squished. The flies were anesthetized using FlyNap (Carolina Biological Supply Company) and put on a cover slip (18 mm x 18 mm) dorsally with halocarbon oil. FlyNap allows a long-term anesthetization that lasts for around 30 to 60 minutes. Following the FlyNap treatment, the wings of the flies were carefully spread out on the cover slip containing the halocarbon oil and air bubble were removed. Halocarbon oil allows the stabilization of the fly body as well as the diffusion of gases. The tested regions are the L1 vein and L3 branch in Figure 19 (the blue circled areas).
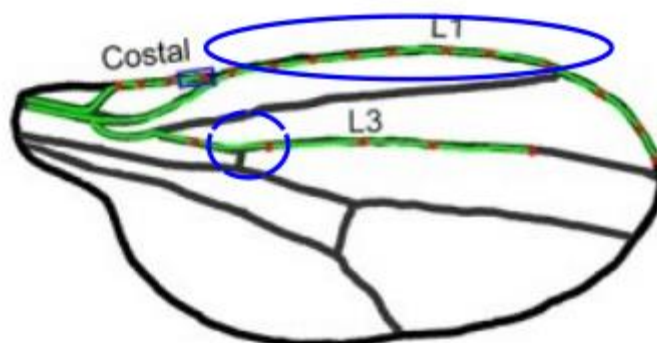
Figure 19: Illustration of a wing of Drosophila melanogaster.

The green highlighted regions are the costal wing nerves, and the red dots depict the neural soma. Blue circled areas are the tested regions, the big circle represents the L1 vein and the smaller, not closed circle shows the "branch"-region. Illustration was taken and slightly modified from the publication of Cao et al. in 2017 [5].

2.6 In vivo imaging of fly wings and analysis of mitochondrial transport

Flies have been prepared as described above and were scanned with the confocal microscope system Leica TCS SP8 (Leica microsystems) using a 63x oil immersion objective, 600 Hz scanning speed, a line average of 2 and a zoom factor of 1.7. The

resolution used was 1024 x 256 and the L1 vein and the first branch in the L3 vein of the fly wing (blue circled are in Figure 19) were recorded for 3 minutes. Quantification was performed using Fiji (NIH, USA) with a kymograph macro script written by Dr. U. Rey (Research Institute of Molecular Pathology, Campus-Vienna-Biocenter 1, 1030 Vienna, Austria). Positions of mitochondria were marked manually and followed throughout 208 frames long videos. Transported mitochondria were observed until the end of the video or when they left the region of interest. 3-minute-long videos were recorded, resulting into 208 frames which were then used to count stationary mitochondria. Here, we used the 5th, 50th and 150th frame of every video and counted the mitochondria manually and averaged these numbers.

2.7 Fly brain dissection protocol and analysis

Flies were anesthetized on ice and dissected in HL3 with either 20 mM N-ethylmalemide (NEM), 20 mM Dithriothreitol (DTT) or 2 mM Diamide (DA) and then kept for 15 minutes in their corresponding solution. Afterwards the brains were incubated in fresh HL3 containing 20 mM NEM on ice for 15 minutes. Afterwards the brains were fixed with 4% PFA for 15 minutes at room temperature and then washed for 5 minutes with PBS for four times. Finally, they were equilibrated in the mounting medium Vectashield (Vector Laboratories) at 4°C over night and then mounted in Vectashield on the next morning. Fly brain images were acquired at room temperature with the Leica Confocal microscopy system TCS-SP8 using a 20x oil immersion objective, a scanning speed of 600 Hz, zoom factor of 1.7 and a line average of 2. The first channel measured GSH levels (excitation wavelength of 488 nm) and the second channel GSSG (excitation of 405 nm). Analysis was performed with Fiji (NIH, USA) and the image stacks were merged using the "maximum-projection" function of Fiji. Fluorescence intensity was measured for both channels and the ratio (405nm/488nm) were calculated using Fiji's innate functions. For antennal lobe analysis, 5 frames in which the antennal lobes' structure were visible the most prominent were chosen manually and then encircled using Fiji's free hand selection tool.

2.5 Statistics

Statistics were performed using GraphPad Prism 6 (GraphPad Software, Inc., San Diego, CA, USA). All results were tested for outliers using Prism's Grubbs test with an α = 0.05 and identified outliers were removed. The cleaned data (without the outliers) were tested for normal distribution using D'Agostino & Pearson test. As a result, all

tests comparing multiple groups were performed with a Kruskal-Wallis test for the data concerning aminergic release. For aging related experiments, GraphPad Prism 6 was used as well, and outliers identified as before, and comparison were performed using one-way ANOVA Turkey's post-hoc tests and Bonferroni correction and two-way ANOVAs with Bonferroni correction. Statistical significances are exhibited as asterisks in the graphs: *, $p < 0.05$; **, $p < 0.01$; ***, $p < 0.0001$; ns, $p > 0.05$.

2.6 Antibodies, media, buffer, and fly stocks list.

The following tables contain the used flies, antibodies, buffers, food, and pharmacological agents used. Commonly used chemicals were ordered from Sigma-Aldrich Chemie GmbH, Germany.

Table 1: List of fly strains. BDSC: Bloomington Drosophila Stock Center

Name	Description	Source
w[1118]	Control; isogenic wildtype, white eyes	BDSC #5905
TDC2-Gal4	Tyrosine decarboxylase 2 gene driver line	Cole et al. [8]
10x UAS-IVS-mCD8-GFP	Expression of a mCD8-tagged GFP under control of 10 UAS sequences with an intron	BDSC #32185
UAS-BRP-RNAi[B3-C8]	UAS-RNAi against BRP	Wagh et al. [50]
UAS-RBP-RNAi	UAS-RNAi against RBP	Turrel et al. [346]
UAS-Unc13A-RNAi-A1	UAS-RNAi against Unc13A	Fulterer et al. [347]
UAS-Unc13B-RNAi-B3	UAS-RNAi against Unc13B	Fulterer et al. [347]
UAS-Brp-WT	Overexpression of wildtype Brp	Wagh et al. [50]
Appl-Gal4	Panneural driver line	Torroja et al., 1999 [348]
Elav-Gal4 (c155x)	Panneural driver line	Liang et al., 2021 [320]
UAS-mito-roGFP2-Grx1	Expression of a glutaredoxin-based fluorescent sensor of	BDSC #67664

	glutathione oxidation within mitochondria under UAS control	
UAS-mitoGFP	Expression of GFP with a mitochondrial import signal	BDSC #8442
UAS-CG8005RNAi	UAS-RNAi against deoxyhypusine synthase	VDCR #103593

Table 2: List of primary antibodies. DSHB: Developmental Studies Hybridoma Bank

Antibody	Antigen	Host species	Antibody type	Dilution	Source
αBRP NC82	Bruchpilot$^{C\text{-}term}$	Mouse	Monoclonal	1:200	DSHB, USA
αGFP	Green fluorescent protein (tag)	Goat	Polyclonal	1:1000	Invitrogen, Germany
αRBP #9172	Rim-BP N-term	Rabbit	Polyclonal	1:500	Sigrist lab [58]
αUnc13A #14gp17	Unc13 isoform A$^{N\text{-}term}$	Guinea Pig	Polyclonal	1:500	Sigrist lab [59]
αUnc13B #rb13031	Unc13 isoform B$^{N\text{-}term}$	Rabbit	Polyclonal	1:500	Sigrist lab [59]

Table 3: List of secondary antibodies

Antibody	Antigen	Host species	Fluorophore	Dilution	Source
αChi Alexa 488	Chicken IgY	Goat	Alexa488	1:500	Invitrogen, Germany

αMs Cy3	Mouse IgG	Goat	Cy3	1:500	Jackson Immuno research, USA
αMs Cy5	Mouse IgG	Goat	Cy5	1:500	Jackson Immuno research, USA
αRb Cy5	Rabbit IgG	Goat	Cy5	1:500	Dianova, Germany
αMs STAR RED	Mouse IgG	Goat	STAR RED	1:300	Abberior, Germany
αRb A594	Rabbit IgG	Goat	Alexa594	1:300	Invitrogen, Germany
Phalloidin 565	Actin-F	-	Atto565	1:5000	Sigma Aldrich, SKU 94072-10NMOL

Table 4: Buffer and media composition

Name	Composition
Haemolymph-like saline 3 (HL3) (pH adjusted to 7.2sss)	70 mM NaCl 5 mM KCl 20 mM MgCl 10 mM NaHCO$_3$ 115 mM Sucrose 5 mM Trehalose 5 mM HEPES
Phosphate-buffered saline (PBS)	137 mM NaCl 2.7 mM KCl 8.1 mM Na$_2$HPO$_4$ 1.5 mM KH$_2$PO$_4$
Phosphate-buffered saline with Triton X-100 (PBT)	PBS + 0.05% Triton X-100
Standard fly food	42 g Agar 83 g Soy flour 75 g Brewer's years

	666 g Corn flour
	183 g Beet syrup
	666 g Malt
	13 g Nipagin (in 100% EtOH)
	53 ml Propionic acid
	(for spermidine in food add 0.625 ml 2M spermidine to 500 ml standard fly food)
	Rest filled up with H_2O up to 10 l
2% yeast fly food	110 g Sucrose
	52 g Corn flour
	7.9 g Agar
	8.9 g Ethanol
	2.3 g Nipagin
	20 g Yeast
	Rest filled up to 1 L H_2O
12% yeast fly food	110 g Sucrose
	52 g Corn flour
	7.9 g Agar
	8.9 g Ethanol
	2.3 g Nipagin
	120 g Yeast
	Rest filled up to 1 L H_2O

3. Results

3.1. Type II innervation and BRP distribution at the IFM during pupal development.

Previous work has shown the importance of octopamine not only in-flight behaviour, but also fight behaviour, hence also called as "fight or flight" hormone of insects and is known to not only act as neuromodulator, but also as a neurohormone (as described in 1.5.2). OA and its precursor TA additionally show antagonistic effect on larval crawling behaviour, indicating the importance of both bioamines. The innervation of the relevant muscles (NMJs and IFMs) is therefore essential. During the larval stages, the necessity to respond to required larval locomotion for foraging behaviour is crucial and octopaminergic/tyraminergic neurons have shown to react dynamically to starvation, where a larva requires more locomotion to find food. Astonished by the flexibility of octopaminergic/tyraminergic neurons being able to react quickly to starvation (within 2 to 6 hours), by extending through synaptopods and by their proximity to type I terminals as octopamine-possessing neuron, we question, whether this flexibility could be a characteristic to quickly find innervation targets during development. As during metamorphosis most muscles and therefore innervation disappear, we were interested in the temporal and spatial distribution of type I and type II boutons and whether the ability to quickly extend and develop synaptopods could be a characteristic used during metamorphosis to find their correct innervation target. Connected to this question, we were also interested in the role of type I boutons in that regard, as they are closely located at some regions to interact. Wondering, if glutamatergic neurons or octopaminergic fibres innervate adult muscles first, we started with *Drosophila* larvae first. To get an overview of spatial and temporal distribution of type II boutons, we began imaging muscle 12 and 13 in L3 instar-larvae and stained for the BRP C-term with the antibody Nc82 and for GFP in my transgenic control group that expresses GFP in TDC2-positive neurons (TDC2-Gal4 > UAS-mCD8-GFP). Consecutively, we started dissecting pupa at different metamorphic stages and checked for remaining muscles and/or newly formed IFM or pretemplates. Using the work of Paul Bainbridge and Mary Bownes [349], the pupal stage was determined. In case of severely histolyzed muscles, we used the still intact CNS to orientate myself during dissection and imaging. During the early pupal stage in P2 (Figure 20A), muscle histolysis has barely started, and muscles could be imaged as

usual. Figure Figure 20A shows muscle 12 with still present type II boutons containing not only BRP spots within type II boutons, but along the whole neuron. During L3 stages, the boutons of octopaminergic/tyraminergic neurons usually only contain a single BRP spot when observed with a confocal microscope. During metamorphosis, in P2 stage, BRP spots are not only visible in synaptopods, but throughout the whole neuron. Furthermore, the usual type I boutons are completely missing at the branch of muscle 12 (white arrows in Figure 20A) when compared to larval innervation (Figure 11C). When looking at further progressed pupa at P5 stage, the larval-like muscles have disintegrated and IFM pretemplates were visible. The TDC2-positive neurons showed no obvious thickenings that would resemble the larval synaptopods and BRP was absent within those neurons (Figure 20B).
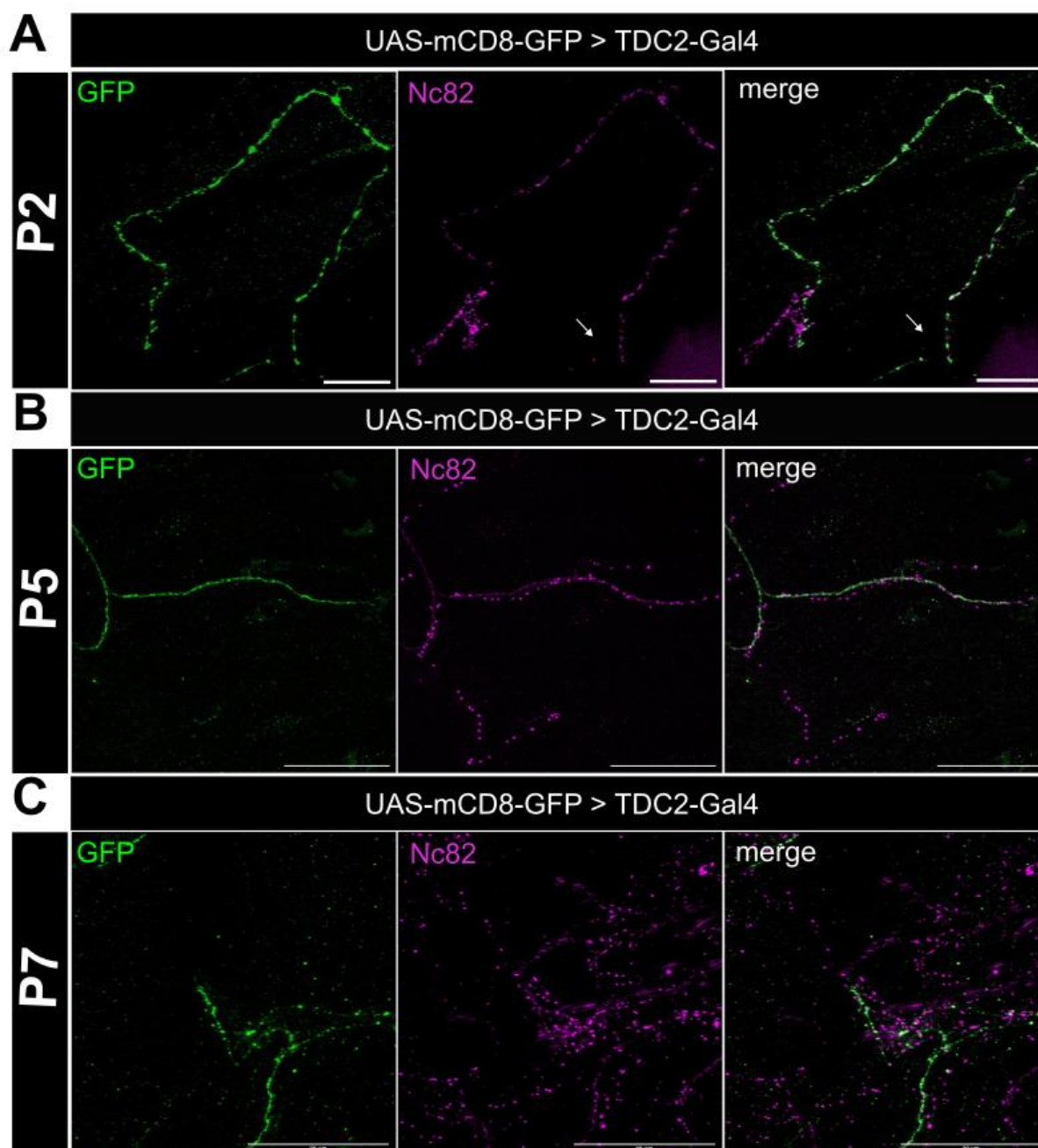
Figure 20: During initial stages of metamorphosis, BRP subsides first upon muscle histolysis and during development of IFMs BRP signal quantity increases visibly.

(A) During P2 larval muscles still retain their larval form, type I boutons are regressing, while type II boutons remain. White arrow: missing BRP staining from type I boutons at muscle 12 branch. **(B)** Images of the pre-template IFMs in P5 stage show TDC2 positive neurons along the muscle with BRP in close vicinity. BRP dots exhibit an organized structure. **(C)** Further into IFM development during P7 stage, BRP distribution within the muscle appears unorganized. Scale bar: 20 μm.

3. Results

BRP labelling can be observed outside within the octopaminergic/tyraminergic neurons, as well as in proximity of OA/TA neurons, but also at a further distance from these neurons. P5 BRP signal showed a more structured and distinct appearance of BRP along the muscle, while in P7 (Figure 20C) the BRP distribution, and therefore possibly also type I neurons, along the muscle showed no obvious structure and BRP seems to be present in abundance. TDC2-positive neurons also show some signal of BRP within, but a "chaotic" overflow of BRP signal around the neuron and along the muscle. The neurons themselves look slightly ragged, like P9 neurons (Figure 21A). Interestingly, the BRP signal in P9 pupa outside the TDC2-positive neurons seem less convoluted than in P7 and seem slightly more structured. Additionally, BRP signal within the octopaminergic/tyraminergic neurons can be observed again. Looking into later pupal stages, P12 (Figure 21B) showed a quite different picture than P9 and P7. Contrary to the previous stages, the BRP signal, and therefore also the type I innervation, over the whole muscle exhibits remarkably more organized structures and the OA/TA neurons show barely any BRP dots inside. The organized BRP spots might indicate the establishment of type I boutons, unlike what was observed in P7, where BRP looked quite diffuse along the whole muscle. P9 showed lesser diffusive picture than in P7 and P12 showed a rather organized BRP picture. Surprisingly, when looking at the almost final pupal stage, P14 (Figure 21C), IFMs showed even less BRP signal, albeit being close to eclosion. Type II innervation also seemed scarcer and BRP signal was very weak. There seemed to be BRP signal within OA/TA neurons again, similar to larval synaptopods. Looking solely at the BRP distribution throughout the investigated pupal stages, it indicates that in P5 type I boutons might develop prior to type II boutons, possibly giving OA/TA neurons a gross direction as to where the adult innervation is going to establish, or perhaps even independently. As the signal during pupal stages differed quite a lot and the consistency of muscles and other innards affected the staining, quantifying single BRP spots might be inaccurate. Therefore, I left this experimental part unquantified and proceeded with another approach. This time, since OA neurons are known to act as neuromodulator and act upon type I neurons, the capability to release OA must be given. The release mechanism in type I terminals is rather well investigated and a lot of active zone proteins have been found and characterized. This is not the case for type II terminals, where the release mechanism is still a mystery yet to be solved. Unlike glutamatergic neurons at the NMJ, the BRP signal in type II boutons is only a dot and the absence of a T-bar in

68

ultrastructural images, further emphasizes the mechanism behind type II terminal's release mechanism.
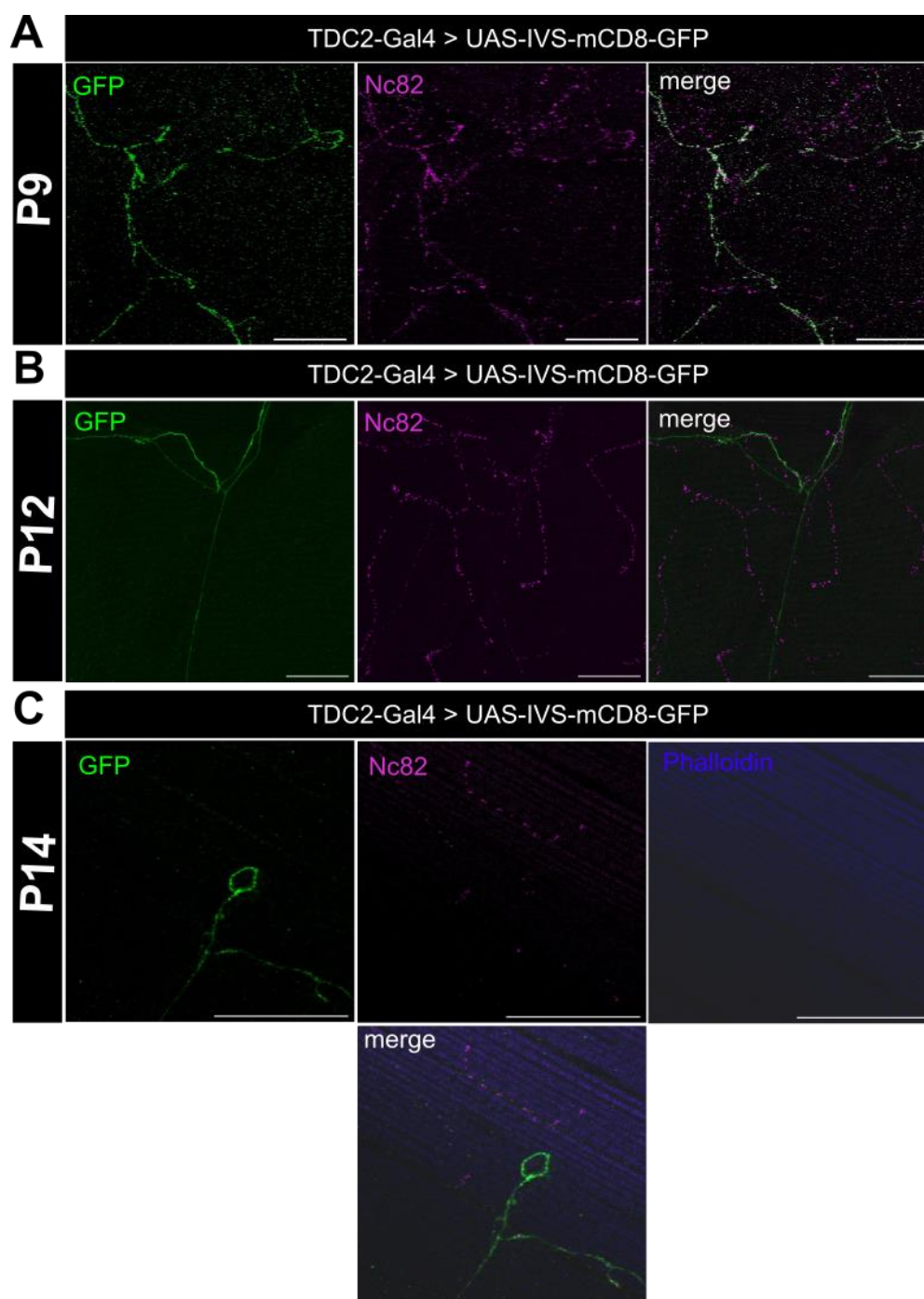
Figure 21: Later stages in the metamorphosis show more structured BRP distribution.

(A) In P9 stage, BRP can be found over the whole muscle, showing no obvious structure in distribution. **(B)** The BRP distribution in P12 pupa is more structured compared to the two previous shown phases. **(C)** The nearly adult pupa in stage P14 is close to emerging from its puparium. The BRP dots has become even fewer compared to the previous shown pupal stages and an additional phalloidin staining (F-actin visualization) shows muscle structure. Scale bar: 20 µm.

3.2. Modification of BRP quantity in octopaminergic neurons did not change synaptopod diameter nor BRP spot diameter.

To investigate the release mechanism in type II terminals, I turned back to better researched models such as the larval NMJ and visualized the octopaminergic neurons via STED. Previous work has shown that the release mechanism and active zone scaffolding in type I boutons involves the interplay of multiple AZ proteins. A vital protein in that process being BRP which has also been shown to localize inside boutons of octopaminergic fibres as a single BRP dot in confocal images. BRP, being a core player in the release mechanism in glutamatergic neurons at larval NMJs and being present in VUM-neurons, suggests that it might contribute to synaptic vesicle release in type II boutons, like its function in type I boutons. Hence, I checked the octopaminergic fibres in L3 larvae and checked for the BRP labels in type II boutons using STED. In previous works, BRP at active zones was shown to form "doughnut"-shaped structures in planar view with multiple BRP labels surrounding a single calcium channel. Interested, whether octopaminergic fibres show a similar BRP structure as type I boutons or not, we performed STED on type II boutons at muscle 12/13 in our transgenic control group TDC2-Gal4 > UAS-mCD8-GFP. We used Nc82 to visualize the BRP$^{C\text{-term}}$ and a GFP antibody for octopaminergic fibres (Figure 22A, first row). STED images show that when manually counting the BRP labels (Figure 22F), in average 1 to 2 BRP spots per type II bouton were observed in my control group, supporting previous findings in confocal images, showing 1 or 2 BRP labels per synaptopod. Through STED recordings, it wasn't possible to discern any obvious formations, unlike in type I bouton recordings, as BRP labels (average 0.0698 µm, Figure 22D) and type II boutons (average 1.16 µm, Figure 22B) are considerably smaller than type I boutons. As criteria to discern between BRP spots that were in proximity as different entities, we set the requirement for the BRP dots to be apart more than 0.002 µm. Since BRP labelling showed no obvious formation and only 1 or 2 BRP dots in type II boutons, we overexpressed BRP in octopaminergic neurons (Figure 22A, third row), and the overexpression, albeit not significant, did show a very slight increase in BRP spots per bouton (Figure 22F, p = 0.081). Simultaneously, we were interested in the opposite scenario and generated a knockdown (KD) mutant for BRP in octopaminergic neurons (Figure 22A, second row). As expected, there was barely any BRP signal left, and only rarely, few dots were visible (Figure 22F, p = 0.0013).
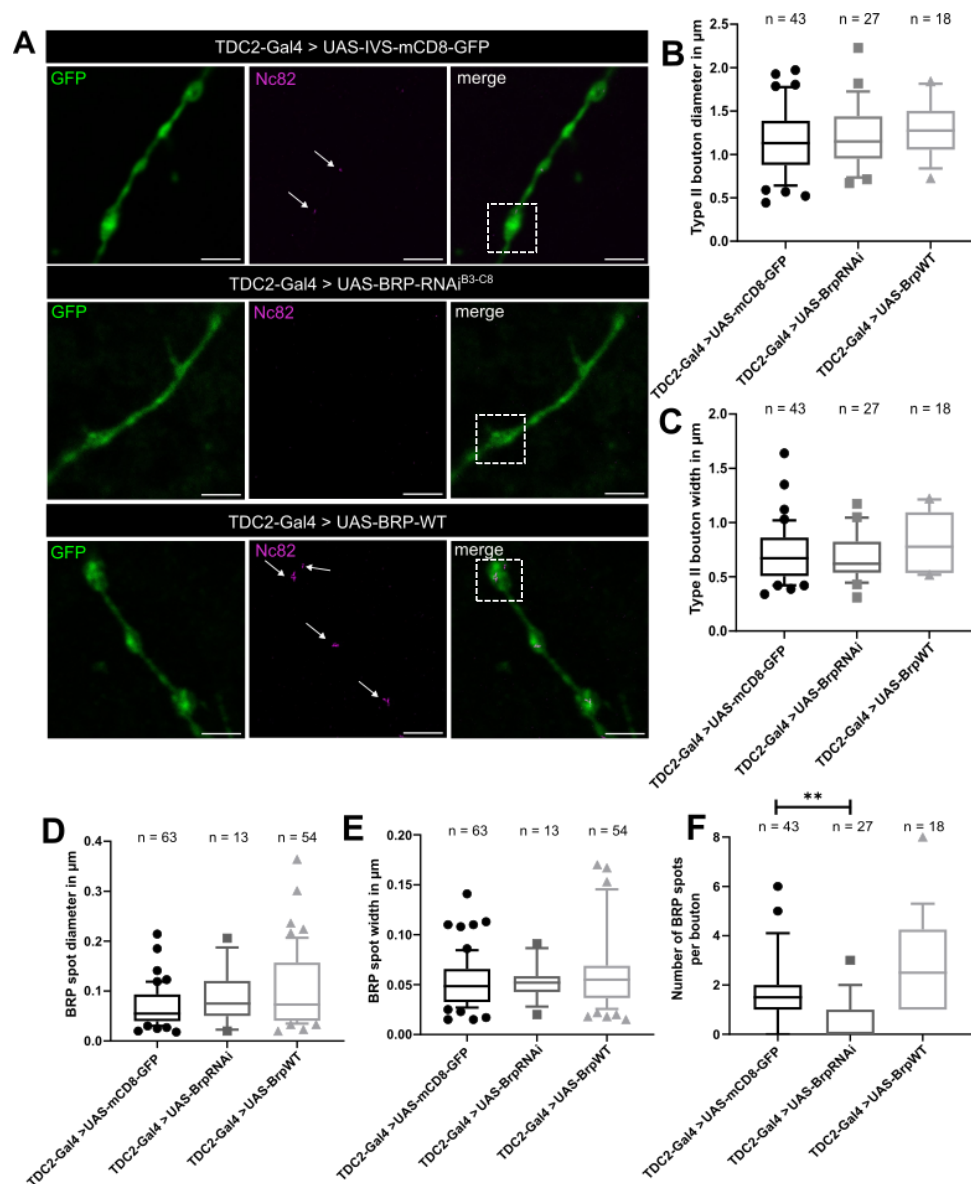
71

Figure 22: BRP knockdown and overexpression alter BRP quantity within TDC2-positive neurons, but not bouton morphology.

(A) GFP visualizes TDC2-positive neurons and Nc82 staining reveals a quantitative decrease in BRP spots in BRP KD mutants (second row) compared to the control group (first row) and the overexpression (third row) exhibit an increase of BRP spots in these neurons. Total flies used for corresponding groups: Control (n=3); *BRP-RNAi[B3-C8]* (n=4); *BRP-WT* (n=2). White arrows point at BRP spots in type II boutons and striped areas are magnified in Figure 19. **B)** Quantification of type II bouton diameter in µm. No significant changes were observed. Control (n=43): 1.16 µm ± 0.3902 µm; *BRP-RNAi[B3-C8]* (n=27): 1.209 µm ± 0.3636 µm, p > 0.999; BRP-WT (n=18): 1.293 µm ± 0.3258, p = 0.2815. (Legend continued the next page)

(C) Quantification of type II bouton width in μm. No significant changes were found. Control (n=43): 0.7048 μm ± 0.2654 μm; BRP-RNAi B3-C8 (n=27): 0.6744 μm ± 0.2095 μm, p > 0.999; BRP-WT (n=18): 0.7893 μm ± 0.2652 μm, p= 0.5047. (D) Quantification of BRP spot diameter. BRP-WT's BRP spot diameter in knockdown as well as in overexpression mutants showed no significant difference overall, even though the overexpression has a slight tendency for an increase in BRP spot diameter. Control (n=63): 0.06982 μm ± 0.04126 μm; BRP-RNAiB3-C8 (n=13): 0.08923 μm ± 0.05302 μm, p = 0.5104; BRP-WT (n=54): 0.1057 μm ± 0.07656 μm, p = 0.0599. (E) Quantification of BRP spot width. Modification in BRP content within type II boutons did not result in significant changes in spot width. Control (n=63): 0.0525 μm ± 0.02589 μm; BRP-RNAiB3-C8 (n=13): 0.05308 μm ± 0.01776 μm, p > 0.999; BRP-WT (n=54): 0.7672 μm ± 0.09335 μm, p = 0.3297. (F) Quantification of BRP spot ratio per type II bouton (Average number of BRP spots / type II bouton). BRP-RNAiB3-C8 shows an absence of BRP spots in most boutons, while BRP-WT shows a slight, albeit not significant increase in BRP spot number per bouton. Control (n=43): 1.75 ± 1.5, BRP-RNAiB3-C8 (n=27): 0.4815 ± 0.849, p = 0.0013; BRP-WT (n=18): 2.944 ± 1.924, p = 0.0810. A BRP spot was considered a separate entity, if the BRP dots were further apart than 0.002 μm. n in (A) and (B) refers to the quantified type II boutons, while n in (D, E) and (F) refers to the observed BRP spots within the analyzed type II boutons in (A) and (B). All images in (A) were deconvolved using Imspector software. All box plots show the mean with 10-90 percentiles ± SD; * p < 0.05, ** p < 0.01, *** p < 0.001. Kruskal-Wallis test and Grubb's outlier test with α = 0.05 in (B-F). Scale bar in (A): 2 μm.

The overexpression of BRP in these synapses didn't result in any significant changes in BRP spot diameter, nor width (Figure 22D and E, diameter: p = 0.0599; width: p = 0.3297). It also didn't affect type II bouton diameter or width (Figure 22B and C; diameter: p = 0.2815; width: p = 0.5047). Overexpressing BRP did not result in any significant differences concerning bouton morphology, and BRP spot morphology, albeit a slight, but not significant increase in BRP spot per bouton (p = 0.081). Similarly, BRP spot diameter in the overexpression mutant showed a slight, but not significant increase in diameter (p = 0.0599). As expected, the BRP-RNAi mutant showed a reduction in BRP spot per bouton, while still leaving some synaptopods with BRP signal. The remaining BRP spots that were observed, did not show any significant difference in diameter, nor in width. The KD of BRP in type II boutons also didn't result in any bouton alteration in terms of diameter and width. Neither modification in BRP amount within octopaminergic neurons showed any phenotypical difference concerning bouton size or BRP spot size. The decrease in BRP spots in the RNAi mutant and slight increase in the overexpression did confirm that the genetic

constructs worked and the change in BRP amount did not alter type II bouton morphology.

3.2.1 Magnification of BRP spots at type II terminal boutons.
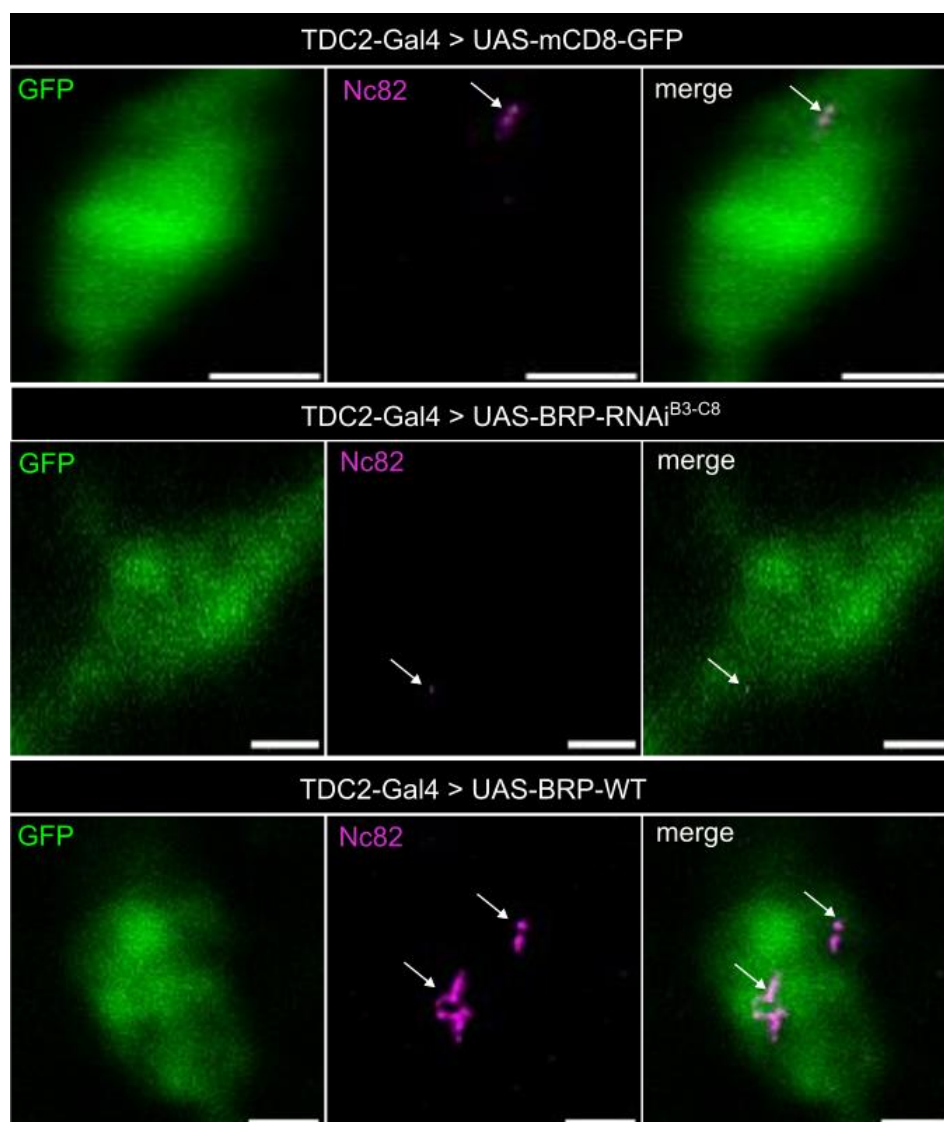
Figure 23: Magnification of type II terminal boutons with BRP signal in different BRP mutants.

A magnification of the striped area in Figure 22 shows that BRP signal in boutons with type II terminals do not only consist of 1 single BRP spot, but occasionally 2 or 3 spots (first row). BRP RNAi KD mutants show either no BRP staining or very weak ones (second row). The BRP overexpression mutant (third row) shows an increase in BRP spots.

To further observe BRP signal inside type II boutons, I checked the BRP spots seen in STED images with a higher magnification (images from Figure 22A) to check for

obvious structures in BRP alignment. When taking a closer look at the STED images, we can see two distinct BRP dots in our control group, while the BRP KD mutants show clearly reduced amount of BRP inside type II terminal boutons (Figure 23). The overexpression shows in STED images an increase in BRP labelling within our tested boutons. It must be mentioned that not all type II boutons in our control group showed two distinct BRP spots, some only showed one or two at different locations inside the bouton. This was also true in our BRP overexpression mutant, as the number of multiple BRP spots within type II terminal boutons differed in individual observed boutons.

3.3 Unc13A did not clearly show signal in type II terminal boutons.
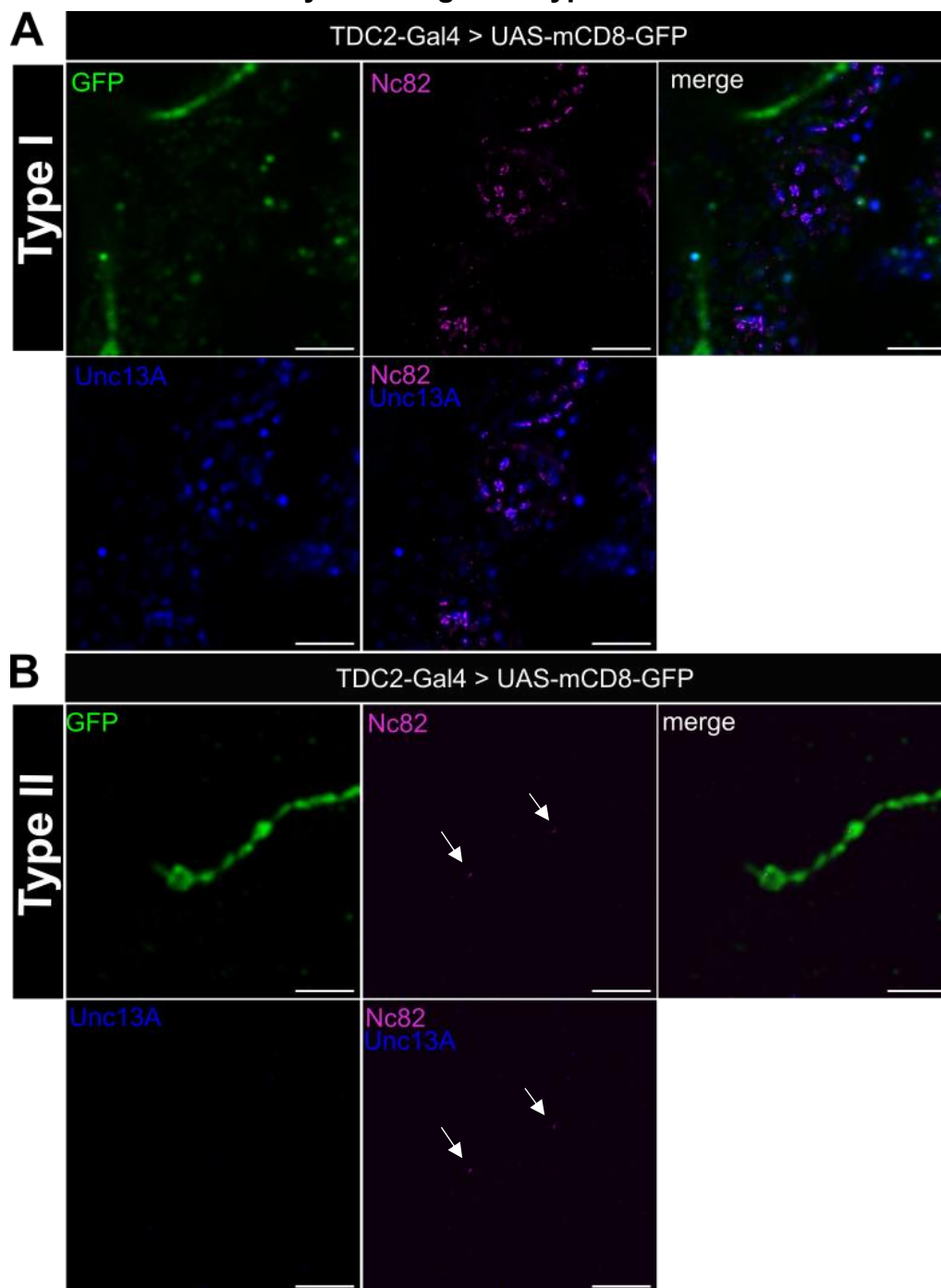
Figure 24: Staining of TDC2-Gal4 > UAS-mCD8-GFP for BRP, Unc13A and GFP did not clearly reveal Unc13A signals in type II terminals.

GFP staining visualizes OA/TA neurons, Nc82 type II boutons and type I presynaptic boutons and Unc13A staining shows no or barely signal in type II boutons but co-localize in type I BRP "doughnut"-structure at muscle 12. **(A)** focusses on type I terminals. **(B)** shows a single branch of an OA/TA neuron on muscle 12 and focusses on type II boutons. **(A,B)** arrows indicate BRP signal in type II boutons. All images were deconvolved using Imspector software.Scale bar: 2 µm.

After testing the effects of modification of BRP quantity in type II boutons, I was interested in other active zone proteins, as little is known about the release machinery in type II terminals. For this matter, I turned to type I terminals and checked for few proteins that are available in there. Therefore, I stained for Unc13A and Unc13B in type II boutons and used STED microscopy to the presence of these proteins. Unc13A and Unc13B have been shown to be present within the AZ in type I terminals and therefore an ideal protein to stain for.

Immunohistochemical staining for Unc13A did not reveal any, or in comparison to other stained proteins, very weak signal. It wasn't distinguishable to background noise, and it was not possible to determine, whether the signal was true or not within type II boutons (Figure 24). In comparison, to confirm, whether the staining worked, we checked the signal at type I terminals, here specifically on muscle 12 at the branch and Unc13A signal could be seen to co-localize to BRP signalling (Figure 24). This indicates that the staining did work, even though it must be mentioned, that the signal was quite weak and had to be amplified using Fiji. Another possible reason for the absence of either Unc13 isoform in STED images could be smaller quantity that might be required in type II terminal boutons.

3.3.1 Unc13B staining did not conclusive presence in neurons with type II terminals.
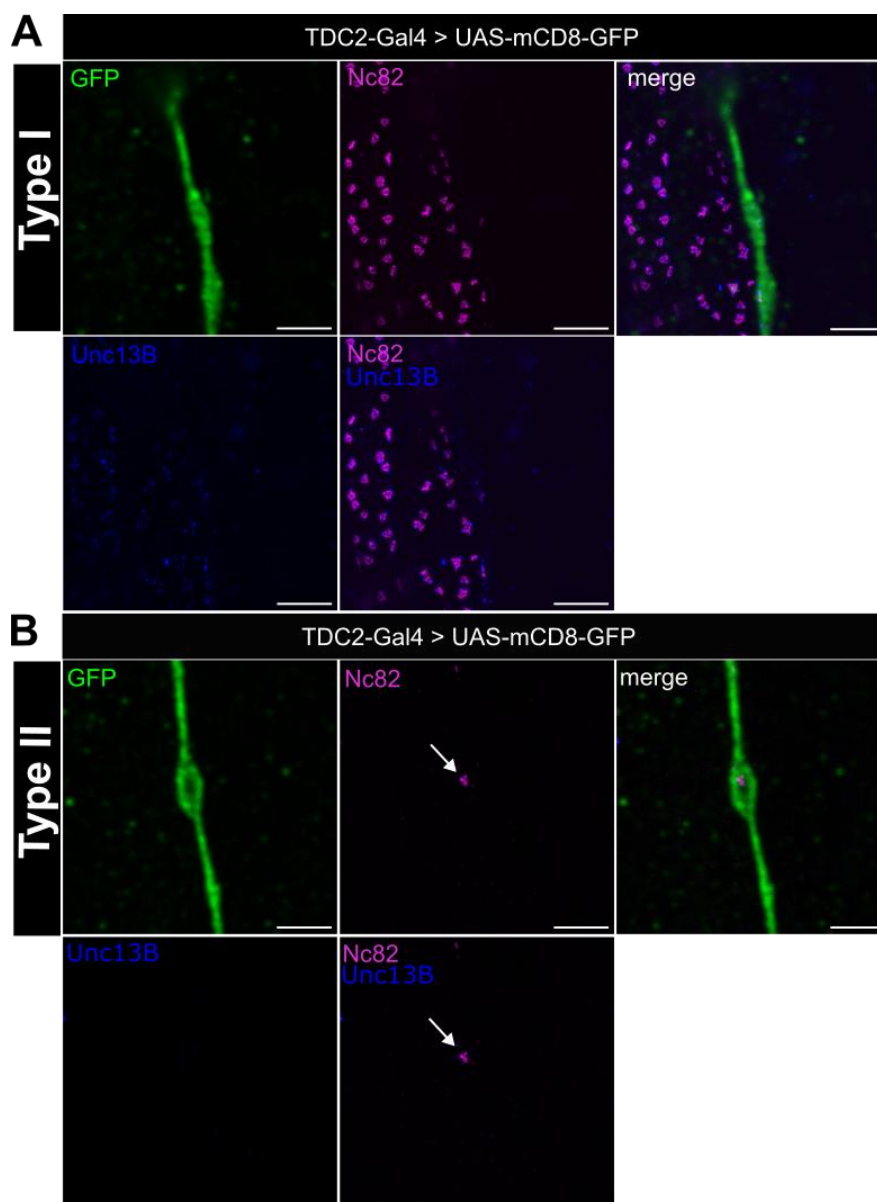
Figure 25: Unc13B staining didn't reveal obvious labelling within type II terminal boutons.

GFP staining visualized OA/TA neurons, while Nc82 marks BRP and Unc13B staining didn't show obvious signal in type II boutons but co-localize in type I terminals at muscle 12. **(A)** focus on type I terminal. **(B)** focus on type a single type II bouton showing the lack of Unc13B signal. **(A, B)** Arrows point at BRP signal in type II boutons. Scale bar: 2 μm.

Immunohistochemical staining for the other known isoform of Unc13, Unc13B, revealed similar results as the staining for the other isoform. Both staining showed the presence of BRP in either terminal, but the lack of Unc13A (Figure 24) and Unc13B

(Figure 25) in type II boutons. When either isoform was checked at type I terminals, it was possible to observe that they co-localize which confirmed, that the antibody did work. Interestingly, when brightness and contrast was increased with the use of ImageJ, Unc13A and Unc13B signal could be observed in type II boutons (data not shown), but whether this was true signal or background signal, remains to be verified with further experimentations. The absence of either isoform might be due to the quantity of the protein within type II terminal boutons, as the dimensions of type II terminal boutons and type I boutons are different.

3.4 Knockdown of certain active zone proteins in OA/TA neurons affect different larval locomotion behaviour.

Larval locomotion is a patterned motor behaviour that's accomplished using CPGs to coordinate neural circuits responsible for[350]. Octopamine and tyramine are known to act on CPG and have agonistic effects on larval locomotion to each other [130]. The existence of BRP in type II terminals and its function in type I boutons suggests the idea that it might also be used in the synaptic vesicle release mechanism in octopaminergic neurons. To investigate this, we used RNAi constructs once again and the IMBA setup. The tested AZ proteins in this thesis are known to be acting in AZ release and scaffolding, which let me pose my hypothesis that some of the tested active zone proteins are potentially available at and required for type II terminal release mechanism. Previous immunohistochemical staining for RBP, Unc13A and Unc13B using STED microscopy didn't show any signal or too much background to differentiate between true signal or background signal (Unc13A: Figure 24, Unc13B: Figure 25, for RBP: data not shown). We then approached the hypothesis differently, by turning to the IMBAtracker from the Gerber lab. Previous larval crawling assays were only capable of crawling behaviour either in a group assay or single animals at a time. Therefore, inter-individual and intra-individual locomotion variability were difficult to test, as locomotion varies between (inter-individual), but also within (intra-individual) individual animals [351-353]. With this approach we were able to evaluate the effects of knocking down certain type I terminal active zone proteins in octopaminergic neurons.

3.4.1 Knockdown of BRP, Unc13A, Unc13B and RBP in octopaminergic neurons showed different effects on larval microbehaviour.
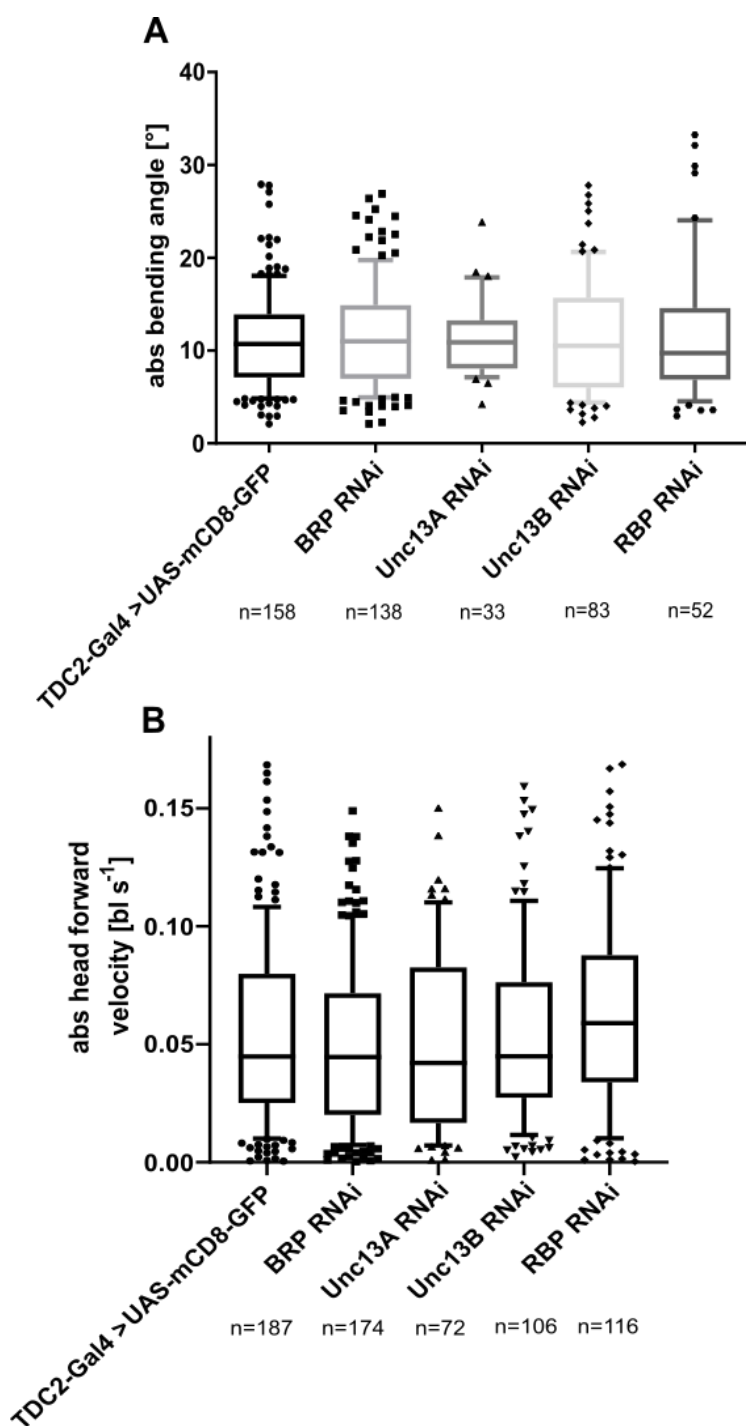

Figure 26: Larval locomotion assay of different AZ protein knockdowns.

(A) The absolute (abs) bending angle showed no significant changes in knockdowns when compared to the control group. Absolute bending angle is the bending angle (left or right bending) of the larva's tail vector and vector from the middle of the larva to the head. Control (n=158): 11.01° ± 5.167°; *BRP-RNAi*[B3-C8] (n=138): 11.62° ± 5.569°, p > 0.9999; *Unc13A-RNAi* (n=33): 11.38° ± 4.108°, p > 0.9999; *Unc13B-RNAi* (n=83): 11.59° ± 6.229°, p > 0.9999; *RBP-RNAi* (n=52): 11.98° ± 7.68°, p > 0.9999. **(B)** Absolute head forward velocity was not affected by the genetic knockdown of tested AZ proteins. Control (n=187): 0.0539 bl/s ± 0.03842 bl/s; *BRP-RNAi*[B3-C8] (n=174): 0.04999 bl/s ± 0.03525 bl/s, p > 0.9999; *Unc13A-RNAi* (n=72): 0.05159 bl/s ± 0.03879 bl/s, p > 0.9999; *Unc13B-RNAi* (n=106): 0.05487 bl/s ± 0.03834 bl/s, p > 0.9999; *RBP-RNAi* (n=116): 0.06343 bl/s ± 0.04121 bl/s, p = 0.1608. All box plots show the mean with 10-90 percentiles ± SD; * p < 0.05, ** p < 0.01, *** p < 0.001. Significances indicated in comparison to control (TDC2-Gal4>UAS-mCD8-GFP) . Kruskal-Wallis test and Grubb's outlier test with α = 0.05 in (A and B). bl = body length.

3. Results

To test larval microbehaviour, we used RNAi lines for BRP, RBP, Unc13A and Unc13B in OA/TA neurons, which are important scaffolding proteins in active zone and release in type I boutons. Through the knockdown of these proteins, we aimed to test the importance of these proteins in OA/TA neurons and if they are potentially responsible or a part of the release or scaffolding machinery responsible for type II terminal release. The locomotive microbehaviour we tested includes several parameters such as bending angle, number of head casts per second, head cast angle and few more of the larvae and were recorded and analyzed with the help of Michael Schleyer from the Bertram Gerber Lab in the Leibniz Institute of Neurobiology in Magdeburg and the use of their IMBA software. The set up of the experiment includes a camera, a light source, and a petri dish with 1% agarose. Around 5-10 larvae were put on the agarose-containing petri dish and recorded for 3 minutes. Video analysis was done by Michael Schleyer. The absolute bending angle (Angle between larva's tail vector and vector from the middle of the larva to the head) of the larvae (Figure 26A) did not show any significant difference in BRP, Unc13A, Unc13B and RBP KD mutants compared to the control group. The head forward velocity also did not exhibit remarkable changes, as BRP, Unc13A Unc13B and RBP KD mutant weren't significantly different from the control group. Subsequently, after finding no significant alteration in absolute bending angle and head forward velocity, we checked the larvae for their absolute head turning velocity as well as head cast (HC) parameters. We saw an increase in HC rate in some mutants, but also a decrease in HC rate in one mutant. The angle didn't significantly change, but a slight increase could be seen in BRP KD mutants. The absolute head turning velocity only showed a slight increase in Unc13B RNAi mutants. Following these data, we tested more parameters such as interstep (IS) data and crawling speed.

3.4.2 HC rate of BRP knockdown mutants decreases, while Unc13A and Unc13B knockdown mutants exhibit increased HC rates.
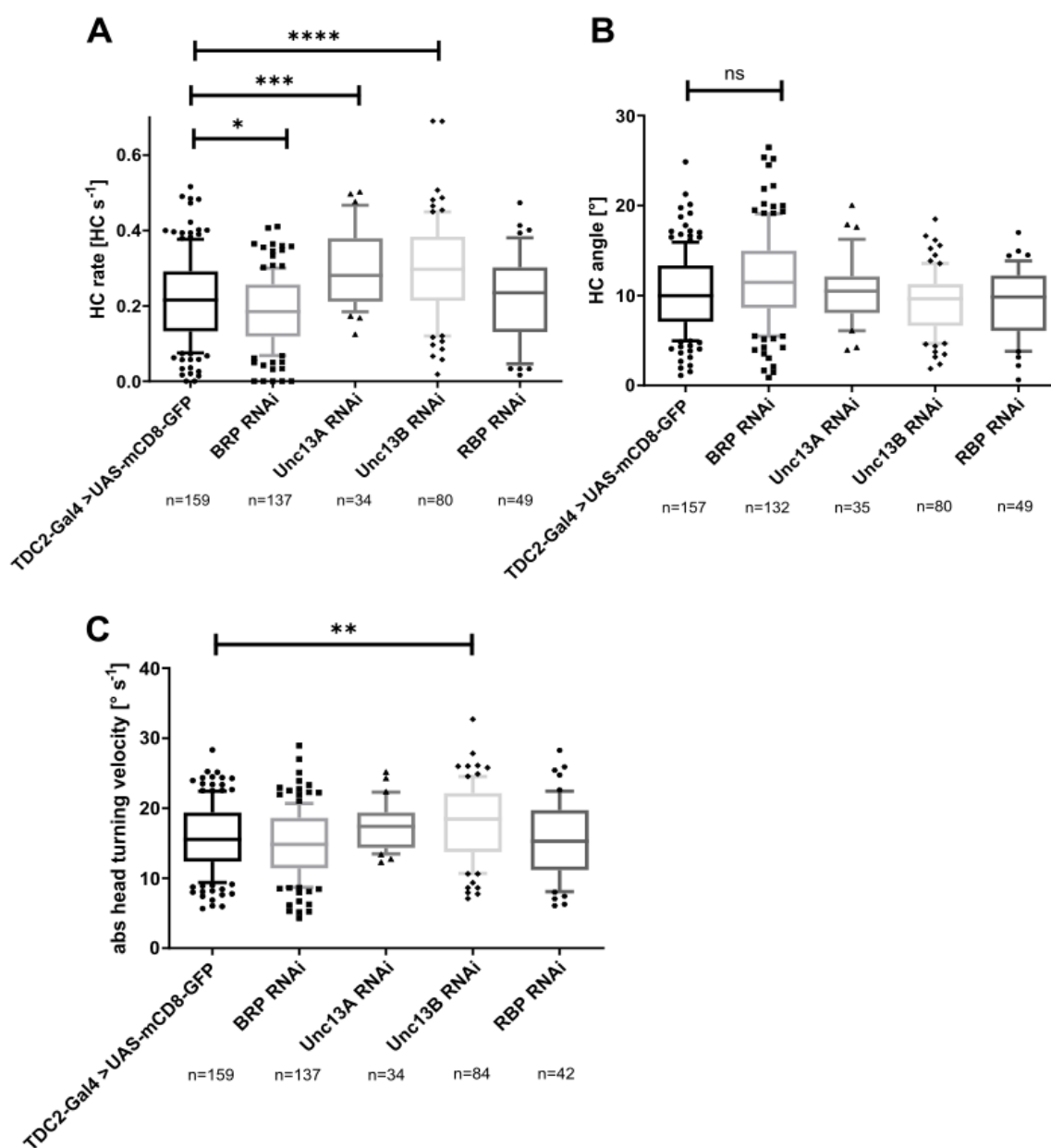
Figure 27: HC rate changes in KD mutants.

(A) The BRP KD mutants show a decrease in head casts per second, while Unc13A and Unc13B KD mutants performed even more head casts than the control group. Control (n=159): 0.2196 ± 0.1104; *BRP-RNAi[B3-C8]* (n=137): 0.185/s ± 0.09194/s, p = 0.0344; *Unc13A-RNAi* (n=34): 0.2958/s ± 0.09953/s, p = 0.0022; *Unc13B-RNAi* (n=80): 0.2989/s ± 0.1282/s, p < 0.0001; *RBP-RNAi* (n=49): 0.2256/s ± 0.1162/s, p > 0.9999. **(B)** The head cast angle remained mainly unaffected, except for BRP KD mutants, which showed a slight increase, albeit not significant in head cast angle. (Legend continued next page)

3. Results

Control (n=157): 10.31° ± 4.253°; *BRP-RNAi*[B3-C8] (n=132): 11.71° ± 5.046°, p = 0.0733; *Unc13A-RNAi* (n=35): 10.63° ± 3.713°, p > 0.9999; *Unc13B-RNAi* (n=80): 9.294° ± 3.441°, p = 0.4111; *RBP-RNAi* (n=49): 9.225° ± 3.704°, p > 0.8237. **(C)** Only Unc13A KD mutants show a significant increase in head turning velocity, while the other KD mutants maintain a similar head turning velocity as the control group. Head turning velocity describes the speed of the executed head cast in degree per second (°/s). Control (n=159): 15.9°/s ± 4.803 °/s; BRP-RNAi[B3-C8] (n=137): 14.97 °/s ± 4.753 °/s, p = 0.4287; Unc13A-RNAi (n=34): 17.47 °/s ± 3.299 °/s, p = 0.348; Unc13B-RNAi (n=84): 18.15 °/s ± 5.289 °/s, p = 0.0059; *RBP-RNAi* (n=42): 15.75 °/s ± 5.416 °/s, p > 0.9999. All box plots show the mean with 10-90 percentiles ± SD; * p < 0.05, ** p < 0.01, *** p < 0.001. Significances indicated in comparison to control (TDC2-Gal4>UAS-mCD8-GFP) . Kruskal-Wallis test and Grubb's outlier test with α = 0.05 in (A and B). bl = body length.

The head turning velocity is the speed of performed lateral reorientation maneuver preceding changes in direction (also called head casts) and is another larval microbehaviour [269]. The head turning velocity (Figure 27C) in BRP (14.97 °/s ± 4.753 °/s), Unc13A (17.47 °/s ± 3.299 °/s) and RBP (15.75 °/s ± 5.416 °/s) KD mutants showed no significant changes, while only the Unc13B KD mutants showed an increase in head turning velocity (18.15 °/s ± 5.289 °/s). Furthermore, we tested the head cast rate (number of head casts per second, Figure 27A) of larvae. The number of head casts per second showed in BRP-RNAi mutants (0.185/s ± 0.09194/s) a slight decrease compared to the control group (0.2196/s ± 0.1104/s), which indicates a slight impairment in locomotive microbehaviour. Contrary to BRP KD mutant, Unc13A (0.2958/s ± 0.09953/s) and Unc13B (0.2989/s ± 0.1282/s) KD mutants performed significantly more head casts per second (Figure 27C) while the RBP (0.2256/s ± 0.1162/s) KD mutants didn't exhibit any significant difference in head casts per second. Looking at the head cast angle (Figure 27B) in those animals, we did not detect any significant differences in the BRP (11.71° ± 5.046°), Unc13A (10.63° ± 3.713°), Unc13B (9.294° ± 3.441°) and RBP (9.225° ± 3.704°) RNAi mutants compared to the control group (10.31° ± 4.253°). Notably, even though the difference was not significant, the BRP KD mutants showed a slight increase in head cast angle (Figure 27D). The increase in head cast rate in Unc13A and Unc13B KD mutants was a result contrary to our expectations, as we hypothesized that a decrease in AZ proteins, if they are used in type II terminals for SV release or AZ scaffolding, would lead to a slight impairment of release or AZ development, resulting in less release and therefore in less modulation of glutamatergic neurons. Possible reasons why this is the case will be discussed in the discussion. Nevertheless, we continued our analysis with further

testable parameters, such as larval interstep (IS) interval, IS distance, IS angle and the crawling speed of the tested larvae.

3.3.2 Knockdown of certain AZ proteins in OA/TA neurons resulted in quicker interstep intervals, but also shorter interstep distance in certain mutants.
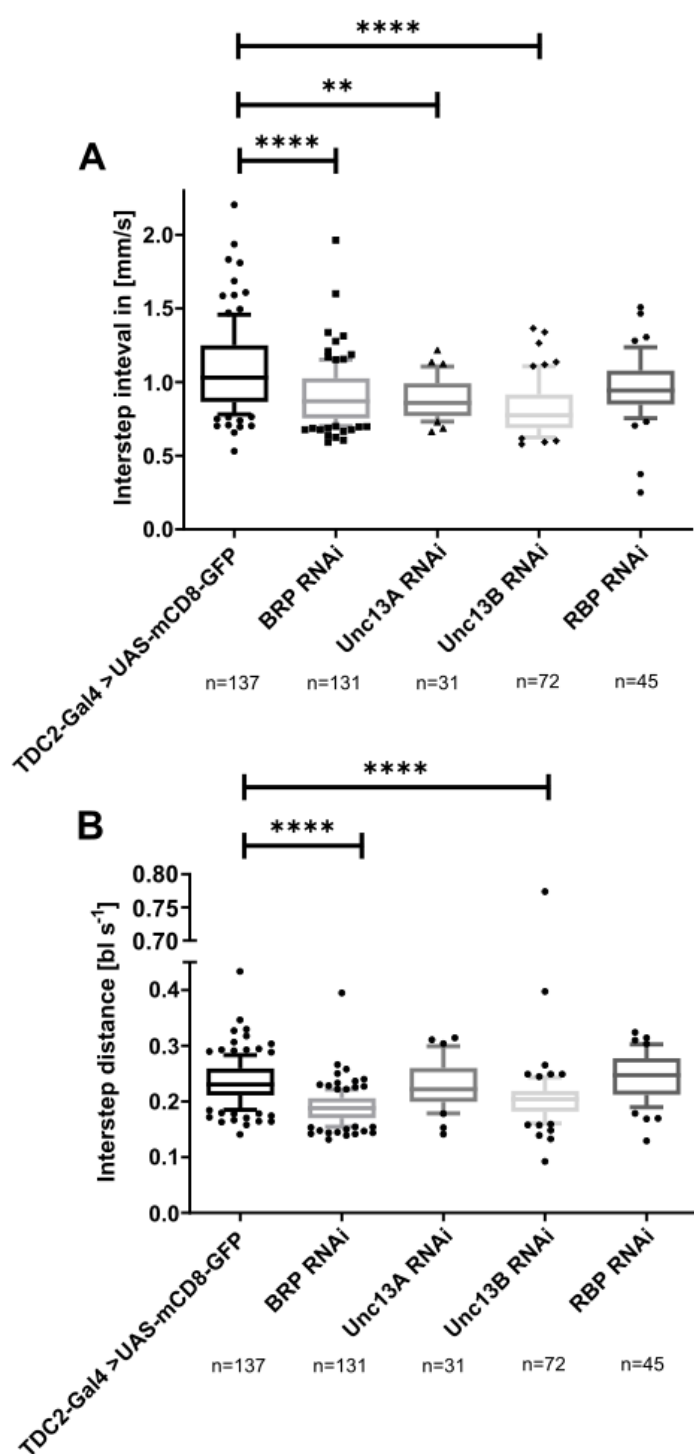
Figure 28: Larval crawling behaviour exhibits significant differences when knocking down certain AZ proteins in OA/TA neurons.

(A) The interstep interval shows significant decrease in Unc13A KD, Unc13B and BRP KD mutants, albeit no remarkable change in RBP KD mutants when compared to the control group. Control (n=137): 1.107 mm/s ± 0.3535 mm/s; *BRP-RNAi^(B3-C8)* (n=131): 0.9555 mm/s ± 0.4298 mm/s, p < 0.0001; *Unc13A-RNAi* (n=31): 0.8893 mm/s ± 0.1338 mm/s, p = 0.0015; *Unc13B-RNAi* (n=72): 0.8433 mm/s ± 0.2648 mm/s, p < 0.0001; *RBP-RNAi* (n=45): 0.9581 mm/s ± 0.2266 mm/s, p = 0.2146. **(B)** BRP RNAi and Unc13B RNAi mutants show a significant decrease in interstep distance in relation to their body length. Control (n=137): 0.236 bl/s ± 0.04145 bl/s; *BRP-RNAi^(B3-C8)* (n=131): 0.1898 bl/s ± 0.03164 bl/s, p < 0.0001; *Unc13A-RNAi* (n=31): 0.2286 bl/s ± 0.0431 bl/s, p > 0.9999; *Unc13B-RNAi* (n=72): 0.2106 bl/s ± 0.07711 bl/s, p < 0.0001; *RBP-RNAi* (n=45): 0.2441 bl/s ± 0.04286 bl/s, p > 0.9999. All box plots show the mean with 10-90 percentiles ± SD; * p < 0.05, ** p < 0.01, *** p < 0.001. Significances indicated in comparison to control (TDC2-Gal4>UAS-mCD8-GFP) . Kruskal-Wallis test and Grubb's outlier test with α = 0.05 in (A and B). bl = body length.

3. Results

Larval locomotion in *Drosophila melanogaster* can be simplified as periods of relatively straight movements by peristaltic waves of muscle contraction along the body wall combined with lateral head movements (head casts) from time to time, which results in a zig-zag pattern towards their targeted location. Such similar pattern of locomotion has also been observed in adult flies and mosquitos [114, 354-363]. Here, we checked for other microbehaviour parameters in larval locomotion such as the interstep interval and interstep distance, which result in the crawling speed of the larvae themselves. The interstep interval measures the time between two steps (step is defined as local maximum of the tail forward velocity during runs), while the interstep distance refers to the distance of the larva's midpoint between two steps. Hence, the crawling speed is defined as interstep distance per interstep interval, where the body length for each individual larva was considered in both interstep parameters. As such, we investigated these parameters with the help of IMBA and discovered that the interstep interval in BRP (0.9555 mm/s ± 0.4298 mm/s), Unc13A (0.8893 mm/s ± 0.1338 mm/s) and Unc13B (0.8433 mm/s ± 0.2648 mm/s): 0.8433 mm/s ± 0.2648 mm/s), but not in RBP (0.9581 mm/s ± 0.2266 mm/s) KD mutants showed a significant decrease in interstep interval when compared to the control group (1.107 mm/s ± 0.3535 mm/s; Figure 28A), which translates into faster steps taken per second of the larvae. Subsequently, looking at the interstep distance, we found that BRP (0.1898 bl/s ± 0.03164 bl/s) and Unc13B (0.2106 bl/s ± 0.07711 bl/s) KD mutants showed a decrease in interstep distance, meaning that the amount of distance covered per step was less than the control group (0.236 bl/s ± 0.04145 bl/s; Figure 28B). Unc13A (0.2286 bl/s ± 0.0431 bl/s) as well as RBP (0.2441 bl/s ± 0.04286 bl/s) KD mutants didn't exhibit any significant changes in interstep distance in comparison (Figure 28B).

3.4.3 Changes in interstep distance and interstep interval affect crawling speed in knockdown mutants.
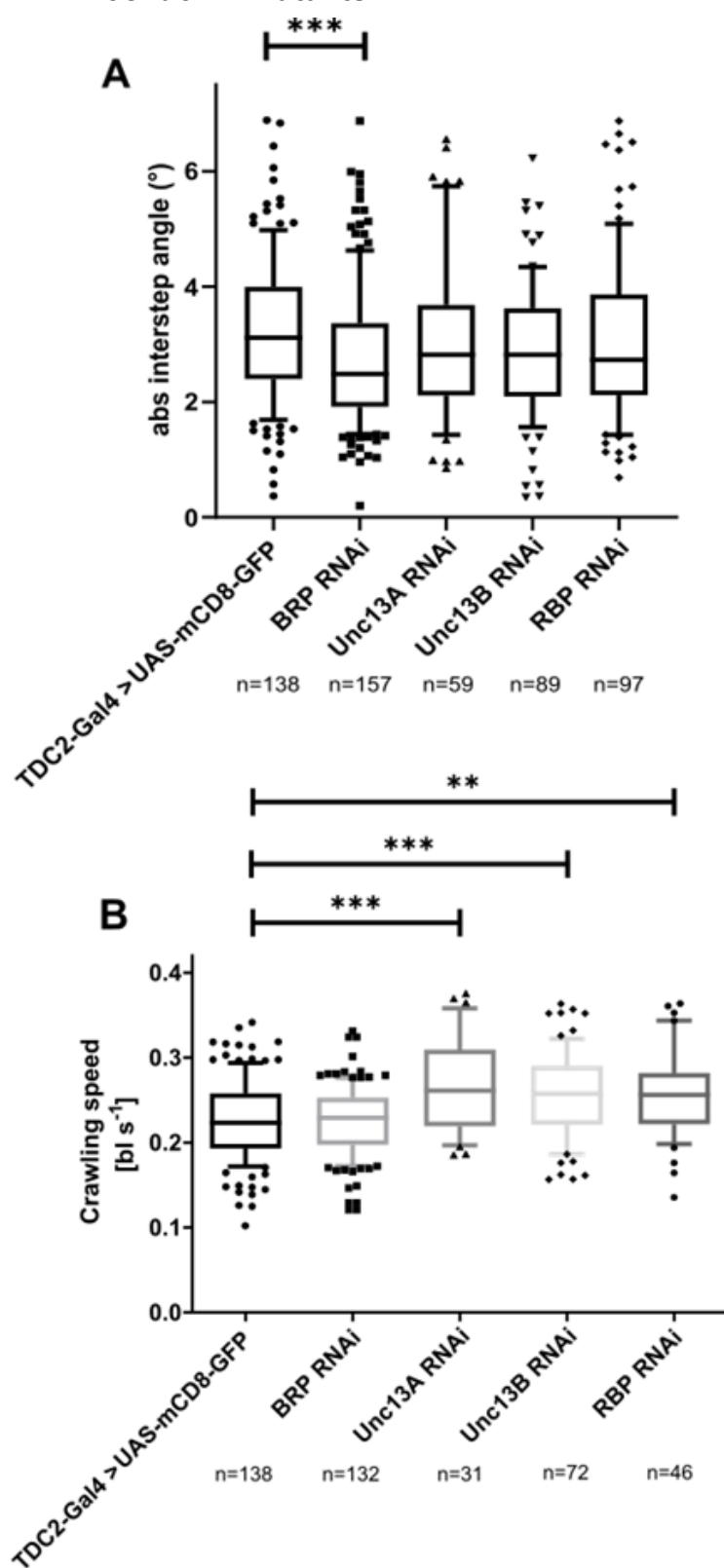
Figure 29: Interstep angle reduces upon BRP knockdown and crawling speed increases in Unc13A, Unc13B and RBP knockdowns.

(A) The absolute interstep angle only decreased in BRP KD mutants, other mutants remained unaffected. Control (n=138): 3.249° ± 1.261°; *BRP-RNAi^{B3-C8}* (n=157): 2.774° ± 1.21°, p = 0.0008; *Unc13A-RNAi* (n=59): 3.07° ± 1.399°, p = 0.733; *Unc13B-RNAi* (n=89): 2.83 ± 1.176°, p = 0.0812; *RBP-RNAi* (n=96): 3.058° ± 1.388°, p > 0.4222. **(B)** The crawling speed of all mutants, except for the BRP KD mutant, show significant increase. Control (n=138): 0.2269 bl/s ± 0.04684 bl/s; *BRP-RNAi^{B3-C8}* (n=132): 0.2258 bl/s ± 0.041 bl/s, p > 0.9999; *Unc13A-RNAi* (n=31): 0.2675 bl/s ± 0.05471 bl/s, p = 0.0011; *Unc13B-RNAi* (n=72): 0.2561 bl/s ± 0.05471 bl/s, p = 0.0003; *RBP-RNAi* (n=46): 0.256 bl/s ± 0.04979 bl/s, p > 0.0025. bl: body length. All box plots show the mean with 10-90 percentiles ± SD; * p < 0.05, ** p < 0.01, *** p < 0.001. Significances indicated in comparison to control (TDC2-Gal4>UAS-mCD8-GFP) . Kruskal-Wallis test and Grubb's outlier test with α = 0.05 in (A and B). bl = body length.

In addition to the IS distance and IS interval, we tested the interstep angle of the larvae as well, which indicates how much the orientation of the larvae changes within one peristaltic forward movement (Figure 29A). When observing the IS angle, we found that only the BRP KD mutants (2.774° ± 1.21°, p = 0.0008) show a significant decrease in IS angle, while the Unc13A (3.07° ± 1.399°), Unc13B (2.83 ± 1.176°) and RBP (3.058° ± 1.388°) KD mutants remained unaffected when compared to the control group (3.249° ± 1.261°). Notably, the Unc13B mutants showed a slight decrease which was barely insignificant (p = 0.0812). Following these data, we investigated the crawling speed in these larvae and discovered that even though interstep interval of BRP KD mutants were significantly shorter (0.9555 bl/s ± 0.4298 bl/s, Figure 28A) and interstep distance was significantly less (0.1898 bl/s ± 0.03164 bl/s; Figure 28B), the crawling speed remained unchanged compared to the control group (0.2269 bl/s ± 0.04684 bl/s, Figure 29C). This result makes sense, since shorter interstep intervals, mean quicker peristaltic movements taken per second, albeit with lesser distance covered (lesser interstep distance), which logically, if the effect in both parameters is close, would nullify their effects on crawling speed. The Unc13A KD mutants showed when compared to the control group a significant decrease in interstep interval as well (Figure 28A), but very similar interstep distance to the control group Figure 28B). Hence, this results in a faster crawling speed (0.2675 bl/s ± 0.05471 bl/s), as the larvae perform faster peristaltic movement than the control, but with similar distance covered per movement. The knockdown of Unc13B in octopaminergic neurons shows similar effects as the BRP KD mutants, the interstep interval and the interstep distance were significantly decreased, while contrary to the BRP KD mutants, their crawling speed did increase (0.2561 bl/s ± 0.05471 bl/s), possibly due to the KD of Unc13B resulting into stronger reduction of interstep intervals (Figure 28A) and lesser reduction of interstep distance than the BRP phenotype (Figure 28B). The RBP KD mutants also show increased crawling speed (0.256 bl/s ± 0.04979 bl/s) mainly due to a slight trend of reduced interstep intervals.

3.4.4 Distance travelled of larvae were not affected in mutants.
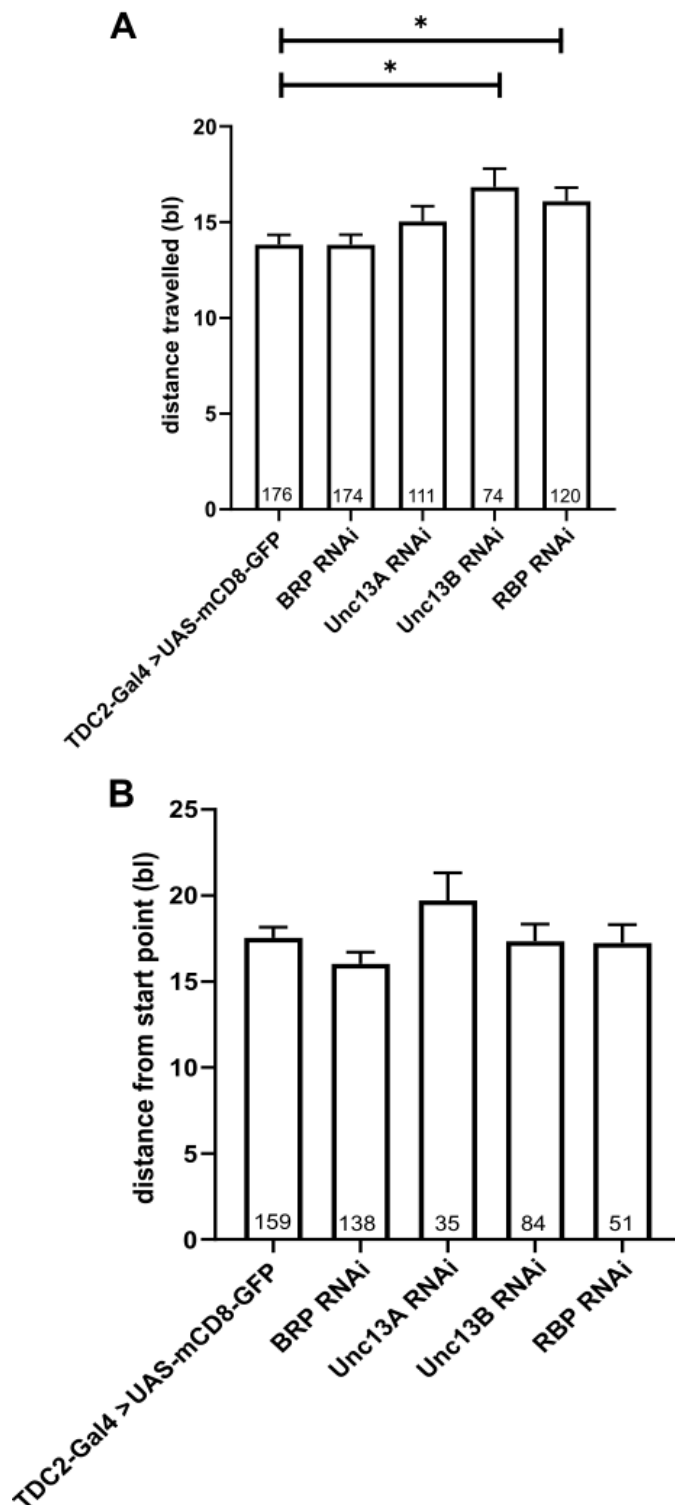
Figure 30: The distance travelled of Unc13B and RBP KD mutants increased while the distance from start point remained unaffected in all mutants.

(A) The distance travelled by the larvae only showed a slightly significant increase in Unc13B and RBP RNAi KD mutants. Unc13A KD mutants show slight increase in travelled distance, but not significant while BRP KD mutants remain similar to the control group. Control (n=176): 13.82 bl ± 0.5117 bl; *BRP-RNAi^{B3-C8}* (n=174): 13.82 bl ± 0.5331 bl, p > 0.9999; *Unc13A-RNAi* (n=111): 15.03 bl ± 0.8041 bl, p = 0.9605; *Unc13B-RNAi* (n=74): 16.82 bl ± 0.9687 bl, p = 0.0197; *RBP-RNAi* (n=120): 16.08 bl ± 0.72 bl, p = 0.0497. (B) Despite the increase in distance travelled, none of the mutants exhibit significant changes their distance from their start points, although Unc13A mutants show a slightly increased distance and BRP mutants a slight decrease, even if they're not significant. Control (n=159): 17.54 bl ± 0.6152 bl; *BRP-RNAi^{B3-C8}* (n=138): 16.03 bl ± 0.6667 bl, p = 0.2889; *Unc13A-RNAi* (n=35): 19.72 bl ± 1.593 bl, p = 0.4998; *Unc13B-RNAi* (n=84): 17.34 bl ± 0.9947 bl, p > 0.9999; *RBP-RNAi* (n=51): 17.23 bl ± 1.069 bl, p > 0.9999. All box plots show the mean with 10-90 percentiles ± SD; * p < 0.05, ** p < 0.01, *** p < 0.001. Significances indicated in comparison to control (TDC2-Gal4>UAS-mCD8-GFP) . Kruskal-Wallis test and Grubb's outlier test with α = 0.05 in (A and B). bl = body length.

Subsequently, we checked for the distance the larvae travelled in general and from their own start point (Figure 30). Here, we saw a significant increase in travelled distance in Unc13B (15.03 bl ± 0.8041 bl, p = 0.0197) and RBP (16.08 bl ± 0.72 bl, p = 0.0497) KD mutants, while BRP (13.82 bl ± 0.5331 bl) and Unc13A (15.03 bl ± 0.8041 bl) remained indifferent when compared to the control group (13.82 bl ± 0.5117 bl). This suggests that Unc13B and RBP KD mutants have increased locomotive capabilities. Regardless of the genotype, the distance of majority of the tested AZ protein KD mutants cover remained similar. Unc13B (17.34 bl ± 0.9947 bl) and RBP (17.23 bl ± 1.069 bl) showed barely any difference in travelled distance. Only Unc13A (19.72 bl ± 1.593 bl, p = 0.4998) showed a slight, but insignificant increase and BRP (16.03 bl ± 0.6667 bl, p = 0.2889) KD mutants a slightly insignificant decrease in distance travelled from the start point.
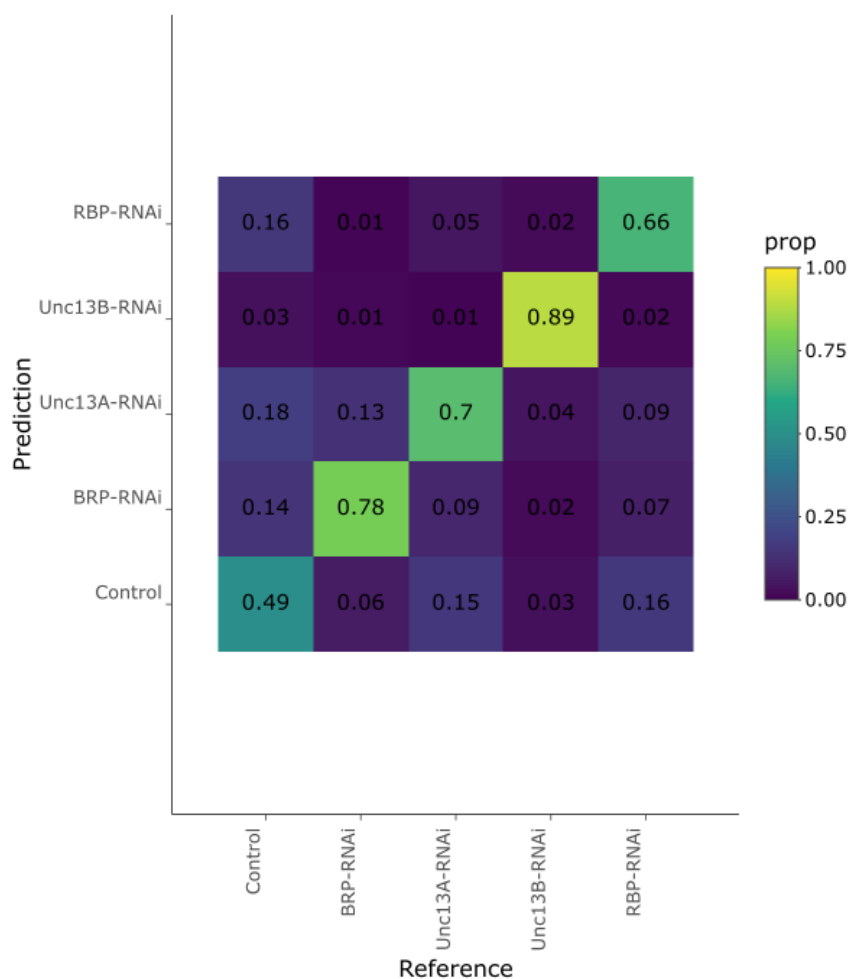
Figure 31: A confusion matrix of the random forest applied to the control group and the different KD mutants.

The confusion matrix used a set of 10 behavioural attributes (Interstep distance, head cast rate, crawling speed, distance travelled, interstep interval, interstep speed, tail forward velocity, head turning velocity, head forward velocity and distance from start point), to display predicted vs reference affiliation of individual larvae to the different genotypes and was run 10 times. Using these 10 sets of behavioural attributes the random forest could discriminate the five genotypes with an accuracy of 0.704. The accuracy is calculated as the average of the five correct assignment rates (0.49, 0.78, 0.7, 0.89 and 0.66).

Finally, we focused on seven specific locomotive behaviour (Absolute bending angle, interstep distance, interstep interval, head cast rate, crawling speed, head cast angle, head turning velocity), and wanted to extend our analysis, as the knockdown of the selected AZ proteins might have affected larval locomotion behaviour in more ways.

3. Results

Thus, we added some more parameters for the random forest and included distance from start point, tail forward velocity and head forward velocity. The random forest is an unbiased, machine-learning based approach to evaluate the behaviours that are the most decisive for differentiating between controls and mutants [4]. The random forest we could distinguish control and mutant larvae with an accuracy of 0.704 (Figure 31) and the three most decisive ones were interstep distance, head cast rate and crawling speed. Distance travelled, tail forwards velocity, head forward velocity and distance from start point were revealed to be interesting as well from our random forest, but did not show any significant differences, when tested.

To summarize the first part of my results, during pupal stages, type I terminal neurons appear to find their innervation target independently from OA/TA neurons and major reorganization of BRP signal (and possibly type I neuron innervation) on the muscle appear to be between P5 and P9 stage, as P12 pupa already show more structured presynaptic BRP alignment along the IFM. BRP KD or overexpression mutants did not affect L3 larval type II terminal bouton morphology, but a significant reduction in BRP quantity in BRP KD mutants within those boutons. The increase in BRP was not significantly higher, but a trend was visible in overexpression mutants. In STED images, a trend of BRP pattern of 2 to 3 spots were observed, albeit not quantified. Additionally, immunohistochemical staining against Unc13A and Unc13B did not show conclusive evidence of their presence inside OA/TA neurons in STED. Contrary, larval locomotive microbehaviour indicated the presence of both isoforms, as knockdowns of Unc13A and Unc13B, as well as RBP did show effects on locomotive behaviour. HC rate of BRP RNAi mutants were reduced, while Unc13A and Unc13B RNAi mutants' HC rate were increased, while the HC angle remained indifferent in all tested mutants. Only BRP KD mutants showed a slight, yet insignificant trend of an increased HC angle. The head turning velocity only increased in Unc13B KD mutants and IS interval reduced in all RNAi mutants, except for RBP RNAi mutants, while IS distance only showed a decrease in BRP and Unc13B RNAi mutants. Only the IS angle of BRP KD mutants were slightly decreased, while the other mutants remained indifferent. The different magnitude in IS interval and IS distance resulted in an increase in crawling speed in all mutants, except for BRP KD mutants. Lastly, when checked for the distance travelled, Unc13B and RBP RNAi mutants showed a slight increase in

93

travelled distance, while the distance from start point remained mainly the same, although slight trends were observable.

3.5 Effects of spermidine and dietary restriction on mitochondrial transport and brain redox state

Aging has been shown to be followed with decline in brain functions which also affect mitochondrial quality, and this has been associated with a possible increase in ROS production within the cell from mitochondria [364-366]. Previous studies have shown that spermidine exhibits anti-aging effects through an autophagy-dependent manner [313, 314, 320, 367-372]. In the second part of my thesis and as a continuation of my master's thesis, I first represent data from my master's thesis and then continue with additional data. Here, we investigated the effects of aging and spermidine on mitochondrial transport and mitochondrial number in adult fly wings. For this, we used a slightly modified protocol from Alessio Vagnoni and Simon L. Bullock's paper from 2016 [345] and analyzed these data with the help of a kymograph macro provided by Dr. Ulises Rey (ex-colleague, now at the IMP, Campus-Vienna-Biocenter). The flies tested were reared normally until they hatched into adults, where they were collected and then put in vials with 5 mM spermidine food or standard fly food. Following these experiments, we tested for effects of spermidine and dietary restriction using a redox sensor for GSH/GSSG, mito-roGFP2-Grx, and checked the oxidative stress levels in adult fly brains. The flies for these experiments were reared as mentioned on spermidine-containing food or not, and for dietary restriction experiments, flies were then put on 2% or 12% yeast food after hatching (data not shown here). In my master's thesis we could show that spermidine, as well as dietary restriction was able to reduce oxidative stress in aged flies (data not shown, my master's thesis, 2019). Here, we continue with the previous results and expand the already existing data from my master's thesis. We first repeated the supplementation of spermidine on adult fly but realized significantly different values than before. To investigate the unexpected results, we tested the range of our redox sensor (mito-roGFP2-Grx1) by fully oxidizing or reducing them via chemical agents. We also tested a different driver (elav-Gal4), which after some tests, came out as the better driver line to use our redox sensor, hence why following experiments, apart from the first set of data from my master's thesis will be continued with this driver.

3.5.1 Aging increases the average number of mitochondria in the L1 vein of adult fly wings.
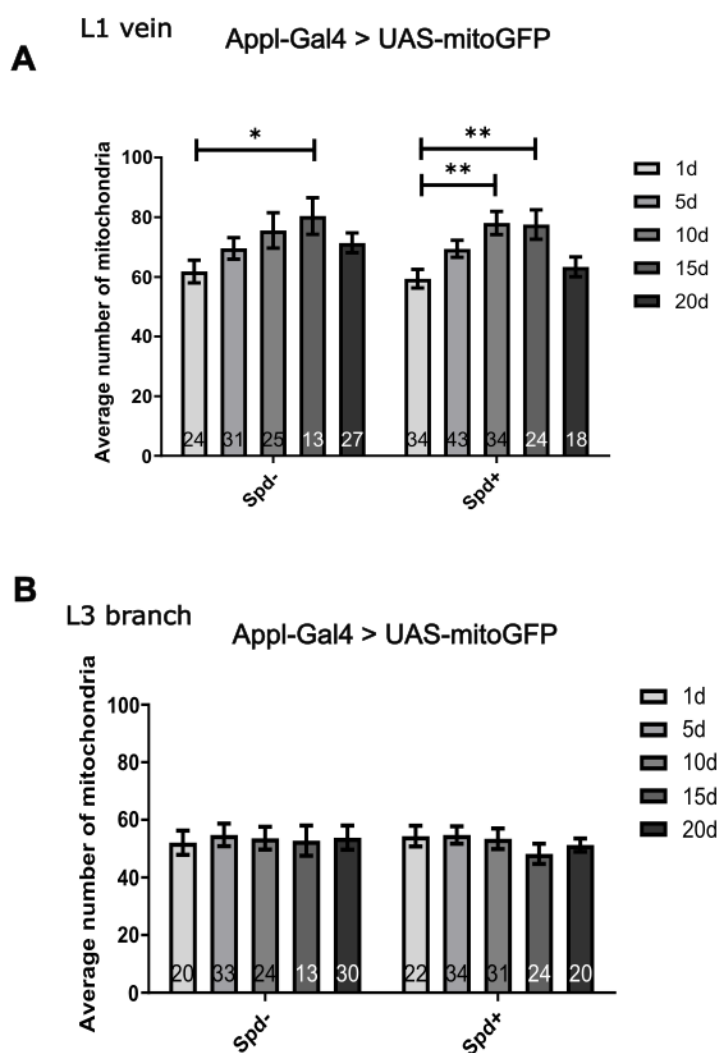
Figure 32: Aging shows an increase in mitochondrial number in L1 veins at later ages.

(A) Mitochondrial quantity shows a trend of increasing quantity within L1 vein area when aged until 15-days old flies, but a decrease in 20-days old flies. The fly cohort with spermidine supplementation showed a similar trend, where mitochondrial numbers increase with age, but at 10-days old flies it plateaus and shows a decrease from then on again. Unlike in flies without spermidine treatment, the difference between 10-days and 15-days old were significant when compared to 1-day old flies. Without spermidine: 1 day (n=24): 61.806 ± 3.809; 5 days (n=31): 69.559 ± 3.623, p = 0.6889; 10 days (n=25): 75.573 ± 5.931, p = 0.0861; 15 days (n=13): 80.397 ± 6.152, p= 0.0404; 20 days (n=27): 71.395 ± 3.326, p = 0.4082. With spermidine treatment: 1 day (n=34): 59.382 ± 3.101; 5 days (n=43): 69.403 ± 2.84, p = 0.1482; 10 days (n=34): 78.054 ± 3.891, p = 0.0011; 15 days (n=24): 77.549 ± 4.929, p = 0.0049; 20 days (n=18): 63.37 ± 3.341, p > 0.9999. (Legend continued next page)

3. Results

(B) Mitochondrial quantity did not change in the first branch at the L3 vein. Regardless of spermidine supplementation or not, mitochondrial number were relative constant even when aged. Without spermidine: 1 day (n=20): 52.1 ± 4.208; 5 days (n=33): 54.808 ± 3.899, p > 0.9999; 10 days (n=24): 53.653 ± 3.978, p > 0.9999; 15 days (n=13): 52.795 ± 5.233, p > 0.9999; 20 days (n=30): 53.8 ± 4.209, p > 0.9999. With spermidine treatment: 1 day (n=22): 54.364 ± 3.589; 5 days (n=34): 54.775 ± 3.049, p > 0.9999; 10 days (n=31): 53.452 ± 3.575, p > 0.9999; 15 days (n=24): 48.194 ± 3.501, p > 0.9999; 20 days (n=20): 51.267 ± 2.314, p > 0.9999. All graphs show the mean ± SEM; * p < 0.05, ** p < 0.01, *** p < 0.001. 2-way ANOVA with Bonferroni correction. SPD+ = with spermidine supplementation; SPD- = without spermidine supplementation; Significances indicated are in comparison to their control inside their group (1d without Spermidine and 1d with spermidine); d = days. N refers to mitochondria counted. Data already described and modified from my master's thesis, 2019.

Initial tests during my master's thesis in 2019 aimed to investigate the effects of spermidine and aging on mitochondrial transport. For this we used our driver line Appl-Gal4 in combination with the UAS-mitoGFP construct to visualize mitochondria with GFP. We looked at adult *Drosophila* wings and used the protocol of Simon L. Bullock [344] to record axonal transport of mitochondria in aged and spermidine treated flies (Figure 32A). We tested different aged flies ranging from 1 day up to 20-days old flies. Here, we checked two regions: the L1 vein at the upper region of the fly wing and the first branch at the L3 vein (Figure 19A). In the L1 vein, we observed a steadily increasing number of mitochondria in tested age groups. At 20-days old flies without spermidine treatment (71.395 ± 3.326), the mitochondrial number within the regions of interest decreased again, closer to the levels of 1-day old flies (61.806 ± 3.809), albeit slightly increased. 5-days (69.559 ± 3.623) and 10-days old flies (78.054 ± 3.891) show steady increases in mitochondrial quantity, while 15-days old flies show the highest number of mitochondria (80.397 ± 6.152) in the L1 vein. Interestingly, the steady increase in mitochondrial number plateaus at 10-days old flies in flies treated with spermidine and 15-days old flies showed a slight decrease, which in 20-days old is even more prominent. Non-spermidine flies only showed a significant increase in 15-days old flies (p = 0.0404) when compared to young flies (1d). Spermidine supplemented flies did, similarly to non-treated flies, show a steady increase in 5-days (69.403 ± 2.84) and significant increases in 10-days (78.054 ± 3.891, p = 0.0011) and 15-days (80.397 ± 6.152, p = 0.0049) old flies, when compared to 1-day old flies (59.382 ± 3.101). Just like the non-spermidine treated flies, 20-days old flies (63.37 ± 3.341,) show a decrease in mitochondrial quantity in L1 vein. When looking at the L3

96

branch (Figure 32B), we did not discover any significant differences in mitochondrial numbers, regardless of age or treatment. Barely any visible trends could be noticed, as the numbers remained very similar for all ages and treatments.

3.5.2 Spermidine and aging did not affect mitochondrial transport velocity nor number of stationary mitochondria.
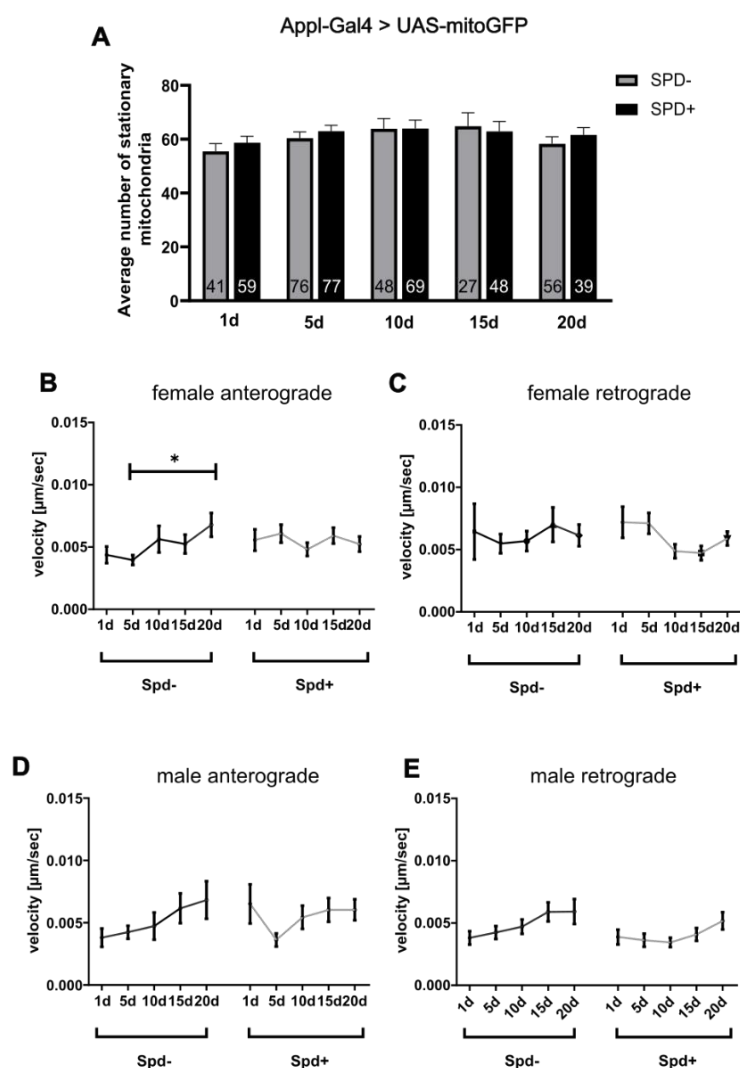
Figure 33: Average number of stationary mitochondria in L1 and L3 branch as well as mitochondrial transport velocity remained unchanged upon spermidine treatment and aging.

(A) Stationary mitochondria of both, L1 vein and L3 branch, remained around the same, regardless of dietary spermidine treatment and age. A subtle increasing trend until 15-days old flies can be observed, which then returns closer to values of young flies in 20-days old flies. Without spermidine treatment: 1 day (n=41): 55.512 ± 2.868; 5 days (n=76): 60.399 ± 2.316, p = 0.9843; 10 days (n=48): 63.875 ± 3.856, p = 0.283; 15 days (n=27): 64.858 ± 4.957, p = 0.3324; 20 days (n=56): 58.292 ± 2.601, p > 0.9999. With spermidine treatment: 1 day (n=59): 58.178 ± 2.363, p > 0.9999; 5 days (n=77): 62.944 ± 2.228, p > 0.9999; 10 days (n=69): 63.959 ± 3.112, p = 0.6964; 15 days (n=48): 62.872 ± 3.678, p > 0.9999; 20 days (n=39): 61.65 ± 2.624, p > 0.9999. **(B, C, D and E)** Regardless of anterograde or retrograde transport and fly gender, no significant difference were observed with age and spermidine supplementation. (Legend continued next page)

3. Results

Only in 5-days old female flies without spermidine treatment were anterograde transport slower than 5-days old female flies with spermidine supplementation. Furthermore, 20-days old female flies also showed a slightly significant decrease in mitochondrial transport velocity compared to 5-days old ones, when supplemented with spermidine food. **(B)** Without spermidine: 1d (n=46): 0.004374 µm/s ± 0.0006655 µm/s; 5d (n=116): 0.003962 µm/s ± 0.0003965 µm/s, p > 0.9999 ; 10d (n=21): 0.005633 µm/s ± 0.001065 µm/s, p > 0.9999 ; 15d (n=41): 0.005244 µm/s ± 0.0007506 µm/s, p > 0.9999 ; 20d (n=73): 0.006781 µm/s ± 0.0009453 µm/s, p > 0.9999. 5d spd- vs 20d spd-: p = 0.0276. With spermidine: 1d (n=47): 0.005564 µm/s ± 0.0008547 µm/s; 5d (n=85): 0.006076 µm/s ± 0.0007143 µm/s, p > 0.9999 ; 10d (n=64): 0.004811 µm/s ± 0.0005352 µm/s, p > 0.9999 ; 15d (n=66): 0.005918 µm/s ± 0.0006410 µm/s, p > 0.9999 ; 20d (n=80): 0.005235µm/s 0.0006052 µm/s, p > 0.9999. **(C)** Without spermidine: 1d (n=30): 0.006443 µm/s ± 0.002232 µm/s; 5d (n=61): 0.005477 µm/s ± 0.0007656 µm/s, p > 0.9999 ; 10d (n=26): 0.005685 µm/s ± 0.0007990 µm/s, p > 0.9999 ; 15d (n=40): 0.006998 µm/s ± 0.001385 µm/s, p > 0.9999 ; 20d (n=54): 0.006137 µm/s ± 0.0008650 µm/s, p > 0.9999. With spermidine: 1d (n=68): 0.007194 µm/s ± 0.001249 µm/s; 5d (n=62): 0.007108 µm/s ± 0.0008352 µm/s, p > 0.9999 ; 10d (n=62): 0.004871 µm/s ± 0.0005595 µm/s, p > 0.9999 ; 15d (n=59): 0.004720 µm/s ± 0.0005752 µm/s, p > 0.9999 ; 20d (n=94): 0.005888 µm/s ± 0.0005532 µm/s, p > 0.9999 **(D)** Without spermidine: 1d (n=27): 0.003804 µm/s ± 0.0007299 µm/s; 5d (n=82): 0.004239 µm/s ± 0.0005184 µm/s, p > 0.9999 ; 10d (n=7): 0.004729 µm/s ± 0.001090 µm/s, p > 0.9999 ; 15d (n=23): 0.006161 µm/s ± 0.001194 µm/s, p > 0.9999 ; 20d (n=42): 0.006824 µm/s ± 0.001505 µm/s, p > 0.9999. With spermidine: 1d (n=22): 0.006514 µm/s ± 0.001569 µm/s; 5d (n=51): 0.003616 µm/s ± 0.0005230 µm/s, p > 0.9999 ; 10d (n=27): 0.005437 µm/s ± 0.0009366 µm/s, p > 0.9999 ; 15d (n=39): 0.006028 µm/s ± 0.0009495 µm/s, p > 0.9999 ; 20d (n=53): 0.006033 µm/s ± 0.0008438 µm/s, p > 0.9999. **(E)** Without spermidine: 1d (n=28): 0.003807 µm/s ± 0.0005406 µm/s; 5d (n=82): 0.004239 µm/s ± 0.0005184 µm/s, p > 0.9999 ; 10d (n=29): 0.004710 µm/s ± 0.0005759 µm/s, p > 0.9999 ; 15d (n=45): 0.005898 µm/s ± 0.0007625 µm/s, p > 0.9999 ; 20d (n=74): 0.005920 µm/s ± 0.0009976 µm/s, p > 0.9999. With spermidine: 1d (n=54): 0.003876 µm/s ± 0.0005894 µm/s; 5d (n=51): 0.003616 µm/s ± 0.0005230 µm/s, p > 0.9999 ; 10d (n=56): 0.003446 µm/s ± 0.0003741 µm/s, p > 0.9999 ; 15d (n=60): 0.004083 µm/s ± 0.0005145 µm/s, p > 0.9999 ; 20d (n=81): 0.005174 µm/s ± 0.0006940 µm/s, p > 0.9999. All graphs show the mean ± SEM; * p < 0.05, ** p < 0.01, *** p < 0.001. 2-way ANOVA with Dunn's correction. SPD+ = with spermidine supplementation; SPD- = without spermidine supplementation; d = days. N refers to mitochondria counted. Significances indicated are in comparison to their control inside their group (1d without Spermidine and 1d with spermidine). Data already described, but reanalyzed and modified, from my master's thesis, 2019.

To further investigate the mitochondrial quality, we checked for the stationary mitochondria within our tested regions. Here, we took together both regions, L1 vein and L3 branch, and manually counted the moving mitochondria and subtracted them from our total observed mitochondria. We used 3 frame points of our recorded stacks: the 5th, 50th and 150th frame and averaged the number of mitochondria and manually checked the amount of retrograde or anterograde moving mitochondria (Figure 33A).

99

3. Results

We saw no significant increases in stationary mitochondria quantity among all ages and treatments. Interestingly, we could observe a non-significant, but slightly increasing trend of mitochondria until 15-days old flies, which was absent in 20-days old flies again. Following these results, we checked for the velocity of the moving mitochondria (Figure 33B, C, D, E). Here, we saw that only in female flies, did anterograde transport velocity of mitochondria show a slightly significant increase in 20-days old flies (0.006781 µm/s $\pm$ 0.0009453 µm/s, $p = 0.0276$) when compared to 5-days old ones (0.003962 µm/s $\pm$ 0.0003965), when no spermidine was supplemented. This significant increase in velocity was abolished with spermidine-treatment. The retrograde transport in female flies, in comparison, did not exhibit such a trend, as well as the retrograde and anterograde moving mitochondria in male flies. Interestingly, we observed a slightly increasing trend in velocity in male flies and surprisingly a drastic, but insignificant decrease in 5-days old, spermidine treated, anterograde transport velocity. Overall, we were not able to see any significant or obvious effects in mitochondrial transport and stationary numbers with age and spermidine supplementation.

3.6 Redox experiments in fly brains with the Appl-Gal4 driver line showed inconsistent results.
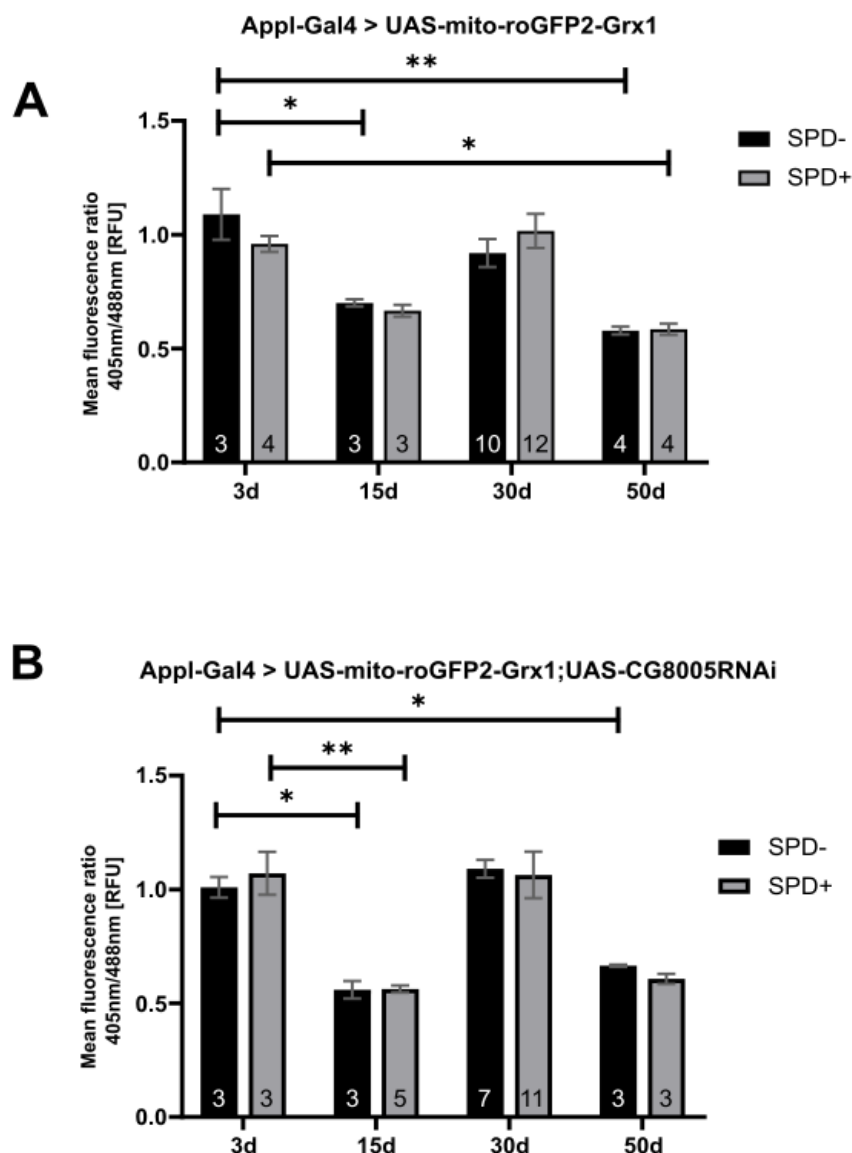
Figure 34: Aging experiments along with dietary spermidine supplementation showed inconsistent fluorescence ratio in different ages.

(A) Mean fluorescence ratio shows unusual differences between 3d, 30d and 15d, 50d old flies in our sensor construct. 3d old flies and 15d old flies' redox ratio were significantly higher than 15d and 50d old ones, Without spermidine: 3d old flies (n=3): 1.089 RFU ± 0.111 RFU; 15d (n=3): 0.701 RFU ± 0.016 RFU, p = 0.0353; 30d (n=10): 0.919 RFU ± 0.062 RFU, p = 0.3494 ; 50d (n=4): 0.579 RFU ± 0.018 RFU, p = 0.0024.With spermidine: 3d (n=4): 0.96 RFU ± 0.035 RFU; 15d (n=3d): 0.666 ± 0.026, p = 0.1077; 30d (n=12): 1.017 RFU ± 0.075 RFU, p = 0.9008; 50d (n=4): 0.585 RFU± 0.025 RFU, p = 0.0181. **(B)** The mean fluorescence ratio in deoxyhypusine synthase knockdown (CG8005RNAi) mutants also fluctuates like the control group. (Legend continued next page)

3. Results

Without spermidine: 3d old flies (n=3): 1.009 RFU ± 0.046 RFU; 15d (n=3): 0.559 RFU ± 0.039 RFU, p = 0.0319; 30d (n=7): 1.091 RFU ± 0.039 RFU, p = 0.8862; 50d (n=3): 0.665 RFU ± 0.005 RFU, p = 0.1209. With spermidine: 3d old flies (n=3): 1.071 RFU ± 0.094 RFU; 15d (n=5): 0.563 RFU ± 0.016 RFU, p = 0.0056; 30d (n=11): 1.064 RFU ± 0.102 RFU, p > 0.9999; 50d (n=3): 0.607 RFU ± 0.022 RFU, p = 0.0253. All graphs show the mean ± SEM; * p < 0.05, ** p < 0.01, *** p < 0.001. 2-way ANOVA with Dunn's correction. SPD+ = with spermidine supplementation; SPD- = without spermidine supplementation; d = days. Significances indicated are in comparison to their control inside their group (1d without Spermidine and 1d with spermidine).

To further investigate mitochondrial quality in aged flies with and without dietary spermidine supplementation, we used the mito-roGFP2-Grx1 construct to determine the oxidative stress levels within adult fly brains. Here, we saw unusual fluctuations between tested ages, regardless of treatment or not. We saw significantly lower mean fluorescence ratio in 15-day and 50-days old flies, regardless of spermidine supplementation or not. The same phenomenon was observed in our CG8005RNAi mutant flies. We saw, just like in our control group, unusual lower mean fluorescence ratio in 15-day and 50-days old flies. Due to these findings, we decided to test our sensor with different driver lines. We used Appl-Gal4 to recheck the driver line in combination with our construct mito-roGFP2-Grx1 and additionally used another driver, elav-Gal4, to rule out that the fluctuations might be the result of our driver line.

3.6.1 Sensor test of Appl-Gal4 driver line shows high fluorescence ratio in younger adult flies.
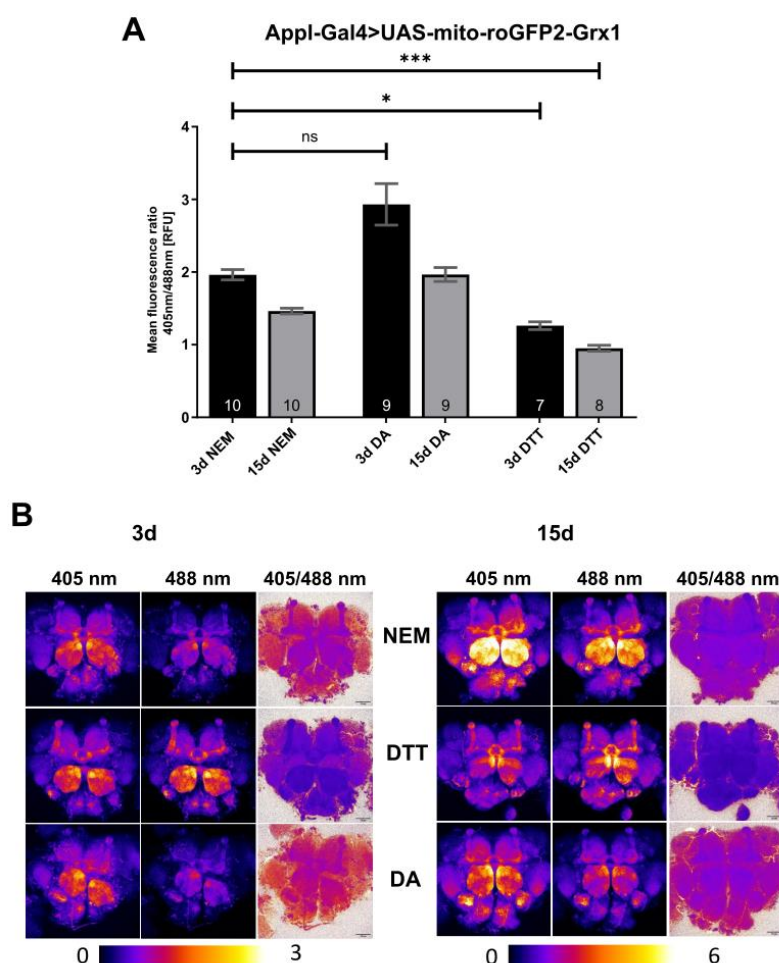
Figure 35: Redox sensor tests with Appl-Gal4 driver line reveal high fluorescence ratio in younger flies.

(A) To determine the range of our redox sensor, NEM was used to stop GSH autooxidation, DA to fully oxidize and DTT to fully reduce disulfide bonds. Flies driven with Appl-Gal4 showed high fluorescence ratio in especially 3-days old flies while previous experiments showed a tremendously lower mean ratio of around 1 RFU (data not shown). NEM: 3d (n=10): 1.953 RFU ± 0.07 RFU; 15d (n=10): 1.463 RFU ± 0.03972 RFU, p = 0.1108; DA: 3d (n=9): 2.932 RFU ± 0.2852 RFU, p = 0.539; 15d (n=9): 1.967 RFU ± 0.09563 RFU, p > 0.9999; DTT: 3d (n=7): 1.262 RFU ± 0.05332 RFU, p = 0.0205; 15d (n=8): 0.951 RFU ± 0.0415 RFU, p = 0.0001. **(B)** Representative fluorescence images of adult fly brains in 405 and 488 nm channels and their ratio pictures with their corresponding chemical treatments. Scale bar: 50 µm. All graphs show the mean ± SEM; * p < 0.05, ** p < 0.01, *** p < 0.001. Kruskal-Wallis tests with Dunn's correction. SPD+ = with spermidine supplementation; SPD- = without spermidine supplementation; d = days. Significances indicated are in comparison to their control inside their group (1d without Spermidine and 1d with spermidine treatment).

3. Results

Upon testing our current driver line, we saw a high fluorescence ratio overall (Figure 35A). Values ranged from 1.262 RFU ± 0.05332 RFU in DTT (the reduced form) up to 2.932 RFU ± 0.2852 RFU (the oxidized form), which was very unusual. Normally the mean fluorescence ratio ranges from around 0.6 to 2.0 RFU maximum. Surprisingly, we also saw higher mean fluorescence ratio in younger flies (3d) than in older flies (15d) in all tested groups (NEM, DA, DTT), which was contrary to the results we saw previously in my master's thesis. Furthermore, when we observed the brain images in Figure 35B, we saw that our fluorescence ranges from 0 to 6 RFU, instead of normally 0 to 3. It was very unlikely for younger flies to exhibit higher oxidative stress than older flies, hence we were skeptical about these results. To check whether our construct was working correctly, we tested the same with another driver, elav-Gal4.

3.7 Redox sensor test with another driver line (elav-Gal4)
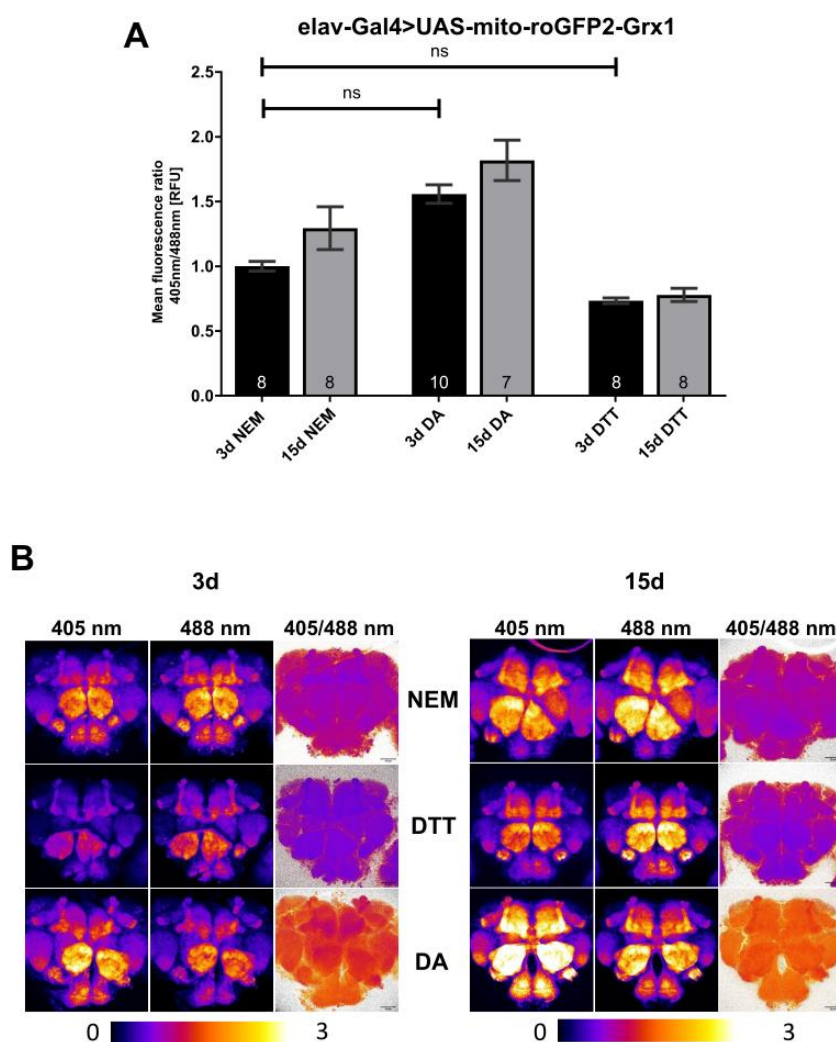
Figure 36: Test of our redox sensor in elav-Gal4 driven flies shows the redox-sensor range more reliably.

(A) Upon driving our sensor with elav-Gal4, we did not see significant differences after treatment of either chemical, DA or DTT, but saw the expected changes with those treatments. The mean fluorescence ratio showed an increase in 15-days old flies across all treatment, confirming the functionality of our redox sensor. NEM: 3d (n=8): 1 RFU ± 0.037 RFU; 15d (n=8): 1.294 RFU ± 0.1654 RFU, p > 0.9999; DA: 3d (n=10): 1.558 RFU ± 0.07153 RFU, p = 0.1776; 15d (n=7): 1.818 RFU ± 0.1562 RFU, p = 0.0517; DTT: 3d (n=8): 0.7331 RFU ± 0.02187 RFU, p = 0.157; 15d (n=8): 0.7788 RFU ± 0.05083 RFU, p = 0.5185. **(B)** Representative mean fluorescence images of 405 and 488 nm channels and their ratio picture when treated with NEM, DTT or DA. Scale bar: 50 µm. All graphs show the mean ± SEM; * p < 0.05, ** p < 0.01, *** p < 0.001. Kruskal-Wallis tests with Dunn's correction. SPD+ = with spermidine supplementation; SPD- = without spermidine supplementation; d = days. Significances indicated are in comparison to their control inside their group (1d without Spermidine and 1d with spermidine treatment).

Due to the results, we saw with our previous driver line, Appl-Gal4, we decided to use elav-Gal4 as another driver to test our redox-sensor construct mito-roGFP2-Grx1, if that construct has any flaws. We did the same experiment (Figure 36) as we did with our previous driver line (Figure 35) and saw very different results. Using the new driver line, we saw our usual mean fluorescence range of around 0.6 to almost 2 RFU and, more importantly, an increase in fluorescence ratio in aged flies. The changes in fluorescence ratio when treated with DTT or DA were not significant, which were within our expectations, as 15-days old flies are not very old animals and shouldn't be experiencing too much oxidative stress with this age. When the flies were treated with DA to fully oxidize disulfide bonds, we saw a strong, but still insignificant increase in 15-days old flies (1.818 RFU ± 0.1562 RFU, $p = 0.0517$) in fluorescence ratio when compared to 3-day old NEM treated flies (1 RFU ± 0.037 RFU). The opposite is true for DTT-treated flies when disulfide bonds are chemically reduced. We also saw a strong reduction in mean fluorescence ratio, which was still barely insignificant in 15-days old DTT-treated flies (0.7788 RFU ± 0.05083 RFU, $p = 0.5185$) when compared to our 3d-old fly treated with NEM (1 RFU ± 0.037 RFU). In the ratio images in Figure 36B, we can also see that the ratio range returned to the usual 0-3 RFU range, unlike with our previous driver line, that had a range up to 6 RFU. These results led us to continue the following experiments with this driver line, as it confirms that our redox-sensor mito-roGFP2-Grx1 is working normally.

3.8. Knockdown of DHPS slightly increased adult flies' brain redox state.
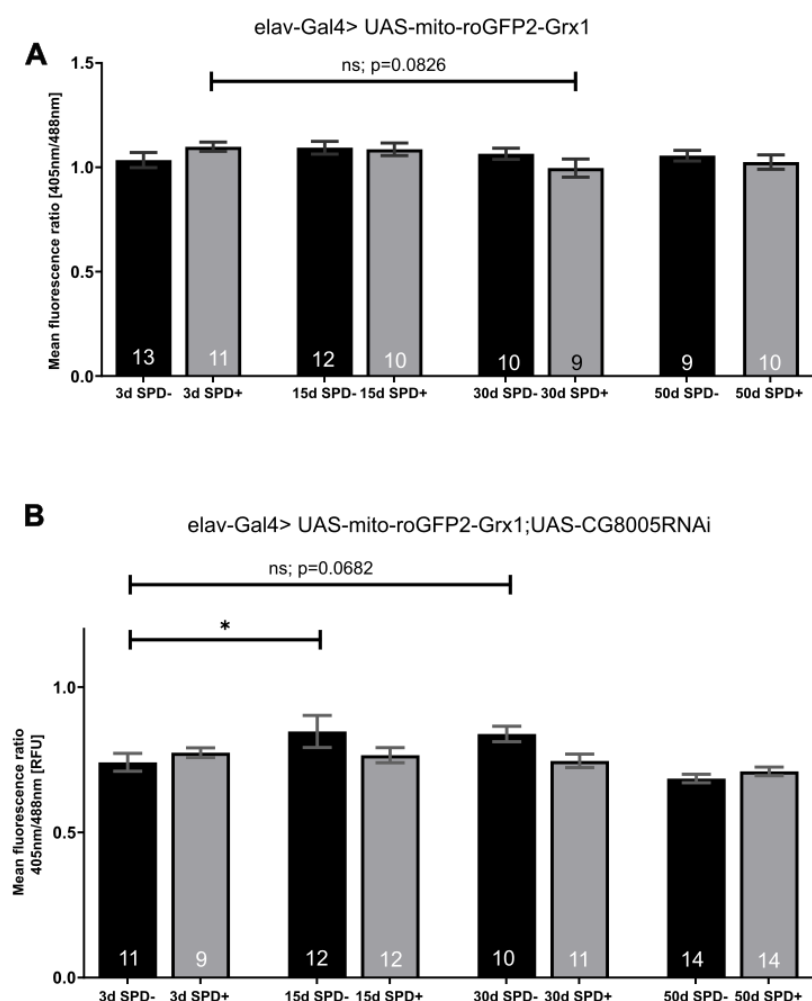
Figure 37: Knockdown of Deoxyhypusine synthase did not majorly affect redox state in adult fly brain.

(A) Upon aging in our control group, did the redox state of the brain stay relatively similar. Even with spermidine supplementation did the brain's redox state show not much difference. A slight decrease in oxidative stress can be observed in 30-days old flies fed with spermidine, albeit not significant. Without spermidine treatment: : 3d old flies (n=13): 1.035 RFU ± 0.037 RFU; 15d (n=12): 1.094 RFU ± 0.031 RFU, p = 0.3604; 30d (n=10): 1.065 RFU ± 0.027 RFU, p = 0.8386; 50d (n=9): 1.056 RFU ± 0.025 RFU, p = 0.9395.With spermidine: 3d (n=11): 1.099 RFU ± 0.022 RFU; 15d (n=10): 1.087 ± 0.03, p = 0.9867; 30d (n=9): 0.997 RFU ± 0.043 RFU, p = 0.0826; 50d (n=10): 1.025 RFU± 0.034 RFU, p = 0.2562. **(B)** Upon knocking down deoxyhypusine synthase, the mean fluorescence ratio was overall in all groups lower when compared to the control group in (A). 15-days old flies showed a slightly significant increase in oxidative stress when compared to 3-day young flies and 30-days old flies were barely insignificant, when treated without spermidine. Flies with dietary spermidine supplementation showed barely any differences across all ages. (Legend continued next page)

Without spermidine treatment: : 3d old flies (n=11): 0.741 RFU ± 0.031 RFU; 15d (n=12): 0.847 RFU ± 0.055 RFU, p = 0.0317; 30d (n=10): 0.839 RFU ± 0.027 RFU, p = 0.0682 ; 50d (n=14): 0.685 RFU ± 0.015 RFU, p = 0.3631.With spermidine: 3d (n=9): 0.774 RFU ± 0.023 RFU; 15d (n=12): 0.766 ± 0.026, p = 0.9952; 30d (n=11): 0.746 RFU ± 0.023 RFU, p = 0.8581; 50d (n=14): 0.71 RFU± 0.015 RFU, p = 0.2964. 2-way ANOVA with Dunn's correction. SPD+ = with spermidine supplementation; SPD- = without spermidine supplementation; d = days. Significances indicated are in comparison to their control inside their group (1d without Spermidine and 1d with spermidine).

Using our new driver line, we repeated the aging and spermidine experiment for our control group and our CG8005RNAi mutant that we did in Figure 34 and saw rather different results than before. Upon aging, without spermidine supplementation, we did not see any significant changes in oxidative stress levels across ages. Here, we only saw a slight increase in mean fluorescence ratio in 15-days (1.094 RFU ± 0.031 RFU, p = 0.3604), 30-days (1.065 RFU ± 0.027 RFU, p = 0.8386) and 50-days old flies (1.025 RFU± 0.034 RFU, p = 0.2562): 1.056 RFU ± 0.025 RFU, p = 0.9395) when compared to the 3-day young flies (1.035 RFU ± 0.037 RFU), albeit not significant. Flies with spermidine supplementation also didn't show significant differences in 15d (1.087 ± 0.03, p = 0.9867), 50d (1.056 RFU ± 0.025 RFU, p = 0.9395) but an almost significant decrease in mean fluorescence ratio can be seen in 30d-old flies (0.997 RFU ± 0.043 RFU, p = 0.0826) when compared to 3d-old flies (1.099 RFU ± 0.022 RFU). In CG8005RNAi mutants, a different picture can be seen. The absence of dietary spermidine supplementation resulted in a slightly significant increase in oxidative stress in 15-days (0.847 RFU ± 0.055 RFU, p = 0.0317) and an almost significant increase in 30-days old flies (0.839 RFU ± 0.027 RFU, p = 0.0682), while 50-days old flies (0.685 RFU ± 0.015 RFU, p = 0.3631) surprisingly showed an even less mean fluorescence ratio when compared to 3-day young flies (0.741 RFU ± 0.031 RFU). Interestingly, CG8005RNAi mutants showed, when compared to the control group, less mean fluorescence ratio. Whereas the fluorescence ratio of the controls ranges from 1.0 to 1.1 RFU, did the DHPS KD mutants show a range of around 0.67 to 0.85 RFU. The reduction of DHPS by genetically knocking it down resulted in a significant increase in oxidative stress in 15-days old flies, and an almost significant increase in 30-days old flies.

4. Discussion

4.1 Type I innervation dissolves ahead of OA/TA neurons during metamorphosis

In the first part of my discussion, I'd like to discuss the first half of my thesis that investigates the release machinery in type II terminal neurons. Previous studies have shown that unlike vertebrate skeletal muscle that are innervated by excitatory cholinergic motor neurons, insect skeletal muscles are innervated by glutamatergic excitatory motor neurons which may receive additional innervation by neuromodulatory or inhibitory neurons [131, 373, 374]. Majority of the neuromodulatory neurons tend to be using the biogenic amine octopamine as neurotransmitter. In *Drosophila melanogaster* larvae, three different types of axon terminals have been discovered, the type I terminal (further subdivided into Is and Ib [14, 169, 375, 376]) that stems from glutamatergic motor neurons forming the NMJs [103, 377, 378], some special neuromodulatory, peptidergic type III terminals [379, 380] and type II terminals that include most of the neuromodulatory axon terminals, such as octopaminergic neurons [115, 169]. These octopaminergic neurons show great dynamic capabilities by extending and building new synaptopods in response to starvation of 2-6 hours and has been shown to use synaptopod extension as a mechanism for expanding type II arbors during larval development [1, 17, 141] and origin from a certain class of unpaired median neurons and possess bilaterally symmetrical axons which cell bodies can be positioned either dorsally (DUM) or ventrally (VUM). The biogenic amine Octopamine is known as an important modulator in the CNS contributing to activation of CPG for flight [159] and its antagonistic relationship with its precursor tyramine [131, 132, 164]. Regardless of terminal type, glutamatergic and OA/TA neurons experience the same fate during metamorphosis, where dramatic changes and histolysis of almost all muscles take place. In my thesis, I imaged different pupal phases and was able to observe a rough temporal and spatial pattern of glutamatergic and OA/TA neuron interplay during pupal stages. During P2, where the puparium starts histolysis of larval muscles, the branch at muscle 12 was void of BRP signal from type I terminals and only further away were some remaining boutons left, albeit with unusual formation. Type I terminals in larval muscles usually show circular forms of BRP rings, which was only partly the case in P2 pupa. The BRP rings didn't show the typical phenotype at synaptic boutons and the missing innervation at muscle 12 branch indicates the dissolving of type I terminal neurons ahead of type II terminal neurons.

4. Discussion

Following the retraction of neurons during P2 pupal stage, P5 pupa already show IFM-like muscles, with thin arborization of octopaminergic/tyraminergic neurons. Interestingly, these extensions of the neuron did not show axonal thickenings resembling larval synaptopods and it was not distinguishable whether the BRP signal were in proximity of the extending neurons or within. Additionally, there were also BRP formations further away from these OA/TA neurons in an already organized form which could suggest an independence from octopaminergic neurons in target-finding during metamorphosis. Interestingly, P7 pupa show increased amount of BRP signal all over the IFMs with rather ragged octopaminergic neuron appearance. The BRP signal in P7 pupa is remarkably higher than in P5 and the BRP signal appears stochastically distributed, contrary to the organized BRP forms seen in P5. In P9, BRP signal seemed to decrease and BRP showed more organized structures again, suggesting the retraction of incorrect targeting sites. The images of P12 pupa and P14 flies supports this idea, as BRP signal starting in P7 pupa progressively decreased along the IFM. These observations, could be linked to a previous work of D.W. Williams and J.W. Truman in 2005 where they refer the remodelling of larval neurons as "cellular metamorphosis" [381]. Here, they also refer back to the paper of Bagri et al. from 2003, that describes the phenomenon in hippocampus of vertebrate CNS of "stereotyped pruning" which, contrary to local pruning refers to the neuronal axons whose growth cone is guided towards an initial target and subsequently pruned back during development [382]. During *Drosophila*'s embryogenesis, neurons extend and form initial axonal and dendritic arbors that grows along the growing muscles. When metamorphosis starts, those larval arborization are pruned back and through an outgrowth of motoneuron growth cone, adult-specific arbors are generated [206, 381]. These described events are likely the observed events in my experimental approach. Similarly, to the pruning events described, glutamatergic and OA/TA neurons regress from the muscle as metamorphosis starts and during metamorphosis, through motoneuronal growth cone extension, innervation of muscle takes place through "trial and error" where individual growth cones may encounter not intended targets. Through molecular cues and intracellular signalling processes within the growth cone, an initiation of synaptogenesis takes place at intended targets, while the incorrect ones are then bypassed [206]. This likely also happens with glutamatergic and octopaminergic neurons here. We saw an increase in BRP signal all over the IFM during P7 that decreases over the following pupal stages (P9, P12, P14). This seems

110

to be the case here as well, where first innervations retract by stereotyped pruning and then adult-like arbors are extended to find their appropriate innervation partner. The images of P5, P7, P9, P12 and P14 suggest that the GFP labelled octopaminergic neurons do not show an obvious guidance of glutamatergic neurons during metamorphosis. The images indicate either a target-finding independent of each other, or even the reverse case, where glutamatergic neurons might be the one guiding OA/TA neuron innervation during pupation. From the data we collected, there is no decisive conclusion that can be made concerning the dependence of innervation of glutamatergic and OA/TA neurons during pupal development, despite their proximity. This thesis only gives a rough overview of temporal and spatial distribution of glutamatergic and OA/TA neuron innervation throughout the pupal stages. The results we found indicate the independence of innervation target finding during metamorphosis, and the chaotic BRP expression during P7 stage could indicate signs of the previous described "stereotyped pruning" events, where the outgrowth of motoneurons to innervate the periphery, takes place. An interesting experiment to further elaborate this subject would be to impair octopamine synthesis with e.g. a mutation in the tyramine β-hydroxylase gene (Tβh-null) and observe the innervation of the OA/TA motoneurons during the pupal stages. Here, the abdominal muscle innervation of female *Drosophila* flies might be an interesting target, as Tβh-null mutants show that even though flies survive to adulthood and male flies remain fertile, female mutant flies become sterile and an impaired egg-retention due to OA deficit [140]. Notably, it was previously reported that TDC2 neurons are in contact with larval crawling motor neurons and show indications of presynaptic release sites of TDC2 neurons contacting motoneuron dendrites [141]. This suggests that TDC2 neurons are in communication with motoneurons, linking the possibility of additional interactions between OA/TA neurons and motoneurons during metamorphosis as the growth cone of motoneuron branches out and starts innervating the periphery first. Additionally, it was shown that TA reduces the excitability of motoneurons and that this effect is fully reversible, while OA did not exhibit to have any effects on motoneuron excitability [141]. One could test the importance of tyraminergic modulation on motoneurons during pupal stages by observing if the innervation of glutamatergic or OA/TA neurons is affected in a *honoka* mutant. Honoka (CG7485) is one of the three G-protein coupled TA receptor that has been suggested to be the receptor to mediate the TA effects on motoneuron excitability and is therefore of interest [136, 141]. If the removal of

111

modulation of OA/TA neurons doesn't show any effects on innervation of neurons with type I and type II terminals during metamorphosis, it could indicate that the images shown in this thesis would suggest the idea that during pupal stages, both terminals and neurons find their innervation target independently and possibly even at different pupal stages, since OA/TA neurons didn't show an "overgrowth" at the muscle, unlike the BRP signal at the muscle.

Another experiment that could be added to this subject would be generating cell-death protein head involution defective (Hid) expressing mutant flies in OA/TA neurons to abolish them and observe the innervation of type I terminals throughout the metamorphosis. If the elimination of OA/TA neurons affect glutamatergic neuronal target-finding during pupal stage, this might indicate a dependence or that certain modulation might be needed from OA/TA neurons during metamorphosis.

4.2 Active zone proteins in OA/TA neurons at the larval NMJ

Plenty of prior works have already described type I terminal active zone proteins, AZ scaffolding and structure [25, 28, 48, 49, 59, 74, 383, 384] in *Drosophila*, but only few have described type II terminals in more detail [1, 17, 115]. Previous works have shown that BRP is a core protein used in active zone scaffolding and release in type I terminals at larval NMJ [48-50]. BRP was also found to be in type II terminals of OA/TA neurons at the larval NMJ [1, 17], providing me with the question what role BRP has in type II terminals. In ultrastructural images of type I terminals, an electron-dense structure can be seen, often referred to as T-bar that's an accumulation of active zone protein at the active zone cytomatrix [385]. A similar structure is missing in electron microscopic pictures of type II terminals, even though BRP, a presynaptic AZ protein, is available in those terminals [17]. Here, I inspected the BRP signal in OA/TA neurons with STED microscopy and could show a better resolution of the BRP signal in type II boutons. Through the analysis of images with better resolution, I was able to observe that the control group shows an average of 1.75 BRP spot per type II bouton, which supports the observations in confocal images of synaptopods containing 1 BRP spot per bouton. With better resolution in STED images, we can observe that it isn't necessarily only 1 BRP labelling per bouton, but often also 2 and sometimes 3 BRP spots in control flies. Not always were the BRP spots close in proximity that could resemble the BRP "doughnut" in type I terminals when stained for BRP[NC82] [48], but sometimes they were even positioned at opposite sides of the bouton in type II

terminals. Here, it is not clear, if the phenomenon of seeing 2 close BRP spots or not in a synaptopod could be due to different view of the AZs (planar or not). As expected, when knocking down BRP in OA/TA neurons, BRP spots disappeared in almost all type II boutons. The remaining BRP spots did not show any alteration in diameter nor width when compared to the control group. Similar results were observed in a BRP overexpression situation, where the BRP spot diameter and width were similar to the control group. The overexpression of BRP in OA/TA neurons did slightly increase the amount of BRP spots within type II boutons. Interestingly, a trend where two or three BRP spots in proximity could be observed in some cases. Here, I show that BRP in type II boutons show single BRP spots when stained with BRP^{NC82}, and occasionally also 2 or 3 spots in a single type II bouton. A knock down of BRP in OA/TA neuron didn't change BRP spot diameter and width, as well as synaptopod morphology itself, but as expected a decrease in BRP labelling. An interesting experiment to continue this project would be staining for the N-term of BRP, as every staining here was done with BRP^{NC82}. Previous work showed that BRP$^{N\text{-}term}$ staining didn't show a "doughnut"-shaped distribution when imaged with STED but would appear within the "doughnut hole" [48]. Here, I would suggest staining both, N-term, and C-term at once, and check whether it is possible to identify BRP when stained at different terms at once with STED microscopy in type II boutons, as the dimensions are different from type I terminals. In type I terminals, a clear BRP structure can be seen which also shows in electron microscopic images as an electron-dense T-bar structure, showing a considerable number of proteins at work. Contrary to type I terminals, since such an electron-dense structure at release sites is missing in type II terminals, the release machinery in type II terminals is likely to have a less packed release apparatus than in type I boutons. This is also conform with the dimensions of the boutons, as it was previously reported that type I terminal's bouton diameter size can range from 3 µm up to 5 µm (3.1 µm ± 1.6 µm) with a maximum of 8 µm and can be further subdivided into type Ib (2-5 µm) and type Is (1-3 µm) [137], while the much smaller type II boutons were reported to have diameters of 1 µm to 2 µm (1.4 µm ± 0.6 µm) [386]. Like previous findings, I can confirm that type II terminal bouton diameter size is in average 1.16 µm ± 0.3902 µm, supporting previous publications. The knock down of BRP or overexpression did not affect type II bouton morphology, indicating that BRP is not necessary for the formation of type II bouton. Interestingly, a previous work has shown that starvation-induced synaptopod formation showed BRP signal, in around 30% of

the newly forming synaptopod, when a "ball on pod" phase is reached. Once the axonal thickening finished and another extension ("Pod on ball") has developed, BRP occurrence was 100% in those synaptopods [1]. This suggests that BRP gradually, once synaptopod formation has finished, is recruited into those terminals, and does not affect synaptopod formation. This supports my finding that BRP overexpression, nor an RNAi knock down resulted into any morphological type II bouton phenotype. An interesting follow-up experiment would be to use BRP overexpression in OA/TA neuron flies and perform electron microscopy on type II terminals and see, whether due to the increase of BRP quantity an electron-dense structure could be seen. If so, that'd confirm that BRP is part of the release machinery in type II terminals and possibly fulfils similar mechanism as in type I terminals. This could be done with other AZ proteins as well then.

4.2.1 Presence of Unc13A and Unc13B at neurons with type II terminals.

To further get a better understanding of the release machinery in type II terminals, I tested for the presence of Unc13A, Unc13B and RBP with an immunohistochemical staining with STED, although these images didn't deliver conclusive results for either tested protein (Figure 24 and Figure 25). Staining showed in type I boutons that the antibody worked, but to confirm this, I'd repeat this experiment and try using a different fixative. I used 4% PFA for 10 minutes, while using pure methanol or Bouin's fixative could perhaps yield different results and improve the staining. The larval locomotion assay with IMBA indicates that Unc13A, Unc13B and RBP are present in OA/TA neurons, contrary to the immunohistochemical staining. Additionally, to the here shown experiments, to further identify whether those AZ proteins are available, it could be worth to overexpress Unc13A and Unc13B separately, to check whether the signal was just too little in previous staining. If the overexpression with the same staining protocol leads to visible signal of said AZ protein, this would confirm that the protein is indeed in type II terminals with probably smaller quantity when compared to type I terminals. This would also be suiting previous findings, as type II terminals don't possess an electron-dense structure at their active zone for release contrary to type I boutons, implying less AZ proteins needed for release of their DSVs. Hence, it'd be logical to deduct that fewer protein diversity or quantity might be needed in synaptic vesicle release. Ultimately, as suggested before, I'd test for the occurrence of more known type I terminal active zone proteins in type II boutons, apart from the ones here

mentioned to deduct which proteins are present. From then on, I'd look for obvious structures in type II boutons such as the BRP "doughnut" structure in type I boutons [48]. In my STED images, when overexpressing BRP, one could see an increase in BRP spots per bouton, furthermore, during analysis, I observed on subjective basis, without quantification since too few animals were tested, a reoccurrence of 2 to 3 BRP spot within type II boutons. It would be interesting to follow this lead by repeating the staining in control flies as well as in BRP overexpression mutants with an increased sample size to confirm this observation. If such a structure is found repeatedly, e.g. 2 BRP spots that align somewhat elliptically or in proximity in a consistent form, this could suggest that the BRP at type II terminals might have similar tasks as the BRP in type I boutons. When this is confirmed, one could then go on and test the presence and localization of e.g. other AZ proteins in relation to the BRP spots and check for similarities between type I terminals. The difficulty here is that, if images are taken and checked near type I terminals, whether the signal comes from a type I bouton or type II bouton might be ambiguous, as OA/TA neurons tend to be close to glutamatergic neurons for interaction.

4.3 Knockdown of BRP, Unc13A, Unc13B and RBP at OA/TA neurons affect larval microbehaviour.

Larval locomotion is a stereotypic behaviour generated by bursts of neuronal activity by CNS networks in form of CPGs [350, 387]. The biogenic amines OA/TA have been shown to affect not only larval locomotion, but also adult flight CPGs [132, 133, 157-159] and alteration of biogenic amine systems have shown to affect locomotive and learning behaviour [111, 136, 388-391]. As previous works have investigated the contrary effects OA and TA have on larval locomotion, we were interested in larval locomotive microbehaviour in association with different knockdown mutants [118, 130]. Here, we tested microbehaviour of larval locomotion in different AZ protein RNAi mutants and used IMBA to analyse those data (Figure 26 and Figure 28). The larval locomotion data showed that the absolute bending angle of the larvae during a run showed no significant changes. The absolute bending angle translates into how much the body of the larva was bent throughout the video. This indicates that larvae didn't show any impairments in their ability to bend their bodies when changing direction. This also suggests that OA/TA modulation does not affect this behaviour. Contrary to these movements, the number of head casts per second increased considerably when

knocking down Unc13A or Unc13B. As mentioned before, head casts are lateral head movements that usually precedes a reorientation event in the larva. Here, we noticed an increase in head casts per second in both Unc13 isoform knockdowns in OA/TA neurons, implying that there were also more directional changes in those larvae. These phenotypes would be in line with previous publications as well, such as Selcho et al (2012) [392] and Kutsukake et al (2000) [136], where they showed that Tdc2[RO54] mutants with tyrosine decarboxylase deficiency, resulting into the absence of TA and OA in OA/TA neurons in those larvae, exhibited significantly reduced locomotion, even when balanced over *CyO.* In homozygous larvae, locomotion was even further reduced. They also showed that an ablation of OA/TA neurons resulted in an alteration of larval locomotion pattern, where the larvae showed a circling behaviour, supporting our finding of increased HC and therefore increased reorientation events. Contrary to the Unc13A and Unc13B knockdown mutants, BRP KD mutants showed a decrease in head casts per second along with a significant increase in head cast angle, unlike the other two mentioned knockdown mutants. These results combined, suggests that less reorientation happens in BRP KD mutants, but with a larger head cast angle. Logically, with increased HC angle, the head cast itself might need slightly more time, which would be a parameter that we did not look at this time. This would be an interesting parameter to look at in following experiments. If an increase in head cast angle results into slower performed head casts in larvae, that could be a possible reason, why BRP KD mutants showed a decrease in head cast per second, unlike Unc13A and Unc13B knockdown mutants. Additionally, to the increase in HC per second, only Unc13B exhibited an increase in head turning velocity, resulting into faster performed head casts, unlike the other groups. Interestingly, RBP RNAi mutants showed no effect whatsoever and were completely unaffected in locomotive behaviour regarding head casts per second, absolute bending angle as well as head turning velocity and head cast angle. Furthermore, when looking at the interstep data in Figure 28, we can observe significant reduction in interstep interval in BRP, Unc13A and Unc13B knockdown mutants, but not in RBP KD mutants, as well as a significant decrease in interstep distance in BRP and Unc13B KD mutants. Following these data, the crawling speed of BRP KD mutants remained unchanged, while all other groups (Unc13A, Unc13B and even RBP) showed an increased crawling speed. Interestingly, Unc13B KD mutants exhibited an increase in crawling speed, contrary to the BRP KD mutants, although both experience a decrease in interstep interval (which translates

116

into faster "steps") and a decrease in interstep distance (this can be translated into shorter "steps"). This is mainly because of the magnitude of locomotive behaviour change in these animals. Unc13B KD mutants showed a more drastic reduction in interstep intervals, with lesser decrease in interstep distance than BRP KD mutants, resulting into a still increased crawling speed. This is not the case for the BRP KD mutants, where one effect basically does not "overshadow" the other effect (here the interstep interval was not reduced enough to cover up the decrease in interstep distance, unlike in Unc13B KD mutants). Unc13A, logically showed increased crawling speed, as interstep interval is significantly reduced, but not interstep distance. Surprisingly, RBP showed no significant effects in interstep interval, as well as in interstep distance, but still showed a significant increase in crawling speed. When observing Figure 28 in closer detail, it is possible to observe the reason why. The interstep interval of RBP RNAi mutants is slightly shorter than the control group, while the interstep distance was also very slightly increased, resulting into an increased crawling speed overall. An interesting issue to point out would be that the changes in locomotive behaviour might not be solely attributed to a defect in modulation at the larval muscles, but the VNC as well. Previous works have shown that OA/TA neurons in the VNC are essential for larval locomotion [392]. Elevating TA and reducing OA levels in OA/TA neurons in the VNC lead to slower locomotion of the larvae, as well as an increased time in pausing episodes as well as reduced linear crawling and circular movement. As these effects occur when TA concentration increases and OA decreases, it isn't too unlikely that Unc13A and Unc13B might contribute to TA release by being involved in the release machinery of tyramine receptors in the neuromodulatory OA/TA neurons. A knockdown of Unc13A and Unc13B could impair the release mechanism for TA and result in a reduced TA modulation, and hence increase OA levels, which would increase locomotion in larvae. Previous findings showed that *honoka* mutants, which is a tyramine receptor hypomorph [167], exhibit increased locomotion in larvae, as well as in adult flies [136, 392]. Following these observations, it wouldn't be too far-fetched to assume that an impairment of TA release might be the cause of increased locomotion in our Unc13A and Unc13B mutant, as well as possibly the RBP KD mutants, which also showed an increase in crawling speed. Solely BRP KD mutant didn't show an increase in crawling speed but exhibited deficits in our tested parameter of interstep distance, but an enhancement in interstep interval, which translates into "smaller, but quicker steps". A possible cause could be

that a knockdown of BRP in OA/TA neurons might lead to a defect in tyramine and octopamine receptor release, leading to the missing modulation of either. This would also indicate that BRP is a part in tyramine and octopamine release and is needed for both receptors. As mentioned earlier, the mutant Tdc2^{RO54} which is a tyrosine decarboxylase mutant, and therefore lacking both OA and TA , showed a reduction in locomotion even in heterozygous larvae and an even stronger effect in homozygous animals [392]. Regarding this, the knockdown of BRP, Unc13A, Unc13B and RBP in these experiments is less invasive and their effect could lead to an only partial release of vesicles, contrary to the complete ablation of OA and TA synthesis pathway of Tdc2^{RO54} mutants.

All in all, further studies will have to further evaluate the localization and presence of AZ proteins such as BRP. Unc13A, Unc13B, and RBP at type II terminals, possibly with ultrastructural images. The release machinery at type II terminals is widely still unknown and remains to be characterized. BRP, Unc13A and Unc13B showed to significantly alter larval locomotive microbehaviour, indicating the presence and their importance for tested parameters. Going forward, future studies will have to carefully approach the different effects of AZ protein alteration in OA/TA neurons at local areas, such as larval body muscles only or in the e.g. the mushroom bodies, since both biogenic amine have been shown to act in both regions [393]. The TDC2-Gal4 construct that was used is not only limited to VUM neurons, but affected all TDC2 positive neurons, including the ones in the brain [8]. The RNAi mutants' effects might not necessarily be solely caused by impaired locomotive actions, but also might be due to alteration of larval behaviour, and possibly also memory such as intermediate-term aversive memory, since OA receptors have also be linked to memory and learning [394, 395]. All in all, further proteins must be looked for in type II terminals, and the ones tested here, must be tested again and with different approaches. A localization of any found active zone protein and a higher resolution of BRP signal in type II terminals as well as discerning whether OA receptors and TA receptors have different release mechanisms would give valuable insights in release machinery of OA/TA neurons.

4.4 Aging affects mitochondrial quantity in L1 wing vein but does not affect L3 branch and mitochondrial transport and.

Aging comes with a decrease in mitochondrial quality and polyamine levels in the brains of rodents and humans, as well as a decline of axonal transport [343, 396-398]. Mitochondrial quality and its transportation throughout the axon are important for the health of the cell. A defect in mitochondria, especially in the respiratory chain system where ROS are produced in physiological concentration, in normal circumstances, could result in damage to mitochondria DNA or nuclear DNA [399]. The maintenance of mitochondria in the cell is essential for the survival of the cell, as GSH, which acts as cysteine storage but also as redox couple to scavenge potentially dangerous ROS, is also present in mitochondria and defending against physiological and pathological oxidative stress [400, 401]. To maintain mitochondrial quality, axonal transport is necessary, to transport newly synthesized mitochondria to regions with high energy demand through anterograde transport, while damaged mitochondria are retrogradely transported back to soma for mitophagy [12, 333, 402]. To test the effects of aging on mitochondrial transport, we previously, in my master's thesis, showed that mitochondrial numbers in our examined areas of the adult fly wings (L1 and first branch in L3) show a steady increase in mitochondrial number with age (until 15 days), regardless of spermidine supplementation or not, followed by a decrease of mitochondria in 20 days old flies (Figure 32). We also showed that stationary mitochondria within fly wing veins did not change with age and spermidine supplementation. The velocity of transported mitochondria remained constant in most cases, except for female anterograde transported mitochondria, where 20-days old female flies without spermidine supplementation showed significantly faster mitochondrial velocity when compared to 5-days old flies. This significant increase in speed wasn't present in spermidine-treated female flies. The increase of mitochondrial number with age isn't unexpected, as mitochondria are known to be transported bidirectional with frequent stops and restarts as well. Furthermore, it isn't atypical for mitochondria to dock at particular stations, where energy and increased calcium homeostasis are in demand [255]. As neurons are dynamic and keeps adapting to an everchanging environment, the idea of increased requirement of energy and calcium homeostasis with age isn't too unlikely. Additionally, a study has shown that in mice, axons become thicker and larger in size with age and mitochondria become less, but longer and larger with an increased production of oxidative stress while generating

119

4. Discussion

less energy [403]. The results we showed here are from mainly younger flies, as *Drosophila* flies age up to around 80 days and we only tested the mitochondrial numbers in 1 to 20 days old flies. We saw a steady increase in mitochondrial numbers until 15-days old flies but a decrease in 20-days old flies, which would also fit in the data presented by Stahon et al. in 2016 [403]. They also reported that mitochondria become elongated with age and this morphological change was correlated with impaired mitochondrial functions. The steady increase in mitochondrial number in the L1 vein also hints at it being a high-trafficking region, as the first branch of the L3 vein showed no such increase and always rather constant mitochondrial numbers. Another interesting paper also found out that stopping of moving mitochondria was not random, but mitochondria showed significantly more stops in gaps between stationary mitochondria [404]. They also reported that mitochondria can space out evenly along the axonal shaft and halt near active growth cones. In our flies with spermidine supplementation, we saw similar increase in mitochondrial numbers, except that at 15-days old flies, the mitochondrial number didn't differ much from 10-days old flies, which was also followed by a decrease in mitochondrial number at 20-days old flies. Spermidine is a polycation shown to exhibit autophagy-mediated anti-aging effects in different species [317, 397]. We were curious about the effects spermidine has on mitochondrial transport and therefore supplemented the flies with spermidine throughout their life and then subjected them to our fly wing assay. Our results were like the control group of non-spermidines fed flies, except for the previously mentioned plateauing of the steady increase in 15-days old flies. As spermidine is thought to boost autophagy, the initial expectation was an increase of mitochondrial transport, potentially lowering the number of stationary mitochondria within the axons. Here, we show that this was not the case. Stationary mitochondrial number remained almost constant in flies throughout their 20th day of living. As we determined the number of mitochondria in our regions of interest, we also investigated the velocity of the moving mitochondria. Here, we didn't find significant differences, regardless of spermidine supplementation and age. The only significant change we saw, was the increase in mitochondrial velocity in anterograde transported mitochondria in female flies between 5-days old and 20-days old flies. We saw an increase in transport velocity in older flies, which was abolished with spermidine supplementation. An increase of transport velocity was contrary to our expectations and could be attributed to our analysis method. We used a macro to manually mark and track the movement of mitochondria,

120

which could result in human mistakes. Additionally, we did not consider bidirectional movement in this analysis. If a mitochondrion stops in its track and starts moving in the other direction, we counted this as a separate, in other direction moving mitochondria. Whether this affects mitochondrial velocity remains to be investigated, but in other works, it has been mentioned, that due to the frequent pausing and reversal of mitochondrial transport direction, the resulting velocity falls in-between that of fast-moving vesicles and slow-moving cytoskeletal proteins [405]. Further experiments are needed to determine the effects of aging in more aged flies, especially 30- to 50-days old ones. Interesting would be to examine old flies' mitochondria, as previous works reported the elongation of mitochondria with age which was also linked to impaired functions [403]. It would be interesting to examine the effects of aging on mitochondrial transport and mitophagy first, before subjecting them to spermidine treatment again.

4.5 Aging as well as spermidine supplementation did not show significant effects in oxidative stress levels when measuring the GSH:GSSG ratio.

Glutathione is an intracellular tripeptide with various functions, such as detoxification of electrophiles, antioxidant defence by scavenging free radicals, maintaining essential thiol status of proteins, and more [273, 406-408]. It has been shown that around 90% of GSH is in the cytosol, 10% in the mitochondria, and a small percentage in the endoplasmic reticulum [409, 410]. The compartmentalization of GSH entails the existence of different redox pools of GSH within the cell and therefore also different redox potential [411]. Only in the endoplasmic reticulum is GSH mainly in its oxidized form (GSSG), while in the other two compartments, the cytosol, and mitochondria, it is predominantly present in reduced form [401, 410, 412]. As mitochondria contain their own GSH/GSSG pool and aging has been associated with an increase in mitochondrial dysfunction via less ATP generation and increased ROS production, likely through defects in the respiratory chain, we used an engineered GFP with a disulfide switch, that allowed us to measure the ratio of GSH and GSSG within mitochondria [413]. We initially started the experiments with our Appl-Gal4 driver, that we also used for our mitochondrial transport experiments, but fluctuations in redox ratio with our mito-roGFP2-Grx1 construct led us to test our construct with Appl-Gal4 and a different driver. Here, we additionally used another pan-neuronal driver, elav-Gal4, and used chemical agents to fully oxidize (DA) or reduce (DTT) disulfide bonds.

4. Discussion

In Appl-Gal4 driven flies, we saw high fluctuating values, while elav-Gal4 driven flies showed GSH/GSSG ratio of around 1 RFU in young flies with NEM application. NEM was used to block the formation of new disulfide crosslinks and maintain current redox state of the adult fly brains. We tested younger flies from 3 days to old flies ranging up to 50-days old flies and investigated the effects of aging and DHPS knockdown in brain redox-state. Here, we observed, with the new driver, contrary to my previous results from my master's thesis, almost no differences in GSH/GSSG ratio with age. Following the unchanging GSH/GSSG ratio, spermidine supplementation also didn't exhibit any major effects on the redox state of the mitochondria. The only notable difference we saw, was a slight decrease in 30-days old flies treated with spermidine, as GSH/GSSG ratio was almost significantly reduced (p = 0.0826) when compared to 3-days young flies subjected to spermidine supplementation. Furthermore, we saw an increase in GSH/GSSG ratio when we knocked down DHPS in 15-days and an almost significant increase in 30-days old flies (p = 0.0682), but not in 50-days old flies. This increase was abolished when flies in the same age group were supplemented with spermidine. These findings indicate, that under normal conditions, aging did not significantly affect mitochondrial GSH/GSSG ratio, but a spermidine supplementation still exhibited a slight decrease in oxidized GSH in 30-days old flies. Notably, the GSH/GSSG ratio decreased in the DHPS KD mutant with and without spermidine supplementation in 50-days old flies. The unchanging GSH/GSSG ratio in mitochondria throughout age was an unexpected result, as it has previously been shown that mitochondrial quality decline with age: membrane potential decreases, mitochondrial DNA accumulate mutations which is followed by increasing deficits in oxidative phosphorylation leading to an increased leakage of ROS of the mitochondria, ultimately leading to initiation of apoptosis [414-416]. These findings led us to the hypothesis that mitochondrial GSH/GSSG might be disturbed with age and spermidine might contribute to improving mitochondrial redox equilibrium. Our findings indicate that aging does not affect mitochondrial GSH/GSSG ratio, but a defect in hypusination of eIF5A affected mitochondrial GSH/GSSG ratio slightly. At 15-days old flies, we saw an increase in oxidative stress and in 30-days old flies an almost significant increase (p = 0.0682). These increases were diminished upon dietary spermidine supplementation, indicating a substantial role of the hypusination of eIF5A in regulation of redox-stress levels in mitochondria. The modification of eIF5A can favour efficient translation elongation of specific mRNAs by tuning translation and in consequence, also

122

4. Discussion

proteomic profiles [417, 418]. Furthermore, eIF5A has been found to decrease with age until mid-age and that this can be augmented by dietary spermidine supplementation [320]. In this paper, we also showed that spermidine supplementation could improve mitochondrial functions in aged fly brains and also an increase in hypusination of eIF5A upon spermidine supplementation. We also showed that eIF5A hypusination affected mitochondrial proteome integrity, as well as, respiratory functions within adult fly brains and that these effects were mediated through the reduction of neuronal hypusination [320]. Here, in this thesis, we saw supporting evidence for these findings. The knockdown of DHPS resulted in an increase in mitochondrial GSH/GSSG ratio. This increase was abolished through spermidine supplementation. As DHPS knockdown lead to spermidine being unusable for hypusination of eIF5A, this was an interesting result. The reduction of GSH/GSSG ratio through spermidine supplementation might indicate either a different way to break down spermidine for the use of hypusination, or a different redox-reducing mechanism mediated by spermidine supplementation. In the scenario of the first mentioned possibility, it'd be essential to examine if there are other possibilities to break down spermidine to donate the amino-butyl group for hypusination of eIF5A. In the second scenario, it'd be interesting to investigate mitophagy in spermidine supplied animals. Notably, the mean fluorescence ratio in DHPS KD mutants were considerably lower than our control flies, regardless of age, indicating overall a reduction of GSSG and an equilibrium shift towards GSH. This was rather unexpected, as a shift towards reduced GSH means a reduction of oxidative stress when eIF5A hypusination was impaired. This result could be explained through the possibility of GSH transport. The cell is capable of transporting GSH from the cytoplasm into the mitochondria, which leads to an increase of reduced GSH within the mitochondrial GSH/GSSG equilibrium, which would shift the equilibrium towards GSH than GSSG. This increased transport could be the effect of DHPS knockdown and remains to be investigated. Another possibility that could be taken into consideration would be that the impairment of eIF5A hypusination could lead to a decrease in membrane fluidity through still unknown means (possibly through lack of eIF5A-mediated translation elongation or cholesterol increase), as previous work have shown that a decrease in mitochondrial membrane fluidity as well as an increase in cholesterol lead to a reduction in mitochondrial GSH levels [419]. Further studies will be needed to evaluate the effects of spermidine supplementation on oxidative stress, as this thesis mainly focussed on mitochondrial

123

GSG/GSSH equilibrium. The next step could be the examination of the cytosolic GSH/GSSG and possibly also the leakage rate of ROS after spermidine supplementation. Another interesting follow up experiment could be the investigation the effect of spermidine, as well as DHPS KD on another redox couple, such as the glutaredoxin system, which has been shown to collaborate with the GSH system [420, 421].

5. Summary

Chemical synapses are fundamental for fast and reliable synaptic transmission and proves as fundamental basis needed for cognitive functions in higher organisms as well as in humans. The ability of synapses to communicate with each other by synaptic vesicle release of neurotransmitters enables them to create a big neuronal network responsible for information relay to other parts of the body. Communication from neuron to neuron happens through release of neurotransmitter-containing synaptic vesicles from presynapse to postsynapse. Synaptic vesicles must be tethered, primed, and then fused with the presynaptic membrane to fulfil their purpose. This is orchestrated by a complex proteinaceous machinery at dedicated cytomatrix sites at the presynapse, known as active zone (AZ). These active zones are essential for synaptic vesicle release and specific scaffolding proteins are needed to assemble and maintain this complex machinery. This synaptic vesicle release machinery has been observed in *Drosophila melanogaster's* glutamatergic type I terminals and can be observed as an electron-dense structure in ultrastructural images. This is not the case for the smaller type II synaptic terminals that emerge from neuromodulatory ventral unpaired median (VUM) neurons in the ventral nerve cord (VNC). These VUM neurons extend their synaptic terminals towards the peripheric larval body wall muscles of *Drosophila* and innervate those muscles. The synapses of these neurons are in proximity of glutamatergic type I terminal neurons and are known to act neuromodulatory on the muscle. Contrary to type I terminals, type II terminals don't possess an electron-dense structure and the synaptic vesicle release machinery is still widely unknown. Previously it has been shown that the presynaptic active zone protein BRP is present in type I as well as in type II terminals.

This thesis can confirm the presence of BRP in the neuromodulatory type II terminals via stimulated emission depletion (STED) microscopy and shows through larval locomotion analyser "IMBA" that other known type I terminal active zone proteins such as Unc13A, Unc13B and RBP are present in those neurons. The use of RNAi lines allowed for a knockdown (KD) of the tested AZ proteins, where different larval locomotive microbehaviour parameters were tested. Analysis of these data have shown that Unc13A, Unc13B and RBP KD mutants show an increased crawling speed via a decrease in "step interval", while BRP KD mutants showed no such increase.

5. Summary

Additionally, Unc13A and Unc13B KD mutants show an increase in lateral head movement that precedes a reorientation event, also known as head cast (HC) in *Drosophila* larvae. Furthermore, STED microscopy was used to check for the tested proteins in better resolution with immunohistochemical approaches , but this remained unsuccessful. STED images confirmed the presence of BRP spots in type II boutons, which were previously only seen through confocal microscopy. Overexpression and KD of BRP in octopaminergic/tyraminergic (OA/TA) neurons didn't alter type II bouton morphology, but number of BRP spots per bouton. Additionally, this thesis inspects the possible interaction between type I and type II terminal neurons during pupal stages throughout the metamorphosis. Immunohistochemical approaches showed no obvious dependence on each other during metamorphosis for innervation target finding.

In the second part of my thesis, we extended our research from our master's thesis and started working from there. Aging is a process that remains mainly ununderstood. Few theories have been proposed, and one of them is the "free radical theory of aging and radiation chemistry" by D. Harman, suggesting the involvement of reactive oxygen species (ROS) in aging. ROS are O2-derived free radicals that are, in high amount, capable of causing several intracellular damages ultimately leading to cell death. Most of the ROS are produced in mitochondria and are within physiological levels, used for intracellular signalling. To maintain a healthy intracellular redox equilibrium, redox couples to scavenge ROS are used in the cell. One of the dominant redox couples is the tripeptide glutathione (GSH) and its oxidized form glutathione disulphide (GSSG). The distribution of GSH/GSSG in cells are around 90% in the cytoplasm, 10% in the mitochondria and a low percentage in the endoplasmic reticulum. Mitochondria are very well known as "the powerhouse of the cell" as they are the main energy producer within cells and are an organelle with their own mitochondrial DNA (mtDNA). With age, mtDNA accumulates mutations, leading to defect in the respiratory chain and ultimately resulting into cell death. To counteract an accumulation of defective mitochondria, mitochondria are transported back to the soma for degradation through mitophagy. Axonal transport declines with age and impaired mitochondrial transport are a key pathogenic change in aging associated neurodegenerative diseases. Spermidine is a polyamine that has been shown to mediate anti-aging effects through boosting autophagy and acts as an amino-butyl group donor for hypusination of the

eukaryotic initiation factor 5A (eIF5A) which has been shown to be involved in spermidine-mediated protection of mitochondrial functionality.

Here, we show through the use of in vivo imaging of adult fly wings, that mitochondrial transport and transport velocity were not affected with age in flies, regardless of dietary spermidine supplementation. We also showed that mitochondrial GSH/GSSG ratio was not affected with age or spermidine supplementation, through the use of an engineered green fluorescent protein (roGFP), containing a disulfide switch with different excitation maxima depending on its oxidation status. Lastly, we used the same construct investigate mitochondrial glutathione redox status to measure the effects of a deoxyhypusine synthase (DHPS) knockdown mutant on mitochondrial GSH/GSSG equilibrium. We saw no significant changes in our control groups, but a significant increase in mid-aged flies when DHPS was genetically reduced, which absent in flies with dietary spermidine supplementation.

Zusammenfassung

Chemische Synapsen sind fundamental für schnelle und zuverlässige synaptische Transmission und bilden daher eine fundamentale Basis gebraucht für kognitive Funktionen in höheren Organismen, als auch in Menschen. Die Fähigkeit der Synapsen, miteinander zu kommunizieren durch synaptische Vesikelfreisetzung von Neurotransmittern, ermöglicht es ihnen ein großes, neuronales Netzwerk, welches für Informationübertragung zu anderen Körperteilen verantwortlich ist, zu erstellen. Kommunikation zwischen Neuronen entsteht durch die Freisetzung von Neurotransmitterhaltigen synaptischen Vesikeln von der Präsynapse an die Postsynapse. Synaptische Vesikel müssen für die Freisetzung vorbereitet werden, um mit der präsynaptischen Membran zu fusionieren. Dies geschieht mithilfe einer komplexen, proteinerge Maschinerie, die sich an spezialisierten Seiten in der Zytomatrix, die aktiven Zonen (AZ) genannt werden, befinden. Diese aktiven Zonen sind essenziell für die Freisetzung von synaptischen Vesikel und spezielle Gerüstproteine sind notwendig, um diese proteinerge Maschinerie zusammenzubauen und zu erhalten. Diese synaptische Vesikelfreisetzungsmaschinerien wurden in glutamatergen Typ I Terminalen in *Drosophila melanogaster* entdeckt und zeichnen sich in elektronmikroskopischen Aufnahmen als eine elektronendichte Struktur aus. Dies ist nicht der Fall in den kleineren Typ II synaptischen Terminalen, die von neuromodulatorischen ventral ungepaarte mediale (VUM) Neuronen aus dem Strickleiternervensystem stammen. Diese VUM-Neuronen erstrecken ihre synaptischen Terminale bis hin zur peripheren larvalen Körperwandmuskeln von *Drosophila* und innerviert diese Muskeln. Die Synapsen dieser Neuronen sind in proximaler Nähe von glutamatergen Typ I Terminalen und agieren neuromodulatorisch auf diese Muskeln. Im Gegenteil zu Typ I Terminalen, besitzen Typ II Terminale keine elektronendichte Struktur und die Maschinerie für synaptische Vesikelfreisetzung ist immernoch unbekannt. Frühere Studien zeigen, dass das präsynaptische Gerüstprotein „Bruchpilot" (BRP) in beiden Terminalen vorkommt.

Diese Doktorarbeit kann die Präsenz von BRP in den neuromodulatorischen Typ II Terminalen mittels „stimulated emission depletion" (STED) Mikroskopie bestätigen und zeigt durch larvale Lokomotionanalysierer „IMBA" andere Gerüstproteine, sowie Unc13A, Unc13B und RBP in diesen Neuronen vorhanden sind. Das Nutzen von RNAi

5. Summary

Linien ermöglicht den Gen-Knockdown von den getesteten AZ-Proteine, an welche lokomotorische Mikroverhalten getestet wurden. Die Analyse dieser Daten zeigten, dass durch Gen-Knockdown von Unc13A-, Unc13B- und RBP zu erhöhten Kriechgesschwindigkeit durch eine Verringerung des „Schrittintervalls" führten, währen die BRP-Mutanten keines solche Erhöhung zeigte. Zudem zeigten Unc13A- und Unc13B-Mutanten einen Anstieg in laterale Kopfbewegung, die vor einer Reorientierungsereignis, die auch als „head cast" (HC) in *Drosophila* Larven bekannt ist. Zudem wurde STED-Mikroskopie genutzt um die getesteten Proteine mit einer immunohistochemischen Ansatz, welches jedoch unerfolgreich bleib. STED-Aufnahmen zeigen die Präsenz von BRP-Signalen in Typ II Boutons, welche vorher nur in konfokalen Mikroskopen gesehen wurden. Die Überexpression und der Gen-Knockdown von BRP in octopaminergen/tyraminergen (OA/TA) Neurone veränderte nicht die Boutonmorphologie, aber die Anzahl der BRP-Signale pro Bouton. Zusätzlich untersucht diese Doktorarbeit mögliche Interaktionen zwischen Neuronen mit Typ I oder Typ II Terminalen während der Metamorphose. Immunohistochemische Ansätze zeigten keine öffentliche Abhängigkeit für die Findung von Innervationszielen in den Puppenstadien.

Im zweiten Teil meiner Doktorarbeit haben wir meine Masterarbeit fortgeführt. Das Altern ist ein immer noch unverstandener Prozess. Einige Theorien wurden vorgeschlagen, wobei eine von denen die „Freie Radikalen Theorie des Alterns und der Strahlungschemie" von D. Harman ist, welche Involvierung von reaktiven Sauerstoffspezies (ROS) vorschlägt. ROS sind Sauerstoff abstammende freie Radikale, die in größerer Menge in der Lage sind, intrazelluläre Schaden hervorzurufen und letztendlich zum Zelltod führen kann. Die Mehrzahl der ROS entsteht in Mitochondrien, welche innerhalb von physiologischen Mengen für intrazelluläre Signalisierungen benutzt werden. Um eine gesunde intrazelluläre Redoxgleichgewicht zu behalten, werden sogenannte Redoxpaare in der Zelle benutzt. Eines der dominanten Redoxpaare ist das Tripeptid Glutathione (GSH) und dessen oxidierte Form Glutathiondisulfid (GSSG). Die Verteilung von GSH/GSSG innerhalb der Zelle liegt in etwa 90% im Zytoplasma, 10% in den Mitochondrien und ein kleiner Prozentsatz im endoplasmatischen Retikulum. Mitochondrien sind weitbekannt als „Kraftwerk der Zelle", da sie die Hauptproduzenten von Energie innerhalb der Zelle sind und sind Organellen mit eigener mitochondrialen DNA

(mtDNA). Im Alter akkumulieren sich Mutationen in der mtDNA an, welche zu Defekten in der Atmungskette führen können, die ultimativ zum Zelltod führen. Um die Akkumulierung von defekten Mitochondrien zu verhindern, transportieren die Zellen die defekten Mitochondrien zurück ins Soma, zur Degradierung mittels Mitophagie. Axonaler Transport verschlechtert sich im Alter und defekter Transport von Mitochondrien sind einer der Hauptsymptome in altersassoziierten neurodegenerativen Krankheiten. Spermidin ist ein Polyamin, welche Effekte gegen das Altern durch das Verbessern von Autophagie erzielen kann und agiert zusätzlich als Aminobutyl-Gruppen Donor für die Hypusinierung vom eukaryotischen Initiationsfaktor 5A (eIF5A), welche involviert in dem Spermidin-vermittelten Schutz der mitochondrialen Funktionalität ist.

In dieser Doktorarbeit zeigen wir durch in vivo Aufnahmen in adulten Fliegenflügeln, dass mitochondrialer Transport und dessen Geschwindigkeit nicht vom Alter beeinflusst werden. Wir zeigen außerdem, dass der mitochondriale GSH/GSSG Verhältnis im Alter und durch Spermidinfütterung nicht beeinflusst wird mithilfe einer konstruierten grünen Fluoreszenzprotein (roGFP), welches einen Disulfid-Schalter mit verschiedenen Erregungsmaxima, welche abhängig von dem Oxidationszustand des Disulfides ist, besitzt. Zuletzt haben wir das gleiche Konstrukt benutzt um den Redoxstatus mitochondrialer Glutathione und Effekte einer genetisch-bedingten Reduzierung von Deoxyhypusin-Synthase (DHPS) auf den mitochondrialen GSH/GSSG Gleichgewicht zu messen. Hier haben wir keine signifikanten Veränderungen in unserer Kontrollgruppe beobachten können, aber eine signifikante Erhöhung in Fliegen mittleren Alters beim genetischen Knockdown von DHPS. Diese Steigerung des GSH/GSSG Verhältnis wurde durch Spermidinfütterung wieder abwesend.

6. Literature

1. Koon, A.C., et al., *Autoregulatory and paracrine control of synaptic and behavioural plasticity by octopaminergic signaling.* Nat Neurosci, 2011. **14**(2): p. 190-9.

2. Ackermann, F., C.L. Waites, and C.C. Garner, *Presynaptic active zones in invertebrates and vertebrates.* EMBO Rep, 2015. **16**(8): p. 923-38.

3. Pauls, D., et al., *A comprehensive anatomical map of the peripheral octopaminergic/tyraminergic system of Drosophila melanogaster.* Scientific Reports, 2018. **8**(1): p. 15314.

4. Thane, M., et al., *High-resolution analysis of individual Drosophila melanogaster larvae uncovers individual variability in locomotion and its neurogenetic modulation.* Open Biol, 2023. **13**(4): p. 220308.

5. Cao, X., et al., *In vivo imaging reveals mitophagy independence in the maintenance of axonal mitochondria during normal aging.* Aging Cell, 2017. **16**(5): p. 1180-1190.

6. Chaudhary, G., et al., *Rearing and handling of Drosophila -A primer for laboratory experiments*. 2021. p. 1-31.

7. Tauc, M., et al., *The eukaryotic initiation factor 5A (eIF5A1), the molecule, mechanisms and recent insights into the pathophysiological roles.* Cell & Bioscience, 2021. **11**(1): p. 219.

8. Cole, S.H., et al., *Two Functional but Noncomplementing Drosophila Tyrosine Decarboxylase Genes: DISTINCT ROLES FOR NEURAL TYRAMINE AND OCTOPAMINE IN FEMALE FERTILITY *.* Journal of Biological Chemistry, 2005. **280**(15): p. 14948-14955.

9. Pereda, A.E., *Electrical synapses and their functional interactions with chemical synapses.* Nature Reviews Neuroscience, 2014. **15**(4): p. 250-263.

10. Takamori, S., et al., *Molecular Anatomy of a Trafficking Organelle.* Cell, 2006. **127**(4): p. 831-846.

11. Aller, I., N. Rouhier, and A.J. Meyer, *Development of roGFP2-derived redox probes for measurement of the glutathione redox*

potential in the cytosol of severely glutathione-deficient rml1 seedlings. Front Plant Sci, 2013. **4**: p. 506.

12. Lu, S.C., *Regulation of glutathione synthesis.* Mol Aspects Med, 2009. **30**(1-2): p. 42-59.

13. Gorczyca, M. and V. Budnik, *Appendix: Anatomy of the Larval Body Wall Muscles and NMJs in the third instar larval stage.* International Review of Neurobiology- INT REV NEUROBIOL, 2006. **75**: p. 367-373.

14. Jia, X.X., M. Gorczyca, and V. Budnik, *Ultrastructure of neuromuscular junctions in Drosophila: comparison of wild type and mutants with increased excitability.* J Neurobiol, 1993. **24**(8): p. 1025-44.

15. Haucke, V., E. Neher, and S.J. Sigrist, *Protein scaffolds in the coupling of synaptic exocytosis and endocytosis.* Nat Rev Neurosci, 2011. **12**(3): p. 127-38.

16. Currie, D.A. and M. Bate, *The development of adult abdominal muscles in Drosophila: myoblasts express twist and are associated with nerves.* Development, 1991. **113**(1): p. 91-102.

17. Stocker, B., et al., *Structural and Molecular Properties of Insect Type II Motor Axon Terminals.* Front Syst Neurosci, 2018. **12**: p. 5.

18. Griffith, L.C. and V. Budnik, *Plasticity and second messengers during synapse development.* Int Rev Neurobiol, 2006. **75**: p. 237-65.

19. Azevedo, F.A.C., et al., *Equal numbers of neuronal and nonneuronal cells make the human brain an isometrically scaled-up primate brain.* Journal of Comparative Neurology, 2009. **513**(5): p. 532-541.

20. Keijzer, F., M. van Duijn, and P. Lyon, *What nervous systems do: early evolution, input–output, and the skin brain thesis.* Adaptive Behaviour, 2013. **21**(2): p. 67-85.

21. Südhof, T.C., *The cell biology of synapse formation.* J Cell Biol, 2021. **220**(7).

22. Nielsen, M.S., et al., *Gap Junctions.* Comprehensive Physiology, 2012.

23. Sheng, M. and C.C. Hoogenraad, *The Postsynaptic Architecture of Excitatory Synapses: A More Quantitative View.* Annual Review of Biochemistry, 2007. **76**(1): p. 823-847.

24. Couteaux, R. and M. Pécot-Dechavassine, *[Synaptic vesicles and pouches at the level of "active zones" of the neuromuscular junction].* C R Acad Hebd Seances Acad Sci D, 1970. **271**(25): p. 2346-9.

25. Zhai, R.G. and H.J. Bellen, *The architecture of the active zone in the presynaptic nerve terminal.* Physiology (Bethesda), 2004. **19**: p. 262-70.

26. Jahn, R. and D. Fasshauer, *Molecular machines governing exocytosis of synaptic vesicles.* Nature, 2012. **490**(7419): p. 201-7.

27. Südhof, T.C., *The presynaptic active zone.* Neuron, 2012. **75**(1): p. 11-25.

28. Schoch, S. and E.D. Gundelfinger, *Molecular organization of the presynaptic active zone.* Cell Tissue Res, 2006. **326**(2): p. 379-91.

29. Südhof, T.C. and J. Rizo, *Synaptic vesicle exocytosis.* Cold Spring Harb Perspect Biol, 2011. **3**(12).

30. Rizo, J. and C. Rosenmund, *Synaptic vesicle fusion.* Nature Structural & Molecular Biology, 2008. **15**(7): p. 665-674.

31. Rizzoli, S.O. and W.J. Betz, *Synaptic vesicle pools.* Nat Rev Neurosci, 2005. **6**(1): p. 57-69.

32. Baumert, M., et al., *Synaptobrevin: an integral membrane protein of 18,000 daltons present in small synaptic vesicles of rat brain.* Embo j, 1989. **8**(2): p. 379-84.

33. Trimble, W.S., D.M. Cowan, and R.H. Scheller, *VAMP-1: a synaptic vesicle-associated integral membrane protein.* Proc Natl Acad Sci U S A, 1988. **85**(12): p. 4538-42.

34. Oyler, G.A., et al., *The identification of a novel synaptosomal-associated protein, SNAP-25, differentially expressed by neuronal subpopulations.* J Cell Biol, 1989. **109**(6 Pt 1): p. 3039-52.

35. Bennett, M.K., N. Calakos, and R.H. Scheller, *Syntaxin: a synaptic protein implicated in docking of synaptic vesicles at presynaptic active zones.* Science, 1992. **257**(5067): p. 255-9.

36. Söllner, T., et al., *A protein assembly-disassembly pathway in vitro that may correspond to sequential steps of synaptic vesicle docking, activation, and fusion.* Cell, 1993. **75**(3): p. 409-18.

37. Gerber, S.H., et al., *Conformational switch of syntaxin-1 controls synaptic vesicle fusion.* Science, 2008. **321**(5895): p. 1507-10.

38. Tang, J., et al., *A complexin/synaptotagmin 1 switch controls fast synaptic vesicle exocytosis.* Cell, 2006. **126**(6): p. 1175-87.

39. Deák, F., et al., *Munc18-1 binding to the neuronal SNARE complex controls synaptic vesicle priming.* J Cell Biol, 2009. **184**(5): p. 751-64.

40. Söllner, T., et al., *SNAP receptors implicated in vesicle targeting and fusion.* Nature, 1993. **362**(6418): p. 318-324.

41. Bombardier, J.P. and M. Munson, *Three steps forward, two steps back: mechanistic insights into the assembly and disassembly of the SNARE complex.* Curr Opin Chem Biol, 2015. **29**: p. 66-71.

42. Tyson, J.R. and T.P. Snutch, *Molecular nature of voltage-gated calcium channels: structure and species comparison.* Wiley Interdisciplinary Reviews: Membrane Transport and Signaling, 2013. **2**(5): p. 181-206.

43. Spafford, J.D. and G.W. Zamponi, *Functional interactions between presynaptic calcium channels and the neurotransmitter release machinery.* Curr Opin Neurobiol, 2003. **13**(3): p. 308-14.

44. Catterall, W.A., *Voltage-gated calcium channels.* Cold Spring Harb Perspect Biol, 2011. **3**(8): p. a003947.

45. Carbone, E. and H.D. Lux, *A low voltage-activated, fully inactivating Ca channel in vertebrate sensory neurones.* Nature, 1984. **310**(5977): p. 501-502.

46. Dunlap, K., J.I. Luebke, and T.J. Turner, *Exocytotic Ca2+ channels in mammalian central neurons.* Trends Neurosci, 1995. **18**(2): p. 89-98.

47. Kawasaki, F., R. Felling, and R.W. Ordway, *A temperature-sensitive paralytic mutant defines a primary synaptic calcium channel in Drosophila.* J Neurosci, 2000. **20**(13): p. 4885-9.

48. Fouquet, W., et al., *Maturation of active zone assembly by Drosophila Bruchpilot.* J Cell Biol, 2009. **186**(1): p. 129-45.

49.   Kittel, R.J., et al., *Bruchpilot promotes active zone assembly, Ca2+ channel clustering, and vesicle release.* Science, 2006. **312**(5776): p. 1051-4.

50.   Wagh, D.A., et al., *Bruchpilot, a protein with homology to ELKS/CAST, is required for structural integrity and function of synaptic active zones in Drosophila.* Neuron, 2006. **49**(6): p. 833-44.

51.   Matkovic, T., et al., *The Bruchpilot cytomatrix determines the size of the readily releasable pool of synaptic vesicles.* J Cell Biol, 2013. **202**(4): p. 667-83.

52.   Klar, T.A., et al., *Fluorescence microscopy with diffraction resolution barrier broken by stimulated emission.* Proceedings of the National Academy of Sciences, 2000. **97**(15): p. 8206-8210.

53.   Hida, Y. and T. Ohtsuka, *CAST and ELKS proteins: structural and functional determinants of the presynaptic active zone.* J Biochem, 2010. **148**(2): p. 131-7.

54.   Mukherjee, K., et al., *Piccolo and bassoon maintain synaptic vesicle clustering without directly participating in vesicle exocytosis.* Proceedings of the National Academy of Sciences, 2010. **107**(14): p. 6504-6509.

55.   Bruckner, J.J., et al., *Fife, a Drosophila Piccolo-RIM Homolog, Promotes Active Zone Organization and Neurotransmitter Release.* The Journal of Neuroscience, 2012. **32**(48): p. 17048-17058.

56.   Hallermann, S., et al., *Naked Dense Bodies Provoke Depression.* The Journal of Neuroscience, 2010. **30**(43): p. 14340-14345.

57.   Kaeser, P.S., et al., *RIM proteins tether Ca2+ channels to presynaptic active zones via a direct PDZ-domain interaction.* Cell, 2011. **144**(2): p. 282-95.

58.   Liu, K.S., et al., *RIM-binding protein, a central part of the active zone, is essential for neurotransmitter release.* Science, 2011. **334**(6062): p. 1565-9.

59.   Böhme, M.A., et al., *Active zone scaffolds differentially accumulate Unc13 isoforms to tune Ca(2+) channel-vesicle coupling.* Nat Neurosci, 2016. **19**(10): p. 1311-20.

60. Siebert, M., et al., *A high affinity RIM-binding protein/Aplip1 interaction prevents the formation of ectopic axonal active zones.* Elife, 2015. **4**.

61. Mittelstaedt, T. and S. Schoch, *Structure and evolution of RIM-BP genes: identification of a novel family member.* Gene, 2007. **403**(1-2): p. 70-9.

62. Hibino, H., et al., *RIM binding proteins (RBPs) couple Rab3-interacting molecules (RIMs) to voltage-gated Ca(2+) channels.* Neuron, 2002. **34**(3): p. 411-23.

63. Wang, Y., S. Sugita, and T.C. Sudhof, *The RIM/NIM family of neuronal C2 domain proteins. Interactions with Rab3 and a new class of Src homology 3 domain proteins.* The Journal of biological chemistry, 2000. **275**(26): p. 20033-20044.

64. Acuna, C., X. Liu, and T.C. Südhof, *How to Make an Active Zone: Unexpected Universal Functional Redundancy between RIMs and RIM-BPs.* Neuron, 2016. **91**(4): p. 792-807.

65. Dai, Y., et al., *SYD-2 Liprin-α organizes presynaptic active zone formation through ELKS.* Nature Neuroscience, 2006. **9**(12): p. 1479-1487.

66. Kaufmann, N., et al., *Drosophila Liprin-α and the Receptor Phosphatase Dlar Control Synapse Morphogenesis.* Neuron, 2002. **34**(1): p. 27-38.

67. Stryker, E. and K.G. Johnson, *LAR, liprin alpha and the regulation of active zone morphogenesis.* J Cell Sci, 2007. **120**(Pt 21): p. 3723-8.

68. Serra-Pagès, C., et al., *The LAR transmembrane protein tyrosine phosphatase and a coiled-coil LAR-interacting protein co-localize at focal adhesions.* Embo j, 1995. **14**(12): p. 2827-38.

69. Schoch, S., et al., *RIM1alpha forms a protein scaffold for regulating neurotransmitter release at the active zone.* Nature, 2002. **415**(6869): p. 321-6.

70. Taru, H. and Y. Jin, *The Liprin homology domain is essential for the homomeric interaction of SYD-2/Liprin-α protein in presynaptic assembly.* J Neurosci, 2011. **31**(45): p. 16261-8.

71. Ko, J., et al., *Interaction of the ERC family of RIM-binding proteins with the liprin-alpha family of multidomain proteins.* J Biol Chem, 2003. **278**(43): p. 42377-85.

72. Serra-Pagès, C., et al., *Liprins, a family of LAR transmembrane protein-tyrosine phosphatase-interacting proteins.* J Biol Chem, 1998. **273**(25): p. 15611-20.

73. Zhen, M. and Y. Jin, *The liprin protein SYD-2 regulates the differentiation of presynaptic termini in C. elegans.* Nature, 1999. **401**(6751): p. 371-375.

74. Owald, D., et al., *A Syd-1 homologue regulates pre- and postsynaptic maturation in Drosophila.* J Cell Biol, 2010. **188**(4): p. 565-79.

75. Owald, D., et al., *Cooperation of Syd-1 with Neurexin synchronizes pre- with postsynaptic assembly.* Nature Neuroscience, 2012. **15**(9): p. 1219-1226.

76. Dai, Y., et al., *SYD-2 Liprin-alpha organizes presynaptic active zone formation through ELKS.* Nat Neurosci, 2006. **9**(12): p. 1479-87.

77. Patel, M.R., et al., *Hierarchical assembly of presynaptic components in defined C. elegans synapses.* Nat Neurosci, 2006. **9**(12): p. 1488-98.

78. Maruyama, I.N. and S. Brenner, *A phorbol ester/diacylglycerol-binding protein encoded by the unc-13 gene of Caenorhabditis elegans.* Proc Natl Acad Sci U S A, 1991. **88**(13): p. 5729-33.

79. Aravamudan, B., et al., *Drosophila Unc-13 is essential for synaptic transmission.* Nature Neuroscience, 1999. **2**(11): p. 965-971.

80. Richmond, J.E., W.S. Davis, and E.M. Jorgensen, *UNC-13 is required for synaptic vesicle fusion in C. elegans.* Nat Neurosci, 1999. **2**(11): p. 959-64.

81. Varoqueaux, F., et al., *Total arrest of spontaneous and evoked synaptic transmission but normal synaptogenesis in the absence of Munc13-mediated vesicle priming.* Proceedings of the National Academy of Sciences, 2002. **99**(13): p. 9037-9042.

82. Kohn, R.E., et al., *Expression of multiple UNC-13 proteins in the Caenorhabditis elegans nervous system.* Mol Biol Cell, 2000. **11**(10): p. 3441-52.

83. Brose, N., et al., *Mammalian homologues of Caenorhabditis elegans unc-13 gene define novel family of C2-domain proteins.* J Biol Chem, 1995. **270**(42): p. 25273-80.

84. Song, Y., M. Ailenberg, and M. Silverman, *Cloning of a novel gene in the human kidney homologous to rat munc13s: its potential role in diabetic nephropathy.* Kidney Int, 1998. **53**(6): p. 1689-95.

85. Koch, H., K. Hofmann, and N. Brose, *Definition of Munc13-homology-domains and characterization of a novel ubiquitously expressed Munc13 isoform.* Biochem J, 2000. **349**(Pt 1): p. 247-53.

86. Hu, Z., X.J. Tong, and J.M. Kaplan, *UNC-13L, UNC-13S, and Tomosyn form a protein code for fast and slow neurotransmitter release in Caenorhabditis elegans.* Elife, 2013. **2**: p. e00967.

87. Xu, X.Z., et al., *Retinal targets for calmodulin include proteins implicated in synaptic transmission.* J Biol Chem, 1998. **273**(47): p. 31297-307.

88. Moss, S.J. and T.G. Smart, *Constructing inhibitory synapses.* Nat Rev Neurosci, 2001. **2**(4): p. 240-50.

89. Greenamyre, J.T. and R.H. Porter, *Anatomy and physiology of glutamate in the CNS.* Neurology, 1994. **44**(11 Suppl 8): p. S7-13.

90. Kohler, R.E., *Lords of the fly: Drosophila genetics and the experimental life*. 1994: University of Chicago Press.

91. Morgan, T.H., *Sex Limited Inheritance in <i>Drosophila</i>.* Science, 1910. **32**(812): p. 120-122.

92. Muller, H.J., *The Production of Mutations by X-Rays.* Proc Natl Acad Sci U S A, 1928. **14**(9): p. 714-26.

93. Tolwinski, N.S., *Introduction: Drosophila-A Model System for Developmental Biology.* J Dev Biol, 2017. **5**(3).

94. Stephenson, R. and N.H. Metcalfe, *Drosophila melanogaster: a fly through its history and current use.* J R Coll Physicians Edinb, 2013. **43**(1): p. 70-5.

95. Brand, A.H. and N. Perrimon, *Targeted gene expression as a means of altering cell fates and generating dominant phenotypes.* Development, 1993. **118**(2): p. 401-15.

96. Jennings, B.H., *Drosophila – a versatile model in biology & medicine.* Materials Today, 2011. **14**(5): p. 190-195.

97. Menon, K.P., R.A. Carrillo, and K. Zinn, *Development and plasticity of the Drosophila larval neuromuscular junction.* WIREs Developmental Biology, 2013. **2**(5): p. 647-670.

98. Jan, L.Y. and Y.N. Jan, *L-glutamate as an excitatory transmitter at the Drosophila larval neuromuscular junction.* The Journal of Physiology, 1976. **262**.

99. Jan, L.Y. and Y.N. Jan, *Properties of the larval neuromuscular junction in Drosophila melanogaster.* J Physiol, 1976. **262**(1): p. 189-214.

100. Ruiz-Cañada, C. and V. Budnik, *Introduction on the use of the Drosophila embryonic/larval neuromuscular junction as a model system to study synapse development and function, and a brief summary of pathfinding and target recognition.* Int Rev Neurobiol, 2006. **75**: p. 1-31.

101. Venken, K.J. and H.J. Bellen, *Emerging technologies for gene manipulation in Drosophila melanogaster.* Nat Rev Genet, 2005. **6**(3): p. 167-78.

102. Sigrist, S.J., et al., *Experience-dependent strengthening of Drosophila neuromuscular junctions.* J Neurosci, 2003. **23**(16): p. 6546-56.

103. Keshishian, H., et al., *The Drosophila Neuromuscular Junction: A Model System for Studying Synaptic Development and Function.* Annual Review of Neuroscience, 1996. **19**(1): p. 545-575.

104. Marqués, G. and B. Zhang, *Retrograde signaling that regulates synaptic development and function at the Drosophila neuromuscular junction.* Int Rev Neurobiol, 2006. **75**: p. 267-85.

105. Packard, M., et al., *The Drosophila Wnt, wingless, provides an essential signal for pre- and postsynaptic differentiation.* Cell, 2002. **111**(3): p. 319-30.

106. Ataman, B., et al., *Nuclear trafficking of Drosophila Frizzled-2 during synapse development requires the PDZ protein dGRIP.* Proc Natl Acad Sci U S A, 2006. **103**(20): p. 7841-6.

107. Green, C.H., B. Burnet, and K.J. Connolly, *Organization and patterns of inter- and intraspecific variation in the behaviour of Drosophila larvae.* Animal Behaviour, 1983. **31**(1): p. 282-291.

108. Gomez-Marin, A. and M. Louis, *Active sensation during orientation behaviour in the Drosophila larva: more sense than luck.* Current Opinion in Neurobiology, 2012. **22**(2): p. 208-215.

109. Lahiri, S., et al., *Two Alternating Motor Programs Drive Navigation in Drosophila Larva.* PLOS ONE, 2011. **6**(8): p. e23180.

110. Heckscher, E.S., S.R. Lockery, and C.Q. Doe, *Characterization of Drosophila Larval Crawling at the Level of Organism, Segment, and Somatic Body Wall Musculature.* The Journal of Neuroscience, 2012. **32**(36): p. 12460-12471.

111. Fox, L.E., D.R. Soll, and C.-F. Wu, *Coordination and Modulation of Locomotion Pattern Generators in Drosophila Larvae: Effects of Altered Biogenic Amine Levels by the Tyramine β Hydroxlyase Mutation.* The Journal of Neuroscience, 2006. **26**(5): p. 1486-1498.

112. Gjorgjieva, J., et al., *Neural circuits for peristaltic wave propagation in crawling Drosophila larvae: analysis and modeling.* Frontiers in computational neuroscience, 2013. **7**: p. 24.

113. Inada, K., et al., *Optical Dissection of Neural Circuits Responsible for Drosophila Larval Locomotion with Halorhodopsin.* PLOS ONE, 2011. **6**(12): p. e29019.

114. Heckscher, E.S., S.R. Lockery, and C.Q. Doe, *Characterization of Drosophila larval crawling at the level of organism, segment, and somatic body wall musculature.* J Neurosci, 2012. **32**(36): p. 12460-71.

115. Monastirioti, M., et al., *Octopamine immunoreactivity in the fruit fly Drosophila melanogaster.* J Comp Neurol, 1995. **356**(2): p. 275-87.

116. Roeder, T., *Tyramine and octopamine: ruling behaviour and metabolism.* Annu Rev Entomol, 2005. **50**: p. 447-77.

117. Roeder, T., *Octopamine in invertebrates.* Prog Neurobiol, 1999. **59**(5): p. 533-61.

118. Roeder, T., et al., *Tyramine and octopamine: Antagonistic modulators of behaviour and metabolism.* Archives of Insect Biochemistry and Physiology, 2003. **54**(1): p. 1-13.

119. Nässel, D.R. and A.M. Winther, *Drosophila neuropeptides in regulation of physiology and behaviour.* Prog Neurobiol, 2010. **92**(1): p. 42-104.

120. Evans, P.D., *The role of cyclic nucleotides and calcium in the mediation of the modulatory effects of octopamine on locust skeletal muscle.* The Journal of Physiology, 1984. **348**(1): p. 325-340.

121. Baier, A., B. Wittek, and B. Brembs, *Drosophila as a new model organism for the neurobiology of aggression?* J Exp Biol, 2002. **205**(Pt 9): p. 1233-40.

122. Schwaerzel, M., et al., *Dopamine and octopamine differentiate between aversive and appetitive olfactory memories in Drosophila.* J Neurosci, 2003. **23**(33): p. 10495-502.

123. Scholz, H., M. Franz, and U. Heberlein, *The hangover gene defines a stress pathway required for ethanol tolerance development.* Nature, 2005. **436**(7052): p. 845-7.

124. Schroll, C., et al., *Light-Induced Activation of Distinct Modulatory Neurons Triggers Appetitive or Aversive Learning in Drosophila Larvae.* Current Biology, 2006. **16**(17): p. 1741-1747.

125. Certel, S.J., et al., *Modulation of <i>Drosophila</i> male behavioural choice.* Proceedings of the National Academy of Sciences, 2007. **104**(11): p. 4706-4711.

126. Hoyer, S.C., et al., *Octopamine in Male Aggression of Drosophila.* Current Biology, 2008. **18**(3): p. 159-167.

127. Crocker, A., et al., *Identification of a Neural Circuit that Underlies the Effects of Octopamine on Sleep:Wake Behaviour.* Neuron, 2010. **65**(5): p. 670-681.

128. Evans, P.D. and M. O'Shea, *An octopaminergic neurone modulates neuromuscular transmission in the locust.* Nature, 1977. **270**(5634): p. 257-9.

129. O'Shea, M. and P.D. Evans, *Potentiation of neuromuscular transmission by an octopaminergic neurone in the locust.* Journal of Experimental Biology, 1979. **79**(1): p. 169-190.

130. Ormerod, K.G., et al., *Action of octopamine and tyramine on muscles of Drosophila melanogaster larvae.* J Neurophysiol, 2013. **110**(8): p. 1984-96.

131. Pflüger, H.J. and C. Duch, *Dynamic neural control of insect muscle metabolism related to motor behaviour.* Physiology (Bethesda), 2011. **26**(4): p. 293-303.

132. Saraswati, S., et al., *Tyramine and octopamine have opposite effects on the locomotion of Drosophila larvae.* J Neurobiol, 2004. **58**(4): p. 425-41.

133. Brembs, B., et al., *Flight initiation and maintenance deficits in flies with genetically altered biogenic amine levels.* J Neurosci, 2007. **27**(41): p. 11122-31.

134. Rillich, J., P.A. Stevenson, and H.J. Pflueger, *Flight and walking in locusts-cholinergic co-activation, temporal coupling and its modulation by biogenic amines.* PLoS One, 2013. **8**(5): p. e62899.

135. Downer, R.G.H., *Trehalose production in isolated fat body of the american cockroach, Periplaneta americana.* Comparative Biochemistry and Physiology Part C: Comparative Pharmacology, 1979. **62**(1): p. 31-34.

136. Kutsukake, M., et al., *A tyramine receptor gene mutation causes a defective olfactory behaviour in Drosophila melanogaster.* Gene, 2000. **245**(1): p. 31-42.

137. Johansen, J., et al., *Stereotypic morphology of glutamatergic synapses on identified muscle cells of Drosophila larvae.* J Neurosci, 1989. **9**(2): p. 710-25.

138. Arakawa, S., et al., *Cloning, localization, and permanent expression of a Drosophila octopamine receptor.* Neuron, 1990. **4**(3): p. 343-54.

139. Saudou, F., et al., *Cloning and characterization of a Drosophila tyramine receptor.* Embo j, 1990. **9**(11): p. 3611-7.

140. Monastirioti, M., J. Charles E. Linn, and K. White, *Characterization of Drosophila Tyramine β-HydroxylaseGene and Isolation of Mutant Flies Lacking Octopamine.* The Journal of Neuroscience, 1996. **16**(12): p. 3900-3911.

141. Schützler, N., et al., *Tyramine action on motoneuron excitability and adaptable tyramine/octopamine ratios adjust <i>Drosophila</i> locomotion to nutritional state.* Proceedings of the National Academy of Sciences, 2019. **116**(9): p. 3805-3810.

142. Hardie, S.L., J.X. Zhang, and J. Hirsh, *Trace amines differentially regulate adult locomotor activity, cocaine sensitivity, and female fertility in Drosophila melanogaster.* Dev Neurobiol, 2007. **67**(10): p. 1396-405.

143. Schüpbach, T. and E. Wieschaus, *Female sterile mutations on the second chromosome of Drosophila melanogaster. II. Mutations blocking oogenesis or altering egg morphology.* Genetics, 1991. **129**(4): p. 1119-36.

144. Homyk, T., Jr. and D.E. Sheppard, *BEHAVIOURAL MUTANTS OF DROSOPHILA MELANOGASTER. I. ISOLATION AND MAPPING OF MUTATIONS WHICH DECREASE FLIGHT ABILITY.* Genetics, 1977. **87**(1): p. 95-104.

145. O'Dell, K. and B. Burnet, *The effects on locomotor activity and reactivity of the hypoactive and inactive mutations of Drosophila melanogaster.* Heredity, 1988. **61**(2): p. 199-207.

146. Bräunig, P., *Suboesophageal DUM neurons innervate the principal neuropiles of the locust brain.* Philosophical Transactions of the Royal Society of London. Series B: Biological Sciences, 1991. **332**(1264): p. 221-240.

147. Sinakevitch, I. and N.J. Strausfeld, *Comparison of octopamine-like immunoreactivity in the brains of the fruit fly and blow fly.* J Comp Neurol, 2006. **494**(3): p. 460-75.

148. Busch, S., et al., *A map of octopaminergic neurons in the Drosophila brain.* J Comp Neurol, 2009. **513**(6): p. 643-67.

149. Vömel, M. and C. Wegener, *Neuroarchitecture of aminergic systems in the larval ventral ganglion of Drosophila melanogaster.* PLoS One, 2008. **3**(3): p. e1848.

150. Burrows, M. and H. Pfluger, *Action of locust neuromodulatory neurons is coupled to specific motor patterns.* Journal of Neurophysiology, 1995. **74**(1): p. 347-357.

151. Baudoux, S., C. Duch, and O.T. Morris, *Coupling of efferent neuromodulatory neurons to rhythmical leg motor activity in the locust.* Journal of neurophysiology, 1998. **79**(1): p. 361-370.

152. Duch, C. and H.-J. Pflüger, *DUM neurons in locust flight: a model system for amine-mediated peripheral adjustments to the requirements of a central motor program.* Journal of Comparative Physiology A, 1999. **184**: p. 489-499.

153. Duch, C., T. Mentel, and H.J. Pflüger, *Distribution and activation of different types of octopaminergic DUM neurons in the locust.* J Comp Neurol, 1999. **403**(1): p. 119-34.

154. Mentel, T., et al., *Activity of neuromodulatory neurones during stepping of a single insect leg.* J Insect Physiol, 2008. **54**(1): p. 51-61.

155. Johnston, R.M., et al., *Patterned activation of unpaired median neurons during fictive crawling in manduca sexta larvae.* J Exp Biol, 1999. **202 (Pt 2)**: p. 103-13.

156. Mentel, T., et al., *Central modulatory neurons control fuel selection in flight muscle of migratory locust.* J Neurosci, 2003. **23**(4): p. 1109-13.

157. Wilson, D.M., *The central nervous control of flight in a locust.* Journal of Experimental Biology, 1961. **38**(2): p. 471-490.

158. Stevenson, P.A. and W. Kutsch, *A reconsideration of the central pattern generator concept for locust flight.* Journal of Comparative Physiology A, 1987. **161**: p. 115-129.

159. Stevenson, P.A. and W. Kutsch, *Demonstration of functional connectivity of the flight motor system in all stages of the locust.* Journal of Comparative Physiology A, 1988. **162**(2): p. 247-259.

160. Hoang, B. and A. Chiba, *Single-Cell Analysis of Drosophila Larval Neuromuscular Synapses.* Developmental Biology, 2001. **229**(1): p. 55-70.

161. Plotnikova, S., *Effector neurons with several axons in the ventral nerve cord of the Asian grasshopper Locusta migratoria.* J. Evol. Biochem. Physiol, 1969. **5**: p. 276-277.

162. Hoyle, G., *A function for neurons (DUM) neurosecretory on skeletal muscle of insects.* Journal of Experimental Zoology, 1974. **189**(3): p. 401-406.

163. Bräunig, P. and H.-J. Pflüger, *The unpaired median neurons of insects.* 2001.

164. Kononenko, N.L., H. Wolfenberg, and H.J. Pflüger, *Tyramine as an independent transmitter and a precursor of octopamine in the locust central nervous system: an immunocytochemical study.* J Comp Neurol, 2009. **512**(4): p. 433-52.

165. Wicher, D., *Metabolic regulation and behaviour: how hunger produces arousal - an insect study.* Endocr Metab Immune Disord Drug Targets, 2007. **7**(4): p. 304-10.

166. Erspamer, V. and G. Boretti, *Identification and characterization, by paper chromatography, of enteramine, octopamine, tyramine, histamine and allied substances in extracts of posterior salivary glands of octopoda and in other tissue extracts of vertebrates and invertebrates.* Arch Int Pharmacodyn Ther, 1951. **88**(3): p. 296-332.

167. Monastirioti, M., C.E. Linn, Jr., and K. White, *Characterization of Drosophila tyramine beta-hydroxylase gene and isolation of mutant flies lacking octopamine.* J Neurosci, 1996. **16**(12): p. 3900-11.

168. Jan, L.Y. and Y.N. Jan, *L-glutamate as an excitatory transmitter at the Drosophila larval neuromuscular junction.* J Physiol, 1976. **262**(1): p. 215-36.

169. Atwood, H.L., C.K. Govind, and C.F. Wu, *Differential ultrastructure of synaptic terminals on ventral longitudinal abdominal muscles in Drosophila larvae.* J Neurobiol, 1993. **24**(8): p. 1008-24.

170. Littleton, J.T., H.J. Bellen, and M.S. Perin, *Expression of Synaptotagmin in Drosophila reveals transport and localization of synaptic vesicles to the synapse.* Development, 1993. **118**: p. 1077-1088.

171. Sherer, L.M., et al., *Octopamine neuron dependent aggression requires dVGLUT from dual-transmitting neurons.* PLOS Genetics, 2020. **16**(2): p. e1008609.

172. Grenningloh, G., E. Jay Rehm, and C.S. Goodman, *Genetic analysis of growth cone guidance in drosophila: Fasciclin II functions as a neuronal recognition molecule.* Cell, 1991. **67**(1): p. 45-57.

173. Harrelson, A.L. and C.S. Goodman, *Growth cone guidance in insects: fasciclin II is a member of the immunoglobulin superfamily.* Science, 1988. **242**(4879): p. 700-8.

174. Nassif, C., A. Noveen, and V. Hartenstein, *Early development of the Drosophila brain: III. The pattern of neuropile founder tracts during the larval period.* J Comp Neurol, 2003. **455**(4): p. 417-34.

175. Nassif, C., A. Noveen, and V. Hartenstein, *Embryonic development of the Drosophila brain. I. Pattern of pioneer tracts.* J Comp Neurol, 1998. **402**(1): p. 10-31.

176. Grenningloh, G., et al., *Molecular genetics of neuronal recognition in Drosophila: evolution and function of immunoglobulin superfamily cell adhesion molecules.* Cold Spring Harb Symp Quant Biol, 1990. **55**: p. 327-40.

177. Wright, J.W., et al., *A role for fasciclin II in the guidance of neuronal migration.* Development, 1999. **126**(14): p. 3217-3228.

178. Hummel, T., et al., *Drosophila Futsch/22C10 Is a MAP1B-like Protein Required for Dendritic and Axonal Development.* Neuron, 2000. **26**(2): p. 357-370.

179. Nathanson, J.A. and P. Greengard, *Octopamine-sensitive adenylate cyclse: evidence for a biological role of octopamine in nervous tissue.* Science, 1973. **180**(4083): p. 308-10.

180. Kim, Y.C., et al., *Appetitive learning requires the alpha1-like octopamine receptor OAMB in the Drosophila mushroom body neurons.* J Neurosci, 2013. **33**(4): p. 1672-7.

181. Farooqui, T., et al., *Modulation of early olfactory processing by an octopaminergic reinforcement pathway in the honeybee.* J Neurosci, 2003. **23**(12): p. 5370-80.

182. Blenau, W. and A. Baumann, *Molecular and pharmacological properties of insect biogenic amine receptors: Lessons from Drosophila melanogaster and Apis mellifera.* Archives of Insect Biochemistry and Physiology, 2001. **48**(1): p. 13-38.

183. Evans, P.D., *Multiple receptor types for octopamine in the locust.* The Journal of Physiology, 1981. **318**(1): p. 99-122.

184. Evans, P.D., *Studies on the Mode of Action of Octopamine, 5-Hydroxytryptamine And Proctolin on A Myogenic Rhythm in the Locust.* Journal of Experimental Biology, 1984. **110**(1): p. 231-251.

185. Evans, P.D., *A modulatory octopaminergic neurone increases cyclic nucleotide levels in locust skeletal muscle.* J Physiol, 1984. **348**: p. 307-24.

186. Evans, P.D., *The role of cyclic nucleotides and calcium in the mediation of the modulatory effects of octopamine on locust skeletal muscle.* J Physiol, 1984. **348**: p. 325-40.

187. Evans, P.D. and B. Maqueira, *Insect octopamine receptors: a new classification scheme based on studies of cloned Drosophila G-protein coupled receptors.* Invert Neurosci, 2005. **5**(3-4): p. 111-8.

188. Nagaya, Y., et al., *A trace amine, tyramine, functions as a neuromodulator in Drosophila melanogaster.* Neurosci Lett, 2002. **329**(3): p. 324-8.

189. Robb, S., et al., *Agonist-specific coupling of a cloned Drosophila octopamine/tyramine receptor to multiple second messenger systems.* Embo j, 1994. **13**(6): p. 1325-30.

190. Evans, P.D., et al., *Chapter 26 Agonist-specific coupling of G-protein-coupled receptors to second-messenger systems*, in *Progress in Brain Research*, P.M. Yu, K.F. Tipton, and A.A. Boulton, Editors. 1995, Elsevier. p. 259-268.

191. Kenakin, T., *Agonist-receptor efficacy. II. Agonist trafficking of receptor signals.* Trends Pharmacol Sci, 1995. **16**(7): p. 232-8.

192. Hannan, F. and L.M. Hall, *Temporal and spatial expression patterns of two G-protein coupled receptors inDrosophila melanogaster.* Invertebrate Neuroscience, 1996. **2**(1): p. 71-83.

193. Han, K.A., N.S. Millar, and R.L. Davis, *A novel octopamine receptor with preferential expression in Drosophila mushroom bodies.* J Neurosci, 1998. **18**(10): p. 3650-8.

194. Davis, R.L., *Physiology and biochemistry of Drosophila learning mutants.* Physiological Reviews, 1996. **76**(2): p. 299-317.

195. Dudai, Y. and S. Zvi, *High-affinity [3H]octopamine-binding sites in Drosophila melanogaster: interaction with ligands and relationship to octopamine receptors.* Comp Biochem Physiol C Comp Pharmacol Toxicol, 1984. **77**(1): p. 145-51.

196. Lee, H.G., et al., *Octopamine receptor OAMB is required for ovulation in Drosophila melanogaster.* Dev Biol, 2003. **264**(1): p. 179-90.

197. Balfanz, S., et al., *A family of octopamine [corrected] receptors that specifically induce cyclic AMP production or Ca2+ release in Drosophila melanogaster.* J Neurochem, 2005. **93**(2): p. 440-51.

198. Roeder, T., *Biogenic amines and their receptors in insects.* Comparative Biochemistry and Physiology Part C: Pharmacology, Toxicology and Endocrinology, 1994. **107**(1): p. 1-12.

199. Orchard, I., *Octopamine in insects: neurotransmitter, neurohormone, and neuromodulator.* Canadian Journal of Zoology, 1982. **60**(4): p. 659-669.

200. Bräunig, P. and M. Burrows, *Projection patterns of posterior dorsal unpaired median neurons of the locust subesophageal ganglion.* Journal of Comparative Neurology, 2004. **478**(2): p. 164-175.

201. Cazzamali, G., D.A. Klaerke, and C.J. Grimmelikhuijzen, *A new family of insect tyramine receptors.* Biochem Biophys Res Commun, 2005. **338**(2): p. 1189-96.

202. Bayliss, A., G. Roselli, and P.D. Evans, *A comparison of the signalling properties of two tyramine receptors from Drosophila.* Journal of Neurochemistry, 2013. **125**(1): p. 37-48.

203. Lange, A.B., *Tyramine: From octopamine precursor to neuroactive chemical in insects.* General and Comparative Endocrinology, 2009. **162**(1): p. 18-26.

204. José A. Campos-Ortega, V.H., *The Embryonic Development of Drosophila melanogaster.* 1985: Springer Berlin, Heidelberg. 227.

205. Broadie, K.S. and M. Bate, *Development of the embryonic neuromuscular synapse of Drosophila melanogaster.* J Neurosci, 1993. **13**(1): p. 144-66.

206. Featherstone, D.E. and K. Broadie, *Surprises from Drosophila: genetic mechanisms of synaptic development and plasticity.* Brain Research Bulletin, 2000. **53**(5): p. 501-511.

207. Chiba, A. and D. Rose, *"Painting" the target: how local molecular cues define synaptic relationships.* BioEssays, 1998. **20**(11): p. 941-948.

208. Rose, D. and A. Chiba, *A single growth cone is capable of integrating simultaneously presented and functionally distinct molecular cues during target recognition.* J Neurosci, 1999. **19**(12): p. 4899-906.

209. Bate, M., M. Landgraf, and M. Ruiz Gómez Bate, *Development of larval body wall muscles.* Int Rev Neurobiol, 1999. **43**: p. 25-44.

210. Rheuben, M.B., M. Yoshihara, and Y. Kidokoro, *Ultrastructural correlates of neuromuscular junction development.* Int Rev Neurobiol, 1999. **43**: p. 69-92.

211. Broadie, K.S. and M. Bate, *Development of larval muscle properties in the embryonic myotubes of Drosophila melanogaster.* J Neurosci, 1993. **13**(1): p. 167-80.

212. Broadie, K. and M. Bate, *Innervation directs receptor synthesis and localization in Drosophila embryo synaptogenesis.* Nature, 1993. **361**(6410): p. 350-3.

213. Chiba, A., et al., *Fasciclin III as a synaptic target recognition molecule in Drosophila.* Nature, 1995. **374**(6518): p. 166-8.

214. Kose, H., et al., *Homophilic synaptic target recognition mediated by immunoglobulin-like cell adhesion molecule Fasciclin III.* Development, 1997. **124**(20): p. 4143-52.

215. Prokop, A., et al., *Presynaptic development at the Drosophila neuromuscular junction: assembly and localization of presynaptic active zones.* Neuron, 1996. **17**(4): p. 617-26.

216. Prokop, A., *Integrating bits and pieces: synapse structure and formation in Drosophila embryos.* Cell Tissue Res, 1999. **297**(2): p. 169-86.

217. Guan, B., et al., *The Drosophila tumor suppressor gene, dlg, is involved in structural plasticity at a glutamatergic synapse.* Curr Biol, 1996. **6**(6): p. 695-706.

218. Zito, K., et al., *Watching a synapse grow: noninvasive confocal imaging of synaptic growth in Drosophila.* Neuron, 1999. **22**(4): p. 719-29.

219. Josephson, R.K., J.G. Malamud, and D.R. Stokes, *Asynchronous Muscle: A Primer.* Journal of Experimental Biology, 2000. **203**(18): p. 2713-2722.

220. Agianian, B., et al., *A troponin switch that regulates muscle contraction by stretch instead of calcium.* Embo j, 2004. **23**(4): p. 772-9.

221. Robertson, C.W., *The metamorphosis of Drosophila melanogaster, including an accurately timed account of the principal morphological changes.* Journal of Morphology, 1936. **59**(2): p. 351-399.

222. Costello, W.J. and R.J. Wyman, *Development of an indirect flight muscle in a muscle-specific mutant of Drosophila melanogaster.* Developmental Biology, 1986. **118**(1): p. 247-258.

223. Crossley, A., *Morphology and development of the Drosophila muscular system.* Genetics and biology of Drosophila, 1978.

224. Fernandes, J., M. Bate, and K. Vijayraghavan, *Development of the indirect flight muscles of Drosophila.* Development, 1991. **113**(1): p. 67-77.

225. Jawkar, S. and U. Nongthomba, *Indirect flight muscles in Drosophila melanogaster as a tractable model to study muscle development and disease.* Int J Dev Biol, 2020. **64**(1-2-3): p. 167-173.

226. Fernandes, J. and K. VijayRaghavan, *The development of indirect flight muscle innervation in Drosophila melanogaster.* Development, 1993. **118**(1): p. 215-227.

227. Ikeda, K. and J.H. Koenig, *Morphological identification of the motor neurons innervating the dorsal longitudinal flight muscle of Drosophila melanogaster.* Journal of Comparative Neurology, 1988. **273**(3): p. 436-444.

228. Hummon, M.R. and W.J. Costello, *Induced neuroma formation and target muscle perturbation in the giant fiber pathway of the Drosophila temperature-sensitive mutant shibire.* Roux's archives of developmental biology, 1988. **197**(7): p. 383-393.

229. Miller, A., *The internal anatomy and histology of the imago of Drosophila melanogaster.* The biology of Drosophila, 1950: p. 421-534.

230. Coggshall, J.C., *Neurons associated with the dorsal longitudinal flight muscles ofDrosophila melanogaster.* Journal of Comparative Neurology, 1978. **177**(4): p. 707-720.

231. Gunage, R.D., et al., *Drosophila adult muscle development and regeneration.* Seminars in Cell & Developmental Biology, 2017. **72**: p. 56-66.

232. Kimura, K. and J. Truman, *Postmetamorphic cell death in the nervous and muscular systems of Drosophila melanogaster.* The Journal of Neuroscience, 1990. **10**(2): p. 403-411.

233. Kuleesha, Y., W.C. Puah, and M. Wasser, *Live imaging of muscle histolysis in Drosophila metamorphosis.* BMC Developmental Biology, 2016. **16**(1): p. 12.

234. Sink, H. and P.M. Whitington, *Location and connectivity of abdominal motoneurons in the embryo and larva of Drosophila melanogaster.* Journal of Neurobiology, 1991. **22**(3): p. 298-311.

235. Carson, H.L. and J.N. Thompson, *The genetics and biology of Drosophila*. 1976.

236. Beramendi, A., et al., *Neuromuscular junction in abdominal muscles of Drosophila melanogaster during adulthood and aging.* Journal of Comparative Neurology, 2007. **501**(4): p. 498-508.

237. Mattson, M.P. and T.V. Arumugam, *Hallmarks of Brain Aging: Adaptive and Pathological Modification by Metabolic States.* Cell Metab, 2018. **27**(6): p. 1176-1199.

238. López-Otín, C., et al., *The hallmarks of aging.* Cell, 2013. **153**(6): p. 1194-217.

239. Gladyshev, V.N., *On the cause of aging and control of lifespan.* BioEssays, 2012. **34**(11): p. 925-929.

240. Franceschi, C., M. Bonafè, and S. Valensin, *Human immunosenescence: the prevailing of innate immunity, the failing of clonotypic immunity, and the filling of immunological space.* Vaccine, 2000. **18**(16): p. 1717-20.

241. Olovnikov, A.M., *[Principle of marginotomy in template synthesis of polynucleotides].* Dokl Akad Nauk SSSR, 1971. **201**(6): p. 1496-9.

242. Olovnikov, A.M., *A theory of marginotomy: The incomplete copying of template margin in enzymic synthesis of polynucleotides and biological significance of the phenomenon.* Journal of Theoretical Biology, 1973. **41**(1): p. 181-190.

243. Harman, D., *Aging: a theory based on free radical and radiation chemistry.* J Gerontol, 1956. **11**(3): p. 298-300.

244. Levine, R.L. and E.R. Stadtman, *Oxidative modification of proteins during aging.* Experimental Gerontology, 2001. **36**(9): p. 1495-1502.

245. Richter, C., J.W. Park, and B.N. Ames, *Normal oxidative damage to mitochondrial and nuclear DNA is extensive.* Proc Natl Acad Sci U S A, 1988. **85**(17): p. 6465-7.

246. Reece, J.B., et al., *Campbell Biology*. 2011: Pearson Education.

247. Nolfi-Donegan, D., A. Braganza, and S. Shiva, *Mitochondrial electron transport chain: Oxidative phosphorylation, oxidant production, and methods of measurement.* Redox Biol, 2020. **37**: p. 101674.

248. Zhao, R.Z., et al., *Mitochondrial electron transport chain, ROS generation and uncoupling (Review).* Int J Mol Med, 2019. **44**(1): p. 3-15.

249. Balaban, R.S., S. Nemoto, and T. Finkel, *Mitochondria, Oxidants, and Aging.* Cell, 2005. **120**(4): p. 483-495.

250. Brand, M.D., *Mitochondrial generation of superoxide and hydrogen peroxide as the source of mitochondrial redox signaling.* Free Radic Biol Med, 2016. **100**: p. 14-31.

251. D'Autréaux, B. and M.B. Toledano, *ROS as signalling molecules: mechanisms that generate specificity in ROS homeostasis.* Nat Rev Mol Cell Biol, 2007. **8**(10): p. 813-24.

252. De Giusti, V.C., et al., *Mitochondrial reactive oxygen species (ROS) as signaling molecules of intracellular pathways triggered by the cardiac renin-angiotensin II-aldosterone system (RAAS).* Front Physiol, 2013. **4**: p. 126.

253. Orrenius, S., V. Gogvadze, and B. Zhivotovsky, *Mitochondrial oxidative stress: implications for cell death.* Annu Rev Pharmacol Toxicol, 2007. **47**: p. 143-83.

254. Nunnari, J. and A. Suomalainen, *Mitochondria: in sickness and in health.* Cell, 2012. **148**(6): p. 1145-59.

255. Yi, M., D. Weaver, and G. Hajnóczky, *Control of mitochondrial motility and distribution by the calcium signal: a homeostatic circuit.* J Cell Biol, 2004. **167**(4): p. 661-72.

256. Alberts, B., *Molecular biology of the cell*. 2017: Garland science.

257. Lane, N. and W. Martin, *The energetics of genome complexity.* Nature, 2010. **467**(7318): p. 929-34.

258. Siekevitz, P., *Powerhouse of the cell.* Scientific American, 1957. **197**(1): p. 131-144.

259. Hamanaka, R.B. and N.S. Chandel, *Mitochondrial reactive oxygen species regulate cellular signaling and dictate biological outcomes.* Trends Biochem Sci, 2010. **35**(9): p. 505-13.

260. De Giusti, V., et al., *Mitochondrial reactive oxygen species (ROS) as signaling molecules of intracellular pathways triggered by the cardiac renin-angiotensin II-aldosterone system (RAAS).* Frontiers in Physiology, 2013. **4**.

261. Short, K.R., et al., *Decline in skeletal muscle mitochondrial function with aging in humans.* Proc Natl Acad Sci U S A, 2005. **102**(15): p. 5618-23.

262. Chakrabarti, S., et al., *Mitochondrial Dysfunction during Brain Aging: Role of Oxidative Stress and Modulation by Antioxidant Supplementation.* Aging Dis, 2011. **2**(3): p. 242-56.

263. Halliwell, B. and C.E. Cross, *Oxygen-derived species: their relation to human disease and environmental stress.* Environ Health Perspect, 1994. **102 Suppl 10**(Suppl 10): p. 5-12.

264. Circu, M.L. and T.Y. Aw, *Reactive oxygen species, cellular redox systems, and apoptosis.* Free Radic Biol Med, 2010. **48**(6): p. 749-62.

265. Ames, B.N., M.K. Shigenaga, and T.M. Hagen, *Oxidants, antioxidants, and the degenerative diseases of aging.* Proc Natl Acad Sci U S A, 1993. **90**(17): p. 7915-22.

266. Turrens, J.F., *Mitochondrial formation of reactive oxygen species.* J Physiol, 2003. **552**(Pt 2): p. 335-44.

267. Jones, D.P., *Redefining oxidative stress.* Antioxid Redox Signal, 2006. **8**(9-10): p. 1865-79.

268. Filomeni, G., G. Rotilio, and M.R. Ciriolo, *Cell signalling and the glutathione redox system.* Biochemical Pharmacology, 2002. **64**(5): p. 1057-1064.

269. Sies, H., *What is oxidative stress?*, in *Oxidative stress and vascular disease*. 1985, Springer. p. 1-8.

270. Sies, H., *Oxidative stress: oxidants and antioxidants.* Exp Physiol, 1997. **82**(2): p. 291-5.

271. Schafer, F.Q. and G.R. Buettner, *Redox environment of the cell as viewed through the redox state of the glutathione disulfide/glutathione couple.* Free Radic Biol Med, 2001. **30**(11): p. 1191-212.

272. Circu, M.L., et al., *Contribution of mitochondrial GSH transport to matrix GSH status and colonic epithelial cell apoptosis.* Free Radical Biology and Medicine, 2008. **44**(5): p. 768-778.

273. Meister, A. and M.E. Anderson, *Glutathione.* Annu Rev Biochem, 1983. **52**: p. 711-60.

274. Finkel, T., *Redox-dependent signal transduction.* FEBS Lett, 2000. **476**(1-2): p. 52-4.

275. Klatt, P. and S. Lamas, *Regulation of protein function by S-glutathiolation in response to oxidative and nitrosative stress.* Eur J Biochem, 2000. **267**(16): p. 4928-44.

276. Flohé, L., *Glutathione peroxidase: fact and fiction.* Ciba Found Symp, 1978(65): p. 95-122.

277. Ghibelli, L., et al., *Non-oxidative Loss of Glutathione in Apoptosis via GSH Extrusion.* Biochemical and Biophysical Research Communications, 1995. **216**(1): p. 313-320.

278. Ghibelli, L., et al., *Rescue of cells from apoptosis by inhibition of active GSH extrusion.* Faseb j, 1998. **12**(6): p. 479-86.

279. Ghibelli, L., et al., *Glutathione depletion causes cytochrome c release even in the absence of cell commitment to apoptosis.* Faseb j, 1999. **13**(14): p. 2031-6.

280. Holmgren, A., *Regulation of ribonucleotide reductase.* Curr Top Cell Regul, 1981. **19**: p. 47-76.

281. Huang, Z.-Z., et al., *Mechanism and significance of increased glutathione level in human hepatocellular carcinoma and liver regeneration.* The FASEB Journal, 2001. **15**(1): p. 19-21.

282. Lu, S.C. and J. Ge, *Loss of suppression of GSH synthesis at low cell density in primary cultures of rat hepatocytes.* American Journal of Physiology-Cell Physiology, 1992. **263**(6): p. C1181-C1189.

283. Shaw, J.P. and I.N. Chou, *Elevation of intracellular glutathione content associated with mitogenic stimulation of quiescent fibroblasts.* Journal of Cellular Physiology, 1986. **129**(2): p. 193-198.

284. Poot, M., et al., *De novo synthesis of glutathione is required for both entry into and progression through the cell cycle.* Journal of cellular physiology, 1995. **163**(3): p. 555-560.

285. Iwata, S., et al., *Thiol-mediated redox regulation of lymphocyte proliferation. Possible involvement of adult T cell leukemia-derived factor and glutathione in transferrin receptor expression.* Journal of immunology (Baltimore, Md.: 1950), 1994. **152**(12): p. 5633-5642.

286. Garcia-Ruiz, C. and J.C. Fernández-Checa, *Redox regulation of hepatocyte apoptosis.* J Gastroenterol Hepatol, 2007. **22 Suppl 1**: p. S38-42.

287. Lemasters, J.J., *Dying a thousand deaths: redundant pathways from different organelles to apoptosis and necrosis.* Gastroenterology, 2005. **129**(1): p. 351-60.

288. Martinez-Lopez, N., D. Athonvarangkul, and R. Singh, *Autophagy and aging.* Adv Exp Med Biol, 2015. **847**: p. 73-87.

289. Mizushima, N., *Autophagy: process and function.* Genes & development, 2007. **21**(22): p. 2861-2873.

290. Nakatogawa, H., et al., *Dynamics and diversity in autophagy mechanisms: lessons from yeast.* Nat Rev Mol Cell Biol, 2009. **10**(7): p. 458-67.

291. Klionsky, D.J., et al., *Guidelines for the use and interpretation of assays for monitoring autophagy (4th edition)(1).* Autophagy, 2021. **17**(1): p. 1-382.

292. Kuma, A., et al., *The role of autophagy during the early neonatal starvation period.* Nature, 2004. **432**(7020): p. 1032-6.

293. Levine, B. and D.J. Klionsky, *Development by self-digestion: molecular mechanisms and biological functions of autophagy.* Dev Cell, 2004. **6**(4): p. 463-77.

294. Lum, J.J., et al., *Growth factor regulation of autophagy and cell survival in the absence of apoptosis.* Cell, 2005. **120**(2): p. 237-48.

295. Yang, Z., et al., *Atg22 recycles amino acids to link the degradative and recycling functions of autophagy.* Mol Biol Cell, 2006. **17**(12): p. 5094-104.

296. Ravikumar, B., et al., *Regulation of mammalian autophagy in physiology and pathophysiology.* Physiol Rev, 2010. **90**(4): p. 1383-435.

297. Ding, W.X., S. Manley, and H.M. Ni, *The emerging role of autophagy in alcoholic liver disease.* Exp Biol Med (Maywood), 2011. **236**(5): p. 546-56.

298. Mizushima, N. and M. Komatsu, *Autophagy: renovation of cells and tissues.* Cell, 2011. **147**(4): p. 728-41.

299. Meijer, A.J. and P. Codogno, *Autophagy: regulation and role in disease.* Crit Rev Clin Lab Sci, 2009. **46**(4): p. 210-40.

300. Zhou, B.P., et al., *HER-2/neu blocks tumor necrosis factor-induced apoptosis via the Akt/NF-kappaB pathway.* J Biol Chem, 2000. **275**(11): p. 8027-31.

301. Chung, J., et al., *Integrin (alpha 6 beta 4) regulation of eIF-4E activity and VEGF translation: a survival mechanism for carcinoma cells.* J Cell Biol, 2002. **158**(1): p. 165-74.

302. Stemke-Hale, K., et al., *An integrative genomic and proteomic analysis of PIK3CA, PTEN, and AKT mutations in breast cancer.* Cancer Res, 2008. **68**(15): p. 6084-91.

303. Alers, S., et al., *Role of AMPK-mTOR-Ulk1/2 in the regulation of autophagy: cross talk, shortcuts, and feedbacks.* Mol Cell Biol, 2012. **32**(1): p. 2-11.

304. Meric-Bernstam, F. and A.M. Gonzalez-Angulo, *Targeting the mTOR signaling network for cancer therapy.* J Clin Oncol, 2009. **27**(13): p. 2278-87.

305. Saxton, R.A. and D.M. Sabatini, *mTOR Signaling in Growth, Metabolism, and Disease.* Cell, 2017. **168**(6): p. 960-976.

306. Okamoto, K., N. Kondo-Okamoto, and Y. Ohsumi, *Mitochondria-anchored receptor Atg32 mediates degradation of mitochondria via selective autophagy.* Dev Cell, 2009. **17**(1): p. 87-97.

307. Narendra, D., et al., *Parkin is recruited selectively to impaired mitochondria and promotes their autophagy.* J Cell Biol, 2008. **183**(5): p. 795-803.

308. Clark, I.E., et al., *Drosophila pink1 is required for mitochondrial function and interacts genetically with parkin.* Nature, 2006. **441**(7097): p. 1162-1166.

309. Ashrafi, G., et al., *Mitophagy of damaged mitochondria occurs locally in distal neuronal axons and requires PINK1 and Parkin.* J Cell Biol, 2014. **206**(5): p. 655-70.

310. Narendra, D.P., et al., *PINK1 Is Selectively Stabilized on Impaired Mitochondria to Activate Parkin.* PLOS Biology, 2010. **8**(1): p. e1000298.

311. Eisenberg, T., et al., *Induction of autophagy by spermidine promotes longevity.* Nature Cell Biology, 2009. **11**(11): p. 1305-1314.
312. Eisenberg, T., et al., *Cardioprotection and lifespan extension by the natural polyamine spermidine.* Nature Medicine, 2016. **22**(12): p. 1428-1438.
313. Wang, I.-F., et al., *Autophagy activators rescue and alleviate pathogenesis of a mouse model with proteinopathies of the TAR DNA-binding protein 43.* Proceedings of the National Academy of Sciences, 2012. **109**(37): p. 15024-15029.
314. Schroeder, S., et al., *Dietary spermidine improves cognitive function.* Cell Reports, 2021. **35**(2): p. 108985.
315. Gupta, V.K., et al., *Restoring polyamines protects from age-induced memory impairment in an autophagy-dependent manner.* Nature Neuroscience, 2013. **16**(10): p. 1453-1460.
316. Gupta, V.K., et al., *Spermidine Suppresses Age-Associated Memory Impairment by Preventing Adverse Increase of Presynaptic Active Zone Size and Release.* PLOS Biology, 2016. **14**(9): p. e1002563.
317. Madeo, F., et al., *Spermidine in health and disease.* Science, 2018. **359**(6374).
318. Park, M.H. and E.C. Wolff, *Hypusine, a polyamine-derived amino acid critical for eukaryotic translation.* J Biol Chem, 2018. **293**(48): p. 18710-18718.
319. Park, M.H., *The post-translational synthesis of a polyamine-derived amino acid, hypusine, in the eukaryotic translation initiation factor 5A (eIF5A).* J Biochem, 2006. **139**(2): p. 161-9.
320. Liang, Y., et al., *eIF5A hypusination, boosted by dietary spermidine, protects from premature brain aging and mitochondrial dysfunction.* Cell Reports, 2021. **35**(2): p. 108941.
321. Dooley, C.T., et al., *Imaging dynamic redox changes in mammalian cells with green fluorescent protein indicators.* J Biol Chem, 2004. **279**(21): p. 22284-93.

322. Palm, G.J., et al., *The structural basis for spectral variations in green fluorescent protein.* Nature structural biology, 1997. **4**(5): p. 361-365.

323. Meyer, A.J. and T.P. Dick, *Fluorescent protein-based redox probes.* Antioxid Redox Signal, 2010. **13**(5): p. 621-50.

324. Schwarzländer, M., et al., *Confocal imaging of glutathione redox potential in living plant cells.* J Microsc, 2008. **231**(2): p. 299-316.

325. Gutscher, M., et al., *Real-time imaging of the intracellular glutathione redox potential.* Nature Methods, 2008. **5**(6): p. 553-559.

326. Morgan, B., M.C. Sobotta, and T.P. Dick, *Measuring E(GSH) and H2O2 with roGFP2-based redox probes.* Free Radic Biol Med, 2011. **51**(11): p. 1943-51.

327. Nicholls, D.G. and S.L. Budd, *Mitochondria and neuronal survival.* Physiol Rev, 2000. **80**(1): p. 315-60.

328. Morris, R.L. and P.J. Hollenbeck, *The regulation of bidirectional mitochondrial transport is coordinated with axonal outgrowth.* J Cell Sci, 1993. **104 (Pt 3)**: p. 917-27.

329. Li, Z., et al., *The importance of dendritic mitochondria in the morphogenesis and plasticity of spines and synapses.* Cell, 2004. **119**(6): p. 873-87.

330. Zhang, C.L., et al., *Activity-dependent regulation of mitochondrial motility by calcium and Na/K-ATPase at nodes of Ranvier of myelinated nerves.* J Neurosci, 2010. **30**(10): p. 3555-66.

331. Amiri, M. and P.J. Hollenbeck, *Mitochondrial biogenesis in the axons of vertebrate peripheral neurons.* Dev Neurobiol, 2008. **68**(11): p. 1348-61.

332. Grafstein, B. and D.S. Forman, *Intracellular transport in neurons.* Physiol Rev, 1980. **60**(4): p. 1167-283.

333. Chang, D.T. and I.J. Reynolds, *Mitochondrial trafficking and morphology in healthy and injured neurons.* Prog Neurobiol, 2006. **80**(5): p. 241-68.

334. Chan, D.C., *Mitochondria: dynamic organelles in disease, aging, and development.* Cell, 2006. **125**(7): p. 1241-52.

335. Stokin, G.B. and L.S. Goldstein, *Axonal transport and Alzheimer's disease.* Annu Rev Biochem, 2006. **75**: p. 607-27.

336. Misgeld, T., et al., *Imaging axonal transport of mitochondria in vivo.* Nat Methods, 2007. **4**(7): p. 559-61.

337. Miller, K.E. and M.P. Sheetz, *Direct evidence for coherent low velocity axonal transport of mitochondria.* J Cell Biol, 2006. **173**(3): p. 373-81.

338. van Spronsen, M., et al., *TRAK/Milton motor-adaptor proteins steer mitochondrial trafficking to axons and dendrites.* Neuron, 2013. **77**(3): p. 485-502.

339. Martin, M., et al., *Cytoplasmic dynein, the dynactin complex, and kinesin are interdependent and essential for fast axonal transport.* Mol Biol Cell, 1999. **10**(11): p. 3717-28.

340. Nangaku, M., et al., *KIF1B, a novel microtubule plus end-directed monomeric motor protein for transport of mitochondria.* Cell, 1994. **79**(7): p. 1209-20.

341. Hirokawa, N., S. Niwa, and Y. Tanaka, *Molecular motors in neurons: transport mechanisms and roles in brain function, development, and disease.* Neuron, 2010. **68**(4): p. 610-38.

342. Pilling, A.D., et al., *Kinesin-1 and Dynein are the primary motors for fast transport of mitochondria in Drosophila motor axons.* Mol Biol Cell, 2006. **17**(4): p. 2057-68.

343. Milde, S., et al., *Axonal transport declines with age in two distinct phases separated by a period of relative stability.* Neurobiol Aging, 2015. **36**(2): p. 971-81.

344. Stewart, B.A., et al., *Improved stability of Drosophila larval neuromuscular preparations in haemolymph-like physiological solutions.* J Comp Physiol A, 1994. **175**(2): p. 179-91.

345. Vagnoni, A. and S.L. Bullock, *A simple method for imaging axonal transport in aging neurons using the adult Drosophila wing.* Nat Protoc, 2016. **11**(9): p. 1711-23.

346. Turrel, O., et al., *Transient active zone remodeling in the Drosophila mushroom body supports memory.* Current Biology, 2022. **32**(22): p. 4900-4913.e4.

347. Fulterer, A., et al., *Active Zone Scaffold Protein Ratios Tune Functional Diversity across Brain Synapses.* Cell Rep, 2018. **23**(5): p. 1259-1274.

348. Torroja, L., et al., *Neuronal overexpression of APPL, the Drosophila homologue of the amyloid precursor protein (APP), disrupts axonal transport.* Curr Biol, 1999. **9**(9): p. 489-92.

349. Bainbridge, S.P. and M. Bownes, *Staging the metamorphosis of Drosophila melanogaster.* Development, 1981. **66**(1): p. 57-80.

350. Marder, E. and D. Bucher, *Central pattern generators and the control of rhythmic movements.* Curr Biol, 2001. **11**(23): p. R986-96.

351. Anreiter, I. and M.B. Sokolowski, *The foraging Gene and Its Behavioural Effects: Pleiotropy and Plasticity.* Annu Rev Genet, 2019. **53**: p. 373-392.

352. Linneweber, G.A., et al., *A neurodevelopmental origin of behavioural individuality in the Drosophila visual system.* Science, 2020. **367**(6482): p. 1112-1119.

353. Werkhoven, Z., et al., *The structure of behavioural variation within a genotype.* Elife, 2021. **10**.

354. Hunter, I., et al., *The Drosophila Larval Locomotor Circuit Provides a Model to Understand Neural Circuit Development and Function.* Front Neural Circuits, 2021. **15**: p. 684969.

355. Caldwell, J.C., et al., *Dynamic analysis of larval locomotion in Drosophila chordotonal organ mutants.* Proc Natl Acad Sci U S A, 2003. **100**(26): p. 16053-8.

356. Risse, B., et al., *Quantifying subtle locomotion phenotypes of Drosophila larvae using internal structures based on FIM images.* Comput Biol Med, 2015. **63**: p. 269-76.

357. Valente, D., I. Golani, and P.P. Mitra, *Analysis of the trajectory of Drosophila melanogaster in a circular open field arena.* PLoS One, 2007. **2**(10): p. e1083.

358. Kohsaka, H., et al., *A group of segmental premotor interneurons regulates the speed of axial locomotion in Drosophila larvae.* Curr Biol, 2014. **24**(22): p. 2632-42.

359. Pulver, S.R., et al., *Imaging fictive locomotor patterns in larval Drosophila.* J Neurophysiol, 2015. **114**(5): p. 2564-77.

360. Fushiki, A., et al., *A circuit mechanism for the propagation of waves of muscle contraction in Drosophila.* Elife, 2016. **5**.

361. Schneider-Mizell, C.M., et al., *Quantitative neuroanatomy for connectomics in Drosophila.* Elife, 2016. **5**.

362. Zwart, M.F., et al., *Selective Inhibition Mediates the Sequential Recruitment of Motor Pools.* Neuron, 2016. **91**(3): p. 615-28.

363. Zarin, A.A., et al., *A multilayer circuit architecture for the generation of distinct locomotor behaviours in Drosophila.* Elife, 2019. **8**.

364. Todorova, V. and A. Blokland, *Mitochondria and Synaptic Plasticity in the Mature and Aging Nervous System.* Curr Neuropharmacol, 2017. **15**(1): p. 166-173.

365. Murman, D.L. *The impact of age on cognition*. in *Seminars in hearing*. 2015. Thieme Medical Publishers.

366. Srivastava, S., *The mitochondrial basis of aging and age-related disorders.* Genes, 2017. **8**(12): p. 398.

367. Eisenberg, T., et al., *Induction of autophagy by spermidine promotes longevity.* Nature cell biology, 2009. **11**(11): p. 1305-1314.

368. Eisenberg, T., et al., *Cardioprotection and lifespan extension by the natural polyamine spermidine.* Nature medicine, 2016. **22**(12): p. 1428-1438.

369. Morselli, E., et al., *Spermidine and resveratrol induce autophagy by distinct pathways converging on the acetylproteome.* Journal of Cell Biology, 2011. **192**(4): p. 615-629.

370. Madeo, F., et al., *Spermidine in health and disease.* Science, 2018. **359**(6374): p. eaan2788.

371. Gupta, V.K., et al., *Restoring polyamines protects from age-induced memory impairment in an autophagy-dependent manner.* Nature neuroscience, 2013. **16**(10): p. 1453-1460.

372. Bhukel, A., F. Madeo, and S.J. Sigrist, *Spermidine boosts autophagy to protect from synapse aging.* Autophagy, 2017. **13**(2): p. 444-445.

373. Usherwood, P.N.R., *Insect muscle.* (No Title), 1975.
374. Wolf, H. and D.M. Lang, *Origin and clonal relationship of common inhibitory motoneurons CI1 and CI3 in the locust CNS.* J Neurobiol, 1994. **25**(7): p. 846-64.
375. Choi, J.C., D. Park, and L.C. Griffith, *Electrophysiological and morphological characterization of identified motor neurons in the Drosophila third instar larva central nervous system.* J Neurophysiol, 2004. **91**(5): p. 2353-65.
376. He, T., et al., *Differences in Ca2+ regulation for high-output Is and low-output Ib motor terminals in Drosophila larvae.* Neuroscience, 2009. **159**(4): p. 1283-91.
377. Feeney, C.J., et al., *Motor nerve terminals on abdominal muscles in larval flesh flies, Sarcophaga bullata: comparisons with Drosophila.* J Comp Neurol, 1998. **402**(2): p. 197-209.
378. Prokop, A. and I.A. Meinertzhagen, *Development and structure of synaptic contacts in Drosophila.* Semin Cell Dev Biol, 2006. **17**(1): p. 20-30.
379. Anderson, M.S., M.E. Halpern, and H. Keshishian, *Identification of the neuropeptide transmitter proctolin in Drosophila larvae: characterization of muscle fiber-specific neuromuscular endings.* J Neurosci, 1988. **8**(1): p. 242-55.
380. Budnik, V., *Synapse maturation and structural plasticity at Drosophila neuromuscular junctions.* Curr Opin Neurobiol, 1996. **6**(6): p. 858-67.
381. Williams, D.W. and J.W. Truman, *Remodeling dendrites during insect metamorphosis.* J Neurobiol, 2005. **64**(1): p. 24-33.
382. Bagri, A., et al., *Stereotyped Pruning of Long Hippocampal Axon Branches Triggered by Retraction Inducers of the Semaphorin Family.* Cell, 2003. **113**(3): p. 285-299.
383. Owald, D. and S.J. Sigrist, *Assembling the presynaptic active zone.* Curr Opin Neurobiol, 2009. **19**(3): p. 311-8.
384. Piao, C. and S.J. Sigrist, *(M)Unc13s in Active Zone Diversity: A Drosophila Perspective.* Frontiers in Synaptic Neuroscience, 2022. **13**.

385. Wichmann, C. and S.J. Sigrist, *The active zone T-bar--a plasticity module?* J Neurogenet, 2010. **24**(3): p. 133-45.

386. Budnik, V. and M. Gorczyca, *SSB, an antigen that selectively labels morphologically distinct synaptic boutons at the Drosophila larval neuromuscular junction.* J Neurobiol, 1992. **23**(8): p. 1054-65.

387. MacKay-Lyons, M., *Central pattern generation of locomotion: a review of the evidence.* Phys Ther, 2002. **82**(1): p. 69-83.

388. Buchner, E., *Genes expressed in the adult brain of Drosophila and effects of their mutations on behaviour: a survey of transmitter- and second messenger-related genes.* J Neurogenet, 1991. **7**(4): p. 153-92.

389. Waddell, S. and W.G. Quinn, *Flies, genes, and learning.* Annu Rev Neurosci, 2001. **24**: p. 1283-309.

390. Tempel, B.L., M.S. Livingstone, and W.G. Quinn, *Mutations in the dopa decarboxylase gene affect learning in Drosophila.* Proc Natl Acad Sci U S A, 1984. **81**(11): p. 3577-81.

391. Murchison, C.F., et al., *A distinct role for norepinephrine in memory retrieval.* Cell, 2004. **117**(1): p. 131-43.

392. Selcho, M., et al., *The role of octopamine and tyramine in Drosophila larval locomotion.* J Comp Neurol, 2012. **520**(16): p. 3764-85.

393. Wong, J.Y.H., et al., *Octopaminergic neurons have multiple targets in Drosophila larval mushroom body calyx and can modulate behavioural odor discrimination.* Learn Mem, 2021. **28**(2): p. 53-71.

394. Wu, C.-L., et al., *An octopamine-mushroom body circuit modulates the formation of anesthesia-resistant memory in Drosophila.* Current Biology, 2013. **23**(23): p. 2346-2354.

395. Sabandal, J.M., et al., *Concerted Actions of Octopamine and Dopamine Receptors Drive Olfactory Learning.* J Neurosci, 2020. **40**(21): p. 4240-4250.

396. Tamura, T., et al., *Aging specifically impairs amnesiac-dependent memory in Drosophila.* Neuron, 2003. **40**(5): p. 1003-11.

397. Vivó, M., et al., *Polyamines in the basal ganglia of human brain. Influence of aging and degenerative movement disorders.* Neurosci Lett, 2001. **304**(1-2): p. 107-11.

398. Sun, N., R.J. Youle, and T. Finkel, *The Mitochondrial Basis of Aging.* Mol Cell, 2016. **61**(5): p. 654-666.

399. DiMauro, S. and E.A. Schon, *Mitochondrial respiratory-chain diseases.* N Engl J Med, 2003. **348**(26): p. 2656-68.

400. Fernández-Checa, J.C., et al., *GSH transport in mitochondria: defense against TNF-induced oxidative stress and alcohol-induced defect.* Am J Physiol, 1997. **273**(1 Pt 1): p. G7-17.

401. Garcia-Ruiz, C. and J.C. Fernandez-Checa, *Mitochondrial glutathione: hepatocellular survival-death switch.* J Gastroenterol Hepatol, 2006. **21 Suppl 3**: p. S3-6.

402. Hollenbeck, P.J. and W.M. Saxton, *The axonal transport of mitochondria.* J Cell Sci, 2005. **118**(Pt 23): p. 5411-9.

403. Stahon, K.E., et al., *Age-Related Changes in Axonal and Mitochondrial Ultrastructure and Function in White Matter.* J Neurosci, 2016. **36**(39): p. 9990-10001.

404. Miller, K.E. and M.P. Sheetz, *Axonal mitochondrial transport and potential are correlated.* J Cell Sci, 2004. **117**(Pt 13): p. 2791-804.

405. Blaker, W.D., J.F. Goodrum, and P. Morell, *Axonal transport of the mitochondria-specific lipid, diphosphatidylglycerol, in the rat visual system.* J Cell Biol, 1981. **89**(3): p. 579-84.

406. Kaplowitz, N., T.Y. Aw, and M. Ookhtens, *The regulation of hepatic glutathione.* Annu Rev Pharmacol Toxicol, 1985. **25**: p. 715-44.

407. DeLeve, L.D. and N. Kaplowitz, *Importance and regulation of hepatic glutathione.* Semin Liver Dis, 1990. **10**(4): p. 251-66.

408. Suthanthiran, M., et al., *Glutathione regulates activation-dependent DNA synthesis in highly purified normal human T lymphocytes stimulated via the CD2 and CD3 antigens.* Proc Natl Acad Sci U S A, 1990. **87**(9): p. 3343-7.

409. Meredith, M.J. and D.J. Reed, *Status of the mitochondrial pool of glutathione in the isolated hepatocyte.* J Biol Chem, 1982. **257**(7): p. 3747-53.

410. Hwang, C., A.J. Sinskey, and H.F. Lodish, *Oxidized redox state of glutathione in the endoplasmic reticulum.* Science, 1992. **257**(5076): p. 1496-502.

411. Marí, M., et al., *Redox control of liver function in health and disease.* Antioxid Redox Signal, 2010. **12**(11): p. 1295-331.

412. Griffith, O.W. and A. Meister, *Origin and turnover of mitochondrial glutathione.* Proc Natl Acad Sci U S A, 1985. **82**(14): p. 4668-72.

413. Chistiakov, D.A., et al., *Mitochondrial aging and age-related dysfunction of mitochondria.* Biomed Res Int, 2014. **2014**: p. 238463.

414. Desler, C., et al., *Is There a Link between Mitochondrial Reserve Respiratory Capacity and Aging?* J Aging Res, 2012. **2012**: p. 192503.

415. Fernandez-Checa, J.C. and N. Kaplowitz, *Hepatic mitochondrial glutathione: transport and role in disease and toxicity.* Toxicol Appl Pharmacol, 2005. **204**(3): p. 263-73.

416. Marí, M., et al., *Mitochondrial glutathione, a key survival antioxidant.* Antioxid Redox Signal, 2009. **11**(11): p. 2685-700.

417. Doerfel, L.K., et al., *EF-P is essential for rapid synthesis of proteins containing consecutive proline residues.* Science, 2013. **339**(6115): p. 85-8.

418. Ude, S., et al., *Translation elongation factor EF-P alleviates ribosome stalling at polyproline stretches.* Science, 2013. **339**(6115): p. 82-5.

419. Coll, O., et al., *Sensitivity of the 2-oxoglutarate carrier to alcohol intake contributes to mitochondrial glutathione depletion.* Hepatology, 2003. **38**(3): p. 692-702.

420. Herrero, E. and J. Ros, *Glutaredoxins and oxidative stress defense in yeast.* Methods Enzymol, 2002. **348**: p. 136-46.

421. Koehler, C.M., K.N. Beverly, and E.P. Leverich, *Redox pathways of the mitochondrion.* Antioxid Redox Signal, 2006. **8**(5-6): p. 813-22.

List of Publications

List of Tables

List of Figures

169

List of Abbrevations

Ach	acetylcholine
ADP	adenosine diphosphate
AEL	after egg laying
AP	action potential
APF	after puparium formation
Atg	autophagy-related gene
ATP	adenosine triphosphate
AZ	active zone
BAP3	BAI1-associated protein 3
bl	body length
BMP	bone morphogenic protein
BRP	bruchpilot
Cac	cacophony
CAZ	cytomatrix of the active zone
CHO	Chinese hamster ovary
CNS	central nervous system
CPG	central pattern generator
DA	diamide
DEOM	dorsal external oblique muscles
DHPS	deoxyhypusine synthase
DIOM	dorsal internal oblique muscles
DLM	dorsal longitudinal flight muscles
dnc	dunce
DOHH	deoxyhypusine hydroxylase
DSV	dense core vesicles
DTT	dithriothreitol
Duf	dumbfounded
DVM	dorsoventral flight muscles
eEPSC	evoked excitatory postsynaptic currents
eIF5A	eukaryotic translation initiation factor 5A
EJP	excitatory junction potentials
ETC	electron transport chain
FasII	Fascilin II
GABA	γ-aminobutyric acid
GFP	green fluorescent protein
GluR	glutamate receptors
GoF	gain of function
Grx1	glutaredoxin-1
GSH/GSSG	glutathione
GSH1	glutamate-cysteine ligase
GSH2	glutathione synthase
GTP	guanosine triphosphate

170

HC	head cast
hid	head involution defective
HL3	hemolymph-like saline
HRP	horseradish peroxidase
HV	head vector
HVA	high-voltage-activated
IFM	indirect flight muscles
IGF1R	insulin-like growth receptor
IMBA	individual maggot behaviour tracker
IRS	insulin receptor substrates
IS	interstep
KD	knockdown
KIF	kinesin superfamily proteins
LAR	leukocyte common antigen-related
LH	liprin-α Homology region
LOF	loss of function
LOM	larval oblique muscles
LVA	low-voltage activated
MAP1B	microtubule-associated protein
MB	mushroom body
mtDNA	mitochondrial DNA
NADPH	nicotinamide adenine dinucleotide phosphaste
NEM	n-ethylmalemide
NGS	normal goat serum
NMJ	neuromuscular junction
NSF	n-ethylmaleimide-sensitive factor
OA	octopamine
OA/TA neurons	octopaminergic/tyraminergic neurons
OctβR	β-adrenergic-like octopamine receptor
P1-P13	pupal stage 1-13
PBS	phosphate-buffered saline
PFA	paraformaldehyde
PIKK	PI3K-related kinase
PINK1	PTEN-induced kinase 1
PSD	post synaptic density
RBP	RIM-binding protein
redox	reduction-oxidation
RFU	relative fluorescence unit
RIM	rab3-interacting molecules
roGFP	redox-sensitive GFP
ROS	reactive oxygen species
RRP	readily releasable pool
rut	rutabaga

SAM	sterile-alpha-motif
SN	segmental nerve
SNAP	soluble NSF attachment protein
SNAP-25	synaptosomal-associated-protein 25
SNARE	soluble N-ethylmaleimide-sensitive factor attachment protein receptors
SOG	subesophageal ganglion
Spd	spermidine
STED	stimulated emission depletion
SV	synaptic vesicles
Syd	synapse-defective
TA	tyramine
TDC	tyrosine decarboxylase
TDT	tergal depressor of the trochanter
TH	tyrosine hydroxylase
TOR	target of rapamycin
TRX	thioredoxin
TyR	tyramine receptors
TβH	tyramine β-hydroxylase
UAS	upstream activation site
UM	unpaired median
Unc13	uncoordinated-13 protein
Unc18	uncoordinated-18 protein
VAMP	vesicle-associated-membrane protein
VGCC	voltage gated Ca^{2+} channels
VNC	ventral nerve cord